On the origin of epithermal Sn-Ag-Zn mineralization at the Pirquitas mine, NW Argentina: fluid inclusion and isotopic constraints

kumulative Dissertation

zur Erlangung des akademischen Grades

„doctor rerum naturalium" (Dr. rer. Nat.)

in der Wissenschaftsdisziplin „Geochemie"

eingereicht an der

MATHEMATISCH-NATURWISSENSCHAFTLICHEN FAKULTÄT DER UNIVERSITÄT POTSDAM

von

Louis Desanois

Potsdam, im Februar 2019

Datum der Disputation: 22.05.2019

Supervisor: Dr. Robert Trumbull
1: Referee GFZ German Research Center for Geosciences, Potsdam, Germany

Supervisor: Prof. Dr. Uwe Altenberger
2: Referee University of Potsdam, Institute of Earth and Environnemental Science, Germany

3: Referee Prof. Dr. Bernd Lehmann Technische Universität Clausthal | TUC · Department of Geology and Paleontology

Published online at the
Institutional Repository of the University of Potsdam:
https://doi.org/10.25932/publishup-43082
https://nbn-resolving.org/urn:nbn:de:kobv:517-opus4-430822

Abstract

Die zentralen Anden beherbergen große Reserven von unedlen und Edelmetallen. Die Region war 2017 ein wichtiger Teil der weltweiten Bergbautätigkeit. Bisher wurden drei Hauptlagerstätten identifiziert und untersucht: 1) Porphyr-Lagerstätten, die sich von Zentralchile und Argentinien bis Bolivien und Nord-Peru erstrecken; 2) Eisenoxid-Kupfer-Gold-Lagerstätten (IOCG), die sich von Zentralperu bis Zentralchile ausdehnen, sowie 3) polymetallische epithermale Zinnlagerstätten, die sich von Südperu bis nach Nordargentinien erstrecken und einen Großteil der Lagerstätten des bolivianischen Zinngürtels (Bolivian Tin Belt - BTB) bilden. Lagerstätten im BTB können in zwei Haupttypen unterteilt werden: (1) polymetallische Lagerstätten aus Zinn-Wolfram-Zink im Zusammenhang mit Plutonen und (2) polymetallische Zinn-Silber-Blei-zink Anlagerungen in epithermalen gangförmigen Lagerstätten.

Mina Pirquitas ist eine epithermale Zinn-Silber-Blei-Zink-Polymetallvenenlagerstätte im Nordwesten Argentiniens, die früher eine der wichtigsten Zinnsilber-Mine meines Landes war. Es wurde als Teil der BTB interpretiert und hat ähnliche Mineralstoffverbände mit südlichen Pluton-bezogenen BTB-Epithermalvorkommen. Es wurden zwei bedeutende Mineralisierungsereignisse identifiziert, die sich auf drei mit meteorischem Wasser gemischte magmatische Fluide beziehen. Das erste Ereignis kann in zwei Stufen unterteilt werden: 1) Stufe I-1, wobei Quarz, Pyrit und Cassiterit aus Fluiden zwischen 233 und 370 ° C und einem Salzgehalt zwischen 0 und 7,5 Gew .-% ausfallen, entsprechend einem ersten Flüssigkeitsimpuls, und 2) Stufe I-2 mit Sphalerit und Zinn-Silber-Blei-Antimonsulfosalzen, die aus Fluiden zwischen 213 und 274 ° C mit einem Salzgehalt von bis zu 10,6 Gew .-% ausfallen, was einem neuen Impuls magmatischer Fluiden im hydrothermalen System entspricht. Durch die Mineralisierung II wurden die reichsten Silbererze bei Pirquitas abgelagert. Die Temperaturen und Salzgehalte von Event II liegen zwischen 190 und 252 ° C bzw. zwischen 0,9 und 4,3 Gew .-%. Dies entspricht der abnehmenden Versorgung mit magmatischen Fluiden. Edelgasisotopenzusammensetzungen und -konzentrationen in mit Erz beherbergten Flüssigkeitseinschlüssen zeigen einen signifikanten Beitrag magmatischer Fluiden zur Pirquitas-Mineralisierung, obwohl keine intrusiven Gesteine im Minengebiet exponiert sind.

Messungen von Blei- und Schwefelisotopen an Erzmineralien zeigen, dass Pirquitas eine ähnliche Signatur mit südlichen Pluton-verwandten polymetallischen Lagerstätten in der BTB teilt. Darüber hinaus liegt der größte Teil der Schwefelisotopenwerte von Sulfid- und Sulfosaltmineralien aus Pirquitas im Bereich von Schwefel aus magmatischem Gestein. Dies deutet darauf hin, dass der Hauptbeitrag von Schwefel zum hydrothermalen System bei Pirquitas wahrscheinlich aus Magma stammt. Das genaue Alter der Lagerstätte ist noch nicht bekannt, aber die Ergebnisse der Wolframit-Datierung von 2,9 ± 9,1 Ma und lokalen Strukturbeobachtungen legen nahe, dass die späten Mineralisierungsereignisse jünger als 12 Ma sind.

Abstract

The Central Andes host large reserves of base and precious metals. The region represented, in 2017, an important part of the worldwide mining activity. Three principal types of deposits have been identified and studied: 1) porphyry type deposits extending from central Chile and Argentina to Bolivia, and Northern Peru, 2) iron oxide-copper-gold (IOCG) deposits, extending from central Peru to central Chile, and 3) epithermal tin polymetallic deposits extending from Southern Peru to Northern Argentina, which compose a large part of the deposits of the Bolivian Tin Belt (BTB). Deposits in the BTB can be divided into two major types: (1) tin-tungsten-zinc pluton-related polymetallic deposits, and (2) tin-silver-lead-zinc epithermal polymetallic vein deposits.

Mina Pirquitas is a tin-silver-lead-zinc epithermal polymetallic vein deposit, located in north-west Argentina, that used to be one of the most important tin-silver producing mine of the country. It was interpreted to be part of the BTB and it shares similar mineral associations with southern pluton related BTB epithermal deposits. Two major mineralization events related to three pulses of magmatic fluids mixed with meteoric water have been identified. The first event can be divided in two stages: 1) stage I-1 with quartz, pyrite, and cassiterite precipitating from fluids between 233 and 370 °C and salinity between 0 and 7.5 wt%, corresponding to a first pulse of fluids, and 2) stage I-2 with sphalerite and tin-silver-lead-antimony sulfosalts precipitating from fluids between 213 and 274 °C with salinity up to 10.6 wt%, corresponding to a new pulse of magmatic fluids in the hydrothermal system. The mineralization event II deposited the richest silver ores at Pirquitas. Event II fluids temperatures and salinities range between 190 and 252 °C and between 0.9 and 4.3 wt% respectively. This corresponds to the waning supply of magmatic fluids. Noble gas isotopic compositions and concentrations in ore-hosted fluid inclusions demonstrate a significant contribution of magmatic fluids to the Pirquitas mineralization although no intrusive rocks are exposed in the mine area.

Lead and sulfur isotopic measurements on ore minerals show that Pirquitas shares a similar signature with southern pluton related polymetallic deposits in the BTB. Furthermore, the major part of the sulfur isotopic values of sulfide and sulfosalt minerals from Pirquitas ranges in the field for sulfur derived from igneous rocks. This suggests that the main contribution of sulfur to the hydrothermal

system at Pirquitas is likely to be magma-derived. The precise age of the deposit is still unknown but the results of wolframite dating of 2.9 ± 9.1 Ma and local structural observations suggest that the late mineralization event is younger than 12 Ma.

Acknowledgements

Firstly, I would like to thanks my supervisor Dr. Volker Lüders for the continuous support of my Ph.D study and related research, for his patience and knowledge. He helps me to learn and understand about this complex subject and guide me in all the time of research of this thesis. Secondly I would like to express my sincere gratitude to my advisor Dr. Robert Trumbull without who it would be impossible to build the relationship with Argentinian people and who gives a lot of his time for answering my numerous questions.

My sincere thanks also goes to Dr Marta Sosnicka who provided me comments and advices in the laboratory and research facilities, Dr. Samuel Niedermann and Prof. Dr. Rolf Romer for they measure and expertise, Prof. Dr. Uwe Altenberger, Prof. Dr. Pablo Caffe, Dr. Marcelo Arnosio, and Dr. Raul Becchio for all the advices, helps and knowledges. Without they precious support it would not be possible to conduct this research.

I thank my fellow Phd student friends and colleagues from STrATEGy for the stimulating discussions, the good time on the field and for all the fun we have had in the last three years. Also I thank my friends in the Salta University in Argentina. In particular Valeria Simon, I am grateful to participated in her project and have the possibility to share our respective expertise.

Last but not the least, I would like to thanks my beloved fiancée, Marie Lefebvre, who was by my side all this time and gives me the straight to finish my thesis beside all the difficulties. My last thank goes to my parents, my brother and sister, and my far away fiends in France for supporting me spiritually throughout writing this thesis and my life in general.

Contents

Figures

Tables

1. General introduction

1.1. The metallogeny of the Central Andes

The Central Andes (Fig 1) have one of the most important reserve of base metals on the planet. Several Andean countries (Chile, Bolivia, Peru, etc.) are among the richest in the world either in production or in geological reserves of antimony, barium, beryllium, bismuth, boron, copper, indium, iodine, lithium, lead, molybdenum, nitrates, platinum, rhenium, selenium, silver, tellurium, tin, tungsten, and zinc (Petersen, 1977). The region represented, in 2017, an important part of the worldwide mining activity with 39% of copper, 23% of silver, 20% of molybdenum, 14% of zinc, and 12% of tin of the world production (Fontboté, 2018). In the last 30 years, numerous new world class deposits were discovered, such as El Indio and Escondida in Chile, and the Andes are still a principal target for exploration. At the same time, there have been a growing number of scientific studies the occurrence and genesis of ore deposits of the central Andes. Three main types have been identified and studied all over the Central Andes and are of interest to this study. Some of them are among the world largest of their type (e.g., Chuquicamata porphyry Cu deposit).

Porphyry deposits

The best studied deposit type of the Central Andes, the porphyry copper type, has been intensively described by Silitoe (1975), Silitoe and Perelló (2005), and Silitoe (2010). It forms due to subvolcanic-related and metasomatic processes during an accretionary orogeny context. The Cenozoic is characterized by an abundant occurrence of Cu-Au-Mo porphyry systems in the Central Andes after massive fluids circulation. This fluids supply has been interpreted to be the consequence of the flattening of the subducted slab, which induced magma trapping in large shallow chambers under the belt (Sillitoe and Perelló 2005). Several orogen-parallel porphyry copper belts occurred along the Andean cordillera. However, compared to Paleozoic and early Mesozoic porphyry Cu deposits, those that formed during the Paleocene to Early Oligocene, and from Miocene to early Pliocene periods are the richest in copper (Sillitoe and Perelló 2005; Fontboté, 2018). They extend from central Chile and Argentina to Bolivia, and northern Peru.

IOCG deposits

A well-known iron oxide-copper-gold (IOCG) deposits belt, defined primarily by their elevated magnetite and/or hematite contents, extends from central Peru to central Chile (Sillitoe & Hedenquist, 2003). The Cu-porphyry and IOCG deposits occur along the main magmatic arc(s) of the Andes. Also, the central Andean IOCG belt is associated to the coastal Cordillera crustal extensional and transtensional phase during the lower Jurassic and the lower Cretaceous (Sillitoe & Hedenquist, 2003).

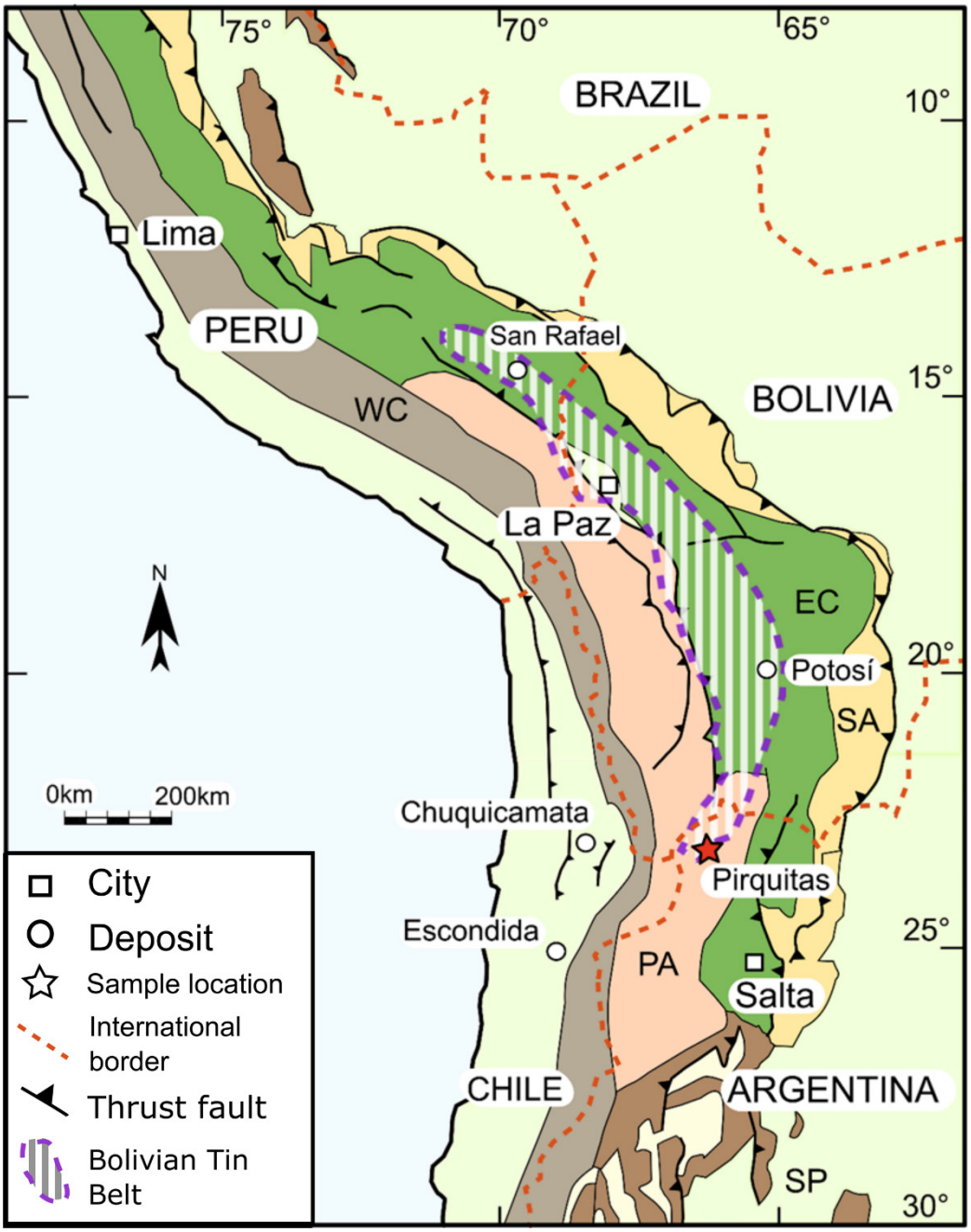

Figure 1: Map of the central Andes with (EC) Eastern Cordillera, (WC) Western Cordillera, (SA) Subandean Cordillera, (PA) Puna-Altiplano, (SP) Sierras Pampeanas.

Andean IOCG deposits are strongly connected to gabrodioritic to dioritic magmas, from which the ore bearing fluid have been generated (Sillitoe & Hedenquist, 2003; De haller and Fontboté, 2009).

Epithermal tin polymetallic deposits

There is an important third belt of mineralization located east of the magmatic arc which shows high concentration of tin, tungsten, silver, and base metals. It is usually known as the Bolivian tin belt (BTB), and it extends from southern Peru to northern Argentina. Numerous tin-polymetallic deposits occurred all along this belt with different mineralization types and ages from Triassic to Cenozoic. The Pirquitas deposit is located at the southern end of the Bolivian Tin Belt.

1.2. The Bolivian Tin-Belt

The Bolivian Tin Belt (BTB) extends from the Peruvian border through Bolivia along the Eastern range of the Andes into northern Argentina for approximately 900 km and hosts a variety of economic ore deposits of regionally different styles and ore associations (Turneaure, 1971; Arce-Burgoa, 1990, 2009; Fontboté, 2018). High grade hydrothermal tin lodes with significant W and Ag contents are in spatial association with peraluminous granites and porphyry intrusive bodies, which are aged from the late Permian to the early Pliocene. Most of the tin deposits hosted in the BTB are late Oligocene to Miocene in age, but a small part of them is dated from late Triassic to early Jurassic (Arce-Burgoa, 2009). Deposits in the BTB can be divided into two major types: (1) Sn–W–Zn pluton-related polymetallic deposits, and (2) Sn–Ag–Pb–Zn epithermal polymetallic vein deposits (including the Bonanza type, a high Au grade deposit type).

1.2.1. Sn–W–Zn pluton related deposits

Sn and Sn-W-Zn deposit types are mostly represented in the Central Cordillera also named Cordillera Real in the northern part of the BTB, and are illustrated by districts as Sayaquira, Caracoles, Araca, Bolsa, Negra, Chojlla, and Milluni. They are generally located in the region from La Paz to the Peruvian border. Most of the tin-tungsten deposits are dominantly tungsten bearing, but between La Paz and Oruro, both tin and tungsten occur sub-equally. They occur within pluton or altered sedimentary rocks of the contact zone and are accompanied by a generation of characteristic widespread tourmaline–related to late hydrothermal alteration. The main mineralizations occur as

cassiterite-quartz and wolframite-quartz veins with scheelite in association with pyrrhotite and sphalerite, the most abundant sulfide minerals. Other sulfides including chalcopyrite, arsenopyrite, and stannite are common, as well as bismuthinite and native bismuth that are characteristic of several deposits. Galena occurs in rarely. The Sn-W-Zn mineralizations form an irregular mineralized belt up to 10km wide on both sides of the batholiths. The southern half of the BTB is dominated by polymetallic tin-silver mineralization however the most important tin type deposits are located there such as Llallagua, Morococala, Huanuni, and Colquiri. The rich tin deposits in the southern BTB are minerallogically similar to those of the Cordillera Real, with quartz-cassiterite-sulfide ores (Turneaure, 1971).

1.2.2. Sn–polymetallic vein type deposits

The polymetallic vein-type deposits in the southern half of the BTB are exemplified by districts including Potosí, Porco, Sieste suyos, Tatasi, San Vicente, and San Antonio de Lipez and include northern Argentina deposits Chinchillas and Pirquitas (this study). Mineralization aging from betwee 22 to 4 Ma, occur as veins, veinlets, stockworks, and disseminated ores hosted in Paleozoic metasediments, volcanic layers, and Paleozoic to Mesozoic plutons (Grant et al., 1979; Coira et al., 2004). Polymetallic Ag-Sn vein-type ore deposits are shallow and are assumed to be genetically related with Miocene and Pliocene subvolcanic intrusions (Grant et al., 1979; Coira et al., 2004). Typically, the southern BTB ore veins are hosted in quartz-poor gangue and are composed of cassiterite, pyrite, base-metal sulfides, and a large variety of sulfosalts including tetrahedrite, pyrargyrite, franckeite, andorite, as well as rare minerals as matildite or aramayoite. The alteration minerals include alunite, chlorite, sericite, and kaolinite with rare tourmaline. The Sn-Zn deposits are characterized by abundant teallite, altered to galena, in association with sphalerite-wurzite, acicular cassiterite, and less abundant minerals as sulfides, franckeite, and cylindrite. Additional deposits can be observed with Ag-Zn or Ag-Pb-Zn shallow mineralization as well as, mostly in the south, Pb-Zn-Sb and Au-W mineralized veins (Turneaure, 1971).

1.3. Mina Pirquitas, overview and history

1.3.1. Geographical characteristics

Mina Pirquitas is a Sn-Ag-(Zn) mine property of Silver Standard Inc located in the Province of Jujuy in northwestern Argentina (22'42"S, 66'30"W). The closet community is the village of Nuevo Pirquitas, ca 10km from the mine site, with a population of about 200 people. Biggers towns, Susques and Abra Pampas, are in ca 130 km distance by road. Approximately 76% of the mine employees are native from the Jujuy province and the majority of them live in the mine camp (Board, 2011).

The deposit is situated in a rugged mountainous terrain at elevations between 4,000 and 4,450 m a.s.l. . The area around the mine is covered by patchy to sparse shrub and grass vegetation that provide habitat for few animal species including vicuña, puna fox, and vizcacha, as well as more than 50 species of birds (Rundel and Palma, 2000). The climate in the area is typical for the Puna plateau, with dry (260 mm annual precipitation) and windy conditions. Occasional rains are concentrated between December and February. Moderate temperatures typify most of the year, with temperatures below freezing during the winter.

1.3.2. General geology

The Pirquitas deposit is located in the Puna plateau, which is mostly composed of a strongly deformed Neoproterozoic to Cambrian metamorphic basement of which is covered by Ordovician metamorphosed shales and sandstones which are intercalated with volcanic layers (Lucassen et al., 2000; Coira et al., 2004). Upon those Ordovician metasediments and volcanic layers, Tertiary continental basins developed. Also, a centripetal drainage network has built depressions partly occupied by salt flats or brackish water bodies (Allmendinger et al., 1997; Gorustovich et al., 2011).

The history of the plateau is dominated by compressional deformations and uplifts related to the Andean Orogeny as well as the magmatic activity of the Andean Central Volcanic Zone (CVZ). The volcanic activity of the Puna is characterized by early Miocene to Pliocene andesitic-dacitic stratovolcanoes along the western margin and large-volume felsic ignimbrites erupted from resurgent calderas of the Altiplano-Puna volcanic complex (de Silva, 1989; Caffe et al., 2002; Kay et al., 2010). The main structures in the Puna are N-S to NNE-SSW striking faults and regional scale striking

lineaments with compressive and transpressive characters. The northern Puna is considered to be in near neutral stress since the end of the Miocene due to a lack of tectonic activity, in contrast to the southern part, where several extensional and transtensional faults are associated with the Pliocene plateau collapse (Allmendinger et al., 1989; Marrett et al., 1994).

The Pirquitas area is composed of Ordovician low-grade metamorphic sandstones and pelites called the Acoite Formation, which is overlain by fluvial and lacustrine sediments of the mid-Miocene Tiomayo Formation, alternating with 15 Ma old ignimbrite deposits. The Acoite Formation layers are folded in the typical deformation style of the Late Ordovician-Lower Devonian WNW-ESE directed Ocloyic compression (Voldman et al., 2012; Mon and Salfity, 1995; Bahlburg and Hervé, 1997). Ordovician normal and strike-slip faults were reactivated as thrust faults during the Tertiary Andean orogeny (Cladouhos et al.,1994) and some of them favored magma ascent and hydrothermal fluids migration in relation with Miocene volcanic centers (Coira et al., 2004; Caffe, 2008). The Pirquitas deposit occurs in an uplifted block of the Acoite Formation with some mineralization cutting the base of the Tiomayo Formation. This suggests a mineralization age younger than 15 Ma. Late Miocene caldera-sourced pyroclastic deposits with ages between 6.6 and 9.8 Ma are found from 12 to 20 km around Mina Pirquitas, but no direct evidence of subvolcanic intrusion at Pirquitas has yet been found. The closest plutonic rock is the granodiorite of Cerro Galán, some 12 km east of Pirquitas (Caffe, 2008).

Mineralization occurs essentially in two types: (1) polymetallic veins with peripheral disseminated mineralization; and (2) mineralized hydrothermal breccia. The vein-type is the dominant one and has been the main source of mined ore. Mineralization of the vein-type is characterized by quartz and massive sulfides (pyrite, sphalerite, galena, or pirquitasite) in association with a large variety of sulfosalts Ag-Sn-As-Sb-Pb-Cu-Bi (pyragyrite, cylindrite, or frankeite) and rare oxides (cassiterite or wolframite). Hydrothermal breccia bodies, found in several part of the area, were formed concomitantly with veins. They host a similar assemblage of pyrite, marcasite, cassiterite, sphalerite, arsenopyrite, galena, and Ag-Sn-As-Sb-Pb-Cu-Bi sulfosalts, except that the abundance of galena is higher (Malvicini, 1978; Paar et al., 1996; Slater, 2016).

1.3.3. History of mining

Mina Pirquitas was one of the most important silver producing mines in Argentina from the early 1930's to its temporary closure in 2017. First, the place was prospected for gold placers in the Orosmayo River drainage, until economic quantities of cassiterite were found in gravel deposits of the Pircas River, situated at the east of the Pirquitas old village. These tin placers were dredged during the period between 1933 and 1949. Silver and tin lode mining began in 1936 from small underground workings, after the discovery of the bedrock source of the cassiterite. Over the last 50 years, the site has become the largest historical producer of tin and silver with twelve mines operated. The principal mines were San Miguel, Chocaya, Llallagua, and Potosí. During the 1970's, almost all the deposits were owned by one company named Sociedad Minera Pirquitas Picchetti and Cia S.A. Approximately 777,600 kg of silver and 18,200 t of tin have been extracted from the vein systems and around 9,100 t of tin from the placer exploitation (Board, 2011). The Argentine subsidiary of Sunshine Mining and Refining Company acquired the deposit in 1995 and began a comprehensive exploration program. In 2002, Silver Standard acquired Sunshine Argentina and invested further in exploration and prospection under the control of the subsidiary Mina Pirquitas, Inc. The current Pirquitas mine began commercial silver-zinc production on December 1, 2009 (Silver Standard Ressources Inc, 2018).

1.4. Open questions, objectives, and methodology

1.4.1. Main motivations and purpose

Pirquitas mineralization is characterized by a complex Ag-Sn-Sb-Pb-Bi mineral association with a lack of more common silver minerals such as argentite or native silver. The principal silver mineral is pyrargyrite (Ag_3SbS_3). Those differences can reflect local variations in the geology and in the mineralization process compared to other similar deposits described in the southern BTB. Furthermore, as no direct relationship with a subvolcanic body was observed, even after a 800m drilling made under the San Miguel open pit, it is risky to define it as a magmatic related deposit. The age of the deposits is still controversy, relative dating only shows that it is younger than 15Ma.

The first study of the actual mine area, regrouping veins systems and breccia, was done by L. Malvicini in 1978. It gives a detailed description of the San Miguel, Chocaya, Potosi, and Oploca vein

systems as well as Potosi and Oploca breccia occurrences. Except for Oploca, all are located in the actual open pit area. In this study, Malvicini defined two events of mineralization resulting of hydrothermal fluid circulation estimated at about 400°C. During the 1990's and the 2000's, the deposit's mineralogy was largely described and studied by W. Paar, R.J. Sureda, and B. Coira. They defined specific sulfides and sulfosalts in Sn-Ag deposit such as the pirquitasite, suredaite, and Coiraite (Paar et al., 1996, 2000, 2001, 2008). In 2011, general information about structures and ores rates in the open pit were given in the Silver standard Technical Report (Board, 2011). The last work about Pirquitas is a general characterization of the Cortadera breccia in the northern part of the mine area which was found during the mine extension exploration campaign in 2014 (Slater, 2016). It was the first time fluid inclusions technics were used on Pirquitas mineralization. However, during the last 40 years, Pirquitas mineralization studies were only focused on structural, mineral observations, SEM, and microprobe analyses, resulting in incomplete knowledge of the history of the deposit. The absence of proper fluid inclusions and isotopic studies was the motivation for the present study of the deposit in order to build a more complete history of Pirquitas mineralization and characterize the geological processes behind it.

The actual state of the art defines the Pirquitas deposit as a Sn-Ag-Zn polymetallic epithermal deposit with characteristics that make it included in the Bolivian tin belt. The temperature of the ore bearing fluid which was previously estimated by Malvicini in 1978 does not fit with typical temperatures measured in deposits presenting similar mineralization. Slater, in 2016, showed a better estimation but still incomplete. The first part of our study is the determination of the ore-bearing fluids temperatures and their possible sources. Those ore-bearing fluids might be magmatic-related despite the absence of any direct pluton observation. In the same way, the origin of the metallic components was questioned. Then, the problem of the age was also pointed and a preliminary dating was made in a way to constraint the age. The most precise age estimation was given by Slater (2016) who estimates it between 12 and 16 Ma. After new observations and measurements in close volcanic centers around Mina Pirquitas, the mineralization could be even younger.

1.5. General information of methods and technologies

Several technics were used in a way to (1) characterize the ore-bearing fluids, (2) trace the origin of fluids and metals, and (3) date the mineralization. Those technics are respectively: fluid inclusions microthermometry, noble gases isotope analysis of fluid inclusions, lead and sulfur isotope analysis of ore minerals, and U-Pb dating of ore minerals.

Fluid inclusions microthermometry

Microthermometry applied to fluid inclusions is a non-destructive technique based on the principle that fluid inclusions are closed systems since their formation. Heating-freezing systems are used to estimate critical temperatures corresponding to phase changes of fluids and solids in the inclusion (freezing, melt, or homogenization temperature) (cf. Bodnar, 2003). The combination of the fluid inclusion petrography and the composition of the solid fluid and gaseous phases of the fluid inclusions is an important diagnostic, classification, and fluid characterization tool. Various models and equation of state, initially developed for P-V-T-X parameters of individual fluid systems, are used to reduce microthermometric data in order to determine (1) the ore bearing fluid temperature at the fluid trapping time, (2) the fluid composition, particularly the salinity, and (3) the pressure i.e. the depth of the deposit during the deposition time (cf. Bodnar, 2003).

Analyses are usually made on transparent minerals such as quartz, calcite, or sphalerite. The previous fluid inclusions study of Slater (2016) was made on quartz and sphalerite from breccia mineralization only, Fluid characterization from opaque sulfides and sulfosalts are lacking. Therefore, two fluid inclusions stages in the Fluid Inclusion laboratory in the GFZ in Potsdam, were used: (1) a FLUID INC-adapted U.S.G.S. gas-flow heating/freezing system mounted on an Olympus BX50 microscope with a long-distance 40× objective in visible light, and (2) a Linkam FTIR 600 heating-cooling stage coupled with an Olympus BHSM- IR infrared microscope with a 50× IR objective coupled to an infrared In-Ga-As camera for observation in the near infrared region (λ=800 to 1800 nm). The first stage was used for transparent minerals like quartz or light sphalerite, whereas the second one was used for opaque minerals like hocartite or dark sphalerite where inclusions are not observable in

visible light. This gives solid informations to characterize precisely the different pulses of ore bearing fluids responsible of the Pirquitas veins and breccia mineralization.

Noble gases isotopes

The group of elements known as noble gases or rare gases owns several unique properties that give them a significant importance as geodynamic tracers. The geochemical composition of the analyzed noble gases gives information about (1) mantle and magma degassing processes, (2) mixing relationships between different mantle, crustal, and atmospheric components, and (3) the formation of the atmosphere and the influence of volatiles.

In our study we mostly focused on the $^{3}He/^{4}He$ ratio as it gives major information about mantle derived fluids and can be used to decipher shallow or deep seated fluids origins (Mamyrin et al, 1969).. Other noble gases, Ne, Ar, Kr, and Xe also provide complementary information to helium, but as most investigators seem to focus on helium first, the database on these gases is rather limited (Sano and Fischer, 2013).

This technique was used to analyze directly the residual ore bearing fluid trapped in the Pirquitas ore minerals fluid inclusions. To achieve this, millimeter size hand-picked minerals separates samples were loaded into an ultra-high vacuum spindle crusher and the released gases were collected and analyzed by a VG5400 noble gases mass spectrometer in the noble gases laboratory of the GFZ (GeoForschungsZentrum) in Potsdam. Analyzing the fluid in the inclusion results in the isotopic composition of the fluid and limits the contribution of He resulting from radioactive decay.

Sulfur isotopes

Sulfur geochemistry helps to better understand its origins, and evolution of the ore depsit it is a well-studied stable isotope with complete references regarding S isotopes geologic reservoirs. For sulfide minerals, the most used isotopic composition is the $^{34}S/^{32}S$ ratio, also named $\delta^{34}S$, but other ratios as $^{33}S/^{32}S$ and $^{36}S/^{32}S$ are also determined in Precambrian sulfide and sulfate minerals and in Martian meteorites (Seal, 2006; Farquhar et al. 2000a, b; Farquhar and Wing 2003). However, only $\delta^{34}S$ were used for Pirquitas as the age of the deposit is estimated to be younger than mid-Miocene. Samples

were hand-picked grains of pure mineral phases from the millimeter scale and are analyzed in the stable isotopes laboratory of the Geologisch-Paläontologisches Institut in Münster.

The high occurrence of sulfides, sulfates, and sulfosalts of the Pirquitas deposit demand the study of sulfur isotopes in order to determine the potential sources of the sulfur in the ore. It is expected to obtain a better estimation of a probable magmatic influence.

Lead and U isotopes and U-Pb dating

In radiogenic geochemistry, Pb is one of the most powerful and useful isotopic tool because of its three parents decay for three isotopes of Pb. For geology, three lead isotopic ratios are used in the Pb-Pb system on a variety of materials in order to provide tracking sources of melts in igneous rocks or sediments: $^{208}Pb/^{204}Pb$, $^{207}Pb/^{204}Pb$, and $^{206}Pb/^{204}Pb$. Also, coupled with the two U decay systems (^{235}U and ^{238}U), it makes Pb isotopes particularly useful in geochronology using the $^{238}U/^{206}Pb$, $^{235}U/^{207}Pb$, and $^{207}Pb/^{206}Pb$ ratios method (White, 2015).

Lead isotopic ratios and U-Pb dating technics were both performed in the geochemistry laboratory of the GFZ in Potsdam. Lead isotopes were analyzed to complete the S isotopes tracking methods by giving complementary information about the metal sources. It helps also to discuss wherein mantel and crustal material have influenced the composition of Pirquitas ores.

Dating by using the U-Pb method in the idea of more precisely estimate an age for the deposit and potentially correlate this age with volcanic and subvolcanic centers in the close area. A wolframite crystal, which was sampled in the mine, was chosen as a dating material following the technic described in Romer et al. (2005) as no other minerals usually used for U-Pb dating are present in the deposit.

References

Allmendinger, R.W., Jordan, T.E., Kay, S.M., Isacks, B. L.,1997. The evolution of the Altiplano-Puna Plateau of the Central Andes. Annu. Rev. Earth. Planet. Sci. 25, 139-174.

Allmendinger, R.W., Strecker, M., Eremchuk, J.E., & Francis, P., 1989. Neotectonic deformation of the southern Puna Plateau, northwestern Argentina. J. S. Am. Earth. Sci. 2, 111–130.

Anderson, D.L., 2007. New theory of the Earth. Cambridge University Press, New York. 384p.

Arce-Burgoa, O., 2009. Metalliferous ore deposits of Bolivia. 2nd edition, La Paz, Bolivia, SPC Impresores S.A, pp. 233.

Arce-Burgoa, O., 1990. Fundamental study on processing of ore from the Huanuni mine, Bolivia. Tesis Doctoral Inedita, Sendai, Japan, Tohoku University, 168 pp.

Bahlburg, H., Hervé, F., 1997. Geodynamic evolution and tectonostratigraphic terranes of northwestern Argentina and northern Chile. Geol. Soc. Am. Bull. 109, 869–884.

Board, W.S., 2011. Technical Report on the Pirquitas mine, Jujuy, Argentina, pp. 52-78.

Bodnar, R.J., 2003. Introduction to fluid inclusions. *In* Fluid inclusion: Analysis and interpretation. Lain Samson, Alan Anderson and Dan Marshall (eds). 374p.

Caffe, P.J., 2008. The Granada ignimbrite: A compound pyroclastic unit and its relationship with Upper Miocene caldera volcanism in the northern Puna. J. South. Am. Earth. Sci. 25, 464-484.

Caffe, P.J., Trumbull, R.B., Coira, B.L., Romer, R.L., 2002. Petrogenesis of Early Neogene magmatism in the northern Puna; implications for magma genesis and crustal processes in the Central Andean Plateau. J. Petrol. 43, 907-942.

Cladouhos, T.T., Allmendinger, R.W., Coira, B., Farrar, E., 1994. Late Cenozoic deformation in the Central Andes: fault kinematics from the northern Puna, northwestern Argentina and southwestern Bolivia. J. South. Am. Earth. Sci. 7, 209-228.

Coira, B., Caffe, P. J., Ramirez, A., Chayle, W., Diaz, A., Rosas, S., 2004. Hoja Geológica 2366-I/ 2166-III Mina Pirquitas. Provincia de Jujuy. Programa Nacional de Cartas Geológicas de la República Argentina 1:250 000(269).

De Haller, A., Fontboté, L.2009 . The Raul-Condestable iron oxide coppergold deposit, central coast of Peru: ore and related hydrothermal alteration, sulfur isotopes, and thermodynamic constraints. Economic Geology. 104: 365-384.

De Silva, S.L., 1989. Altiplano-Puna volcanic complex of the central Andes. Geology 17, 1102-1106.

Farquhar J, Bao H, Thiemens M (2000a) Atmospheric influence of Earths earliest sulfur cycle. Science 289: 756-758

Farquhar J, Savarino J, Jackson TL, Thiemens MH (2000b) Evidence of atmospheric sulphur in the martian regolith from sulphur isotopes in meteorites. Nature 404:50-52

Farquhar J, Wing B (2003) Multiple sulfur isotopes and the evolution of the atmosphere. Earth Planet Sci Lett 213:1-13

Fontboté, L. 2018. Ore deposits of the central andes. Elements. 16: 257-261.

Grant, J.N., Halls, C., Salinas, W.A., Snelling, N.J., 1979. K-Ar ages of igneous rocks and mineralization in part of the Bolivian Tin Belt. Econ. Geol. 74, 838-851.

Gorustovich, S.A., Monaldi, C.R., Salfity, J.A., 2011. Geology and metal ore deposits in Argentine Puna. Cenozoic Geology of the Central Andes of Argentina, SCS Publisher, pp. 169-187.

Kay, S.M., Coira, B.L., Caffe, P.J., Chen, C.H., 2010. Regional chemical diversity, crustal and mantle sources and evolution of central Andean Puna plateau ignimbrites. J. Volc. Geoth. Res. 198, 81-111.

Lucassen, F., Becchio, R., Wilke, H.G., Thirlwall, M.F., Viramonte, J., 2000. Proterozoic–Paleozoic development of the basement of the central Andes (18°S–26°S) – a mobile belt of the South American craton. J. S. Am. Earth. Sci. 13, 697–715.

Malvicini, L., 1978. Las vestas de estano y plata de Minas Pirquitas (Pircas) PCIA. de Jujuy, Rebublica Argentina. Revista de la Asociación Argentina de Mineralogía, Petrología y Sedimentología 9(1-2), 1-25.

Mamyrin, B.A., Tolstikhin, IN., Anufriyev, G.S., Kamenskiy, I.L. 1969. Isotopic analysis of terrestrial helium on a magnetic resonance mass spectrometer. Geokhimiya 1969, 595-602.

Marrett, R.A., Allmendinger, R.W., Alonso, R.N., Drake, R.E., 1994. Late Cenozoic tectonic evolution of the Puna Plateau and adjacent foreland, northwestern Argentine Andes. J. South. Am. Earth. Sci. 7, 179-208.

Mon, R., Salfity, J.A., 1995. Tectonic evolution of the Andes of northern Argentina. In: Tankard, A.J., Suarez, R., Welsink, H.J. (Eds.), Petroleum basins of South America. Am. Assoc. Petr. Geol. Mem. 62, 269-283.

Paar, W.H., Moëlo, Y., Mozgova, N.N., Organova, N.I., Stanley, C.J., Roberts, A.C., Culetto, F.J., Effenberger, H.S., Topa, D., Putz, H., Sureda, R.J., de Brodtkorb, M.K. 2008. Coiraite, $(Pb,Sn^{2+})_{12.5}As_3Fe^{2+}Sn^{4+}{}_5S_{28}$: a franckeite-type new mineral species from Jujuy Province, NW Argentina. Mineralogical Magazine. 72: 1083-1101

Paar, W.H., de Brodtkorb, M.K., Sureda, R.J., Topa, D. 2001. Mineralogía y quimismo de sulfuros y sulfosales de estaño y plomo en las vetas de Mina Pirquitas, Jujuy, Argentina (22°41'S66°28'W). Revista geológica de Chile. 28(2): 259-268.

Para, W.H., Miletich, R., Topa, D., Criddle, A.J., Brodtkorb, M.K., Amthaur, G., Tippelt, G. 2000. Suredaite, PbSnS3, a new mineral species, from the Pirquitas Ag-Sn deposit, NW-Argentina: mineralogy and crystal structure. Am. Mineral. 85: 1066-1075.

Paar, W.H., Brodtkorb, M.K., Topa, D., Sureda, R.J., 1996. Caracterización mineralógica y química de algunas especies metalíferas del Yacimiento Pirquitas, Provinca de Jujuy, República Argentina: Parte 1. XIII Congr. Geol. Argent y III Congreso de Exploración de Hidrocarburos(III), pp. 141-158.

Petersen, U., 1977. Metallogenic Provinces in South America. Geol. Rundschau B.1, 174-183.

Romer, R.L., Heinrich, W., Schröder-Smeibidl, B., Meixner, A., Fischer, C.O., Schulz, C. 2005. Elemental dispersion and stable isotope fractionation during reactive fluidflow and fluid immiscibility in the Bufa del Diente aureole, NE-Mexico: evidence from radiographies and Li, B, Sr, Nd, and Pb isotope systematics. Contributions to Mineralogy and Petrology. 149:400–429

Rundel, P.W., Palma, B. 2000. Preserving the Unique Puna Ecosystems of the Andean Altiplano: A Descriptive Account of Lauca National Park, Chile. Mountain Research and Development. 20, 262-271

Sano, Y., Fischer, T.P. 2013. The analysis and interpretation of noble gases in modern hydrothermal systems. Burnard P. (eds). The Noble Gas as geochemical tracers. pp 249-317.

Seal RR.2006. Sulfur isotope geochemistry of sulfide minerals. Rev. Mineral. Geochem. 61:633–667

Sillitoe, R.H. 2010. Porphyry Copper Systems. Economic Geology ; 105 (1): 3–41

Sillitoe, R.H., Perelló, J. 2005. Andean copper province: tectonomagmatic settings, deposit types, metallogeny, exploration, and discovery. In: Hedenquist JW, Thompson JFH, Goldfarb RJ, Richards JR (eds) Economic Geology 100th Anniversary Volume. Society of Economic Geologists Inc. 845-890.

Sillitoe, R.H., Hedenquist, J.W., 2003. Linkages between volcanotectonic settings, ore-fluid compositions, and epithermal precious-metal deposits. Society of .Econ. Geol. Special Publication. 10, 315-343.

Sillitoe, R.H., Halls, C., Grant, J.N., 1975. Porphyry tin deposits in Bolivia. Econ. Geol. 70, 913-927.

Silver Standard Ressources Inc. Puna Operation; Brownfields Development for Mine Life Extension. http://www.ssrmining.com/operations/production/puna/ (accessed 07 December 2018).

Slater, E.T., 2016. The Cortaderas zone, Pirquitas Mine, NW Argentina: An example of Miocene epithermal Ag-Zn-Pb-Sn mineralization in the Andean Tin Belt. MSc thesis Laurentian University Sudbury, Ontario, Canada, 113 p.

Turneaure, F.S., 1971. The Bolivian Tin-Silver Province. Econ. Geol. 66, 215-225.

Voldman, G.G., Albanesi, G.L., Ortega, G., Monaldi, C.R., Zeballo, F.J., Giuliano, M.E., 2012. Biostratigraphy of the Santa Rosita Formation (Furongian-Tremadocian) in its type area, Eastern Cordillera, NW Argentina. Geophysical Research Abstracts p 14.

White, W.M, 2014. Isotope Geochemistry. John Wiley & Sons (eds). 496 p

2. Fluid inclusion studies in ore minerals from the polymetallic epithermal Sn-Ag Pirquitas deposit, Jujuy Province, NW Argentina

2.1. Abstract.

The Pirquitas epithermal Sn-Ag deposit is located near the Bolivian border in the Argentinian Puna Plateau and used to be historically a great source of Sn and Ag in the country. The Pirquitas deposit is considered to be an analogue to the Bolivian Sn-Ag epithermal deposits but the origin of the ore-bearing fluids is still controversial. Fluid inclusions studies in quartz, Sn-Ag minerals and sphalerite from e.g. the Oploca vein system in transmitted and near infrared light show variable salinity from 10.6 to 0.8 wt.% NaCl equiv. and homogenous temperature from 274° to 190° C probably due to mixing of saline metal-rich fluids with meteoric water. Fluid inclusion evidence for flashing and boiling suggested in previous studies from the Cortaderas breccia body was not observed in samples from the Oploca vein system. All results obtained are in agreement with data from Bolivian epithermal Ag deposits (e.g. Potosi, San Rafael).

Keywords:

Pirquitas, Bolivian tin belt, epithermal polymetallic, massive sulfide, vein type, fluid inclusion, tin, silver.

Published as:

Desanois L, Lüders V, Trumbull RB (2017) Fluid inclusion studies in ore minerals from the polymetallic epithermal Sn-Ag Pirquitas deposit, Jujuy Province, NW Argentina. 14th SGA Biennal Meeting (Quebec, Canada). 1:343-346.

2.2. Introduction

Pirquitas is a Bolivian-type epithermal Sn-Ag deposit located in Jujuy Province of NW Argentina (Rosas et al., 2013). The Pirquitas mine is one of the most important economic Sn-Ag mines in Argentina, with both primary Sn-Ag sulfide mineralization as well as alluvial tin and gold accumulations (Paar et al., 2000). Between 1933 and 1989 Pirquitas was the largest producer of tin

and silver in Argentina (Board, 2011). Production in 2015 was 309 t of silver and 2,134 t of zinc (www.silverstandard.com).

The source of ore fluids in the Pirquitas deposit is still controversial. In this contribution, we report results of fluid inclusion studies in quartz, sphalerite and silver ore minerals from the Oploca vein which is the most southern vein-type mineralization in the Pirquitas deposit (Fig. 3). The results are compared with fluid inclusion data from breccia-hosted ores from the Cortaderas breccia, 500 m north of the open pit (Slater, 2016).

2.3. Regional setting

Pirquitas mine is located on the Altiplano-Puna Plateau, near the Bolivian border, at an elevation of about 4200 m. Vein type mineralization at Pirquitas is hosted in metamorphosed Ordovician marine sedimentary rocks covered by Tertiary continental sedimentary units and salars (Gorustovich et al., 2011). The main tectonic structures are NNE striking faults, and faults sub-parallel to the Neogene N-S to NNE-SSW fold axes with compressive or transgressive nature (Slater, 2016).

Although the mineralization at Pirquitas is considered as an analogue to the Bolivian Sn-Ag epithermal deposits, there is no direct association with magmatism. The closest intrusion is the granodioritic Cerro Galàn some 12 km to the east of the Pirquitas mine (Soler, et al., 2008). The Bolivian epithermal deposit model and geophysical results suggest a subvolcanic body or breccia pipe between 400 and 600 m beneath the Pirquitas open pit, however, a 800 m deep borehole did not confirm its existence so far (Soler et al., 2008).

2.3.1.Local geology

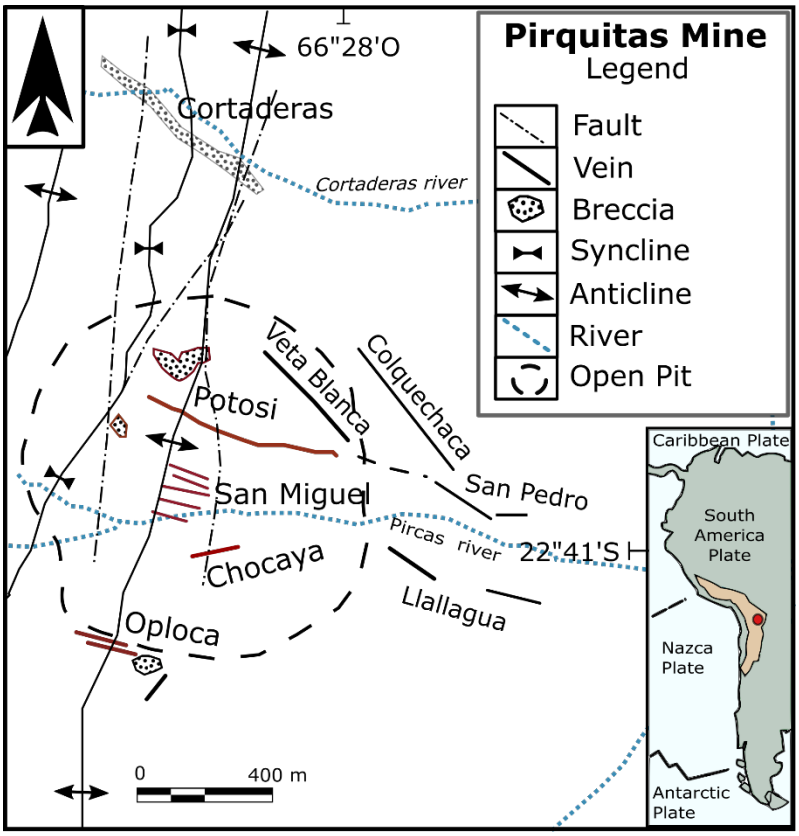

Figure 2. . Location map of the Pirquitas mine also showing major structures and ore bodies. Modified after Rosas et al. (2013) and Slater (2016).

The Ordovician metasediment-hosted ore at Pirquitas occurs in three types, namely (1) polymetallic veins, (2) disseminated mineralization and (3) hydrothermal breccia ore bodies. The vein systems are exposed in an area of the current open pit. The Potosi, San Miguel, Chocaya, Oploca, San Pedro, Llallagua, Chicharron and Colquiri veins are deep-stipping (N to S) polymetallic veins striking close to 105°. Disseminated mineralization occurs north of Potosi, San Miguel area, and comprises the Veta Blanca and Colquechaca veins with a NW-SE trend near 305°. (Rosas et al., 2013; Salter, 2016). Veins and breccia-hosted mineralization consists of iron and zinc sulfides with accessory cassiterite and a large variety of Ag-Sn-Zn (-Pb-Sb-As-Cu-Bi) sulfides and sulfosalts. All mineralized veins are subvertical with an average thickness of 30 to 50 cm (Malvicini, 1978; Paar, et al., 1996). Disseminated ores occur in small veins, stockworks and disseminate minerals in the host rock, especially common in the San Miguel area. Hydrothermal breccia bodies, characterised by sulphide and quartz mineralization occur in the Oploca and Potosi vein systems. A subject of recent exploration

(Slater, 2016) is the Ag-Zn-rich breccia system in the Cortaderas zone, north of the current open pit (Fig. 2).

2.3.2. Paragenesis and mineralogy

In the southern veins system, Oploca, San Miguel and Chacoya, four ore assemblages were distinguished by Paar et al. (1996): (1) sphalerite, pyrargyrite-miargyrite, freibergite, wolframite and cassiterite; (2) stannite and other tin sulphides; (3) Pb-Ag sulfoantimony minerals; and (4) bismuth minerals such including frankeite and andorite.

Malvicini (1978) described two stage of ore deposition. The first stage is dominated by early pyrrhotite partly replaced by pyrite with accessory cassiterite and arsenopyrite; the second stage comprises colloform bands of sphalerite ("schalenblende") with stannite and other Sn-sulfides, minor galena and various Sn-Ag sulfosalts replacing pyrrhotite, cassiterite, sphalerite and galena. Most of the Pb-Sb-Ag minerals were deposited during this second stage of ore formation. (Fig. 3)

2.4. Results

2.4.1. Fluid inclusion petrography

The samples studied here mostly come from the veins of the Oploca and San Miguel systems. Fluid inclusions occur in quartz as well as in ore minerals hocartite-pirquitasite, pyrargyrite, sphalerite and cassiterite. Fluid inclusions in quartz, pyrargyrite and bright sphalerite were studied in transmitted light whereas fluid inclusions hosted in dark sphalerite, miargyrite and hocartite-pirquitasite were studied using an infrared light microscope.

Fluid inclusions hosted in different ore minerals are always aqueous two-phase but show variable L-V ratios (Fig. 4 and 5).

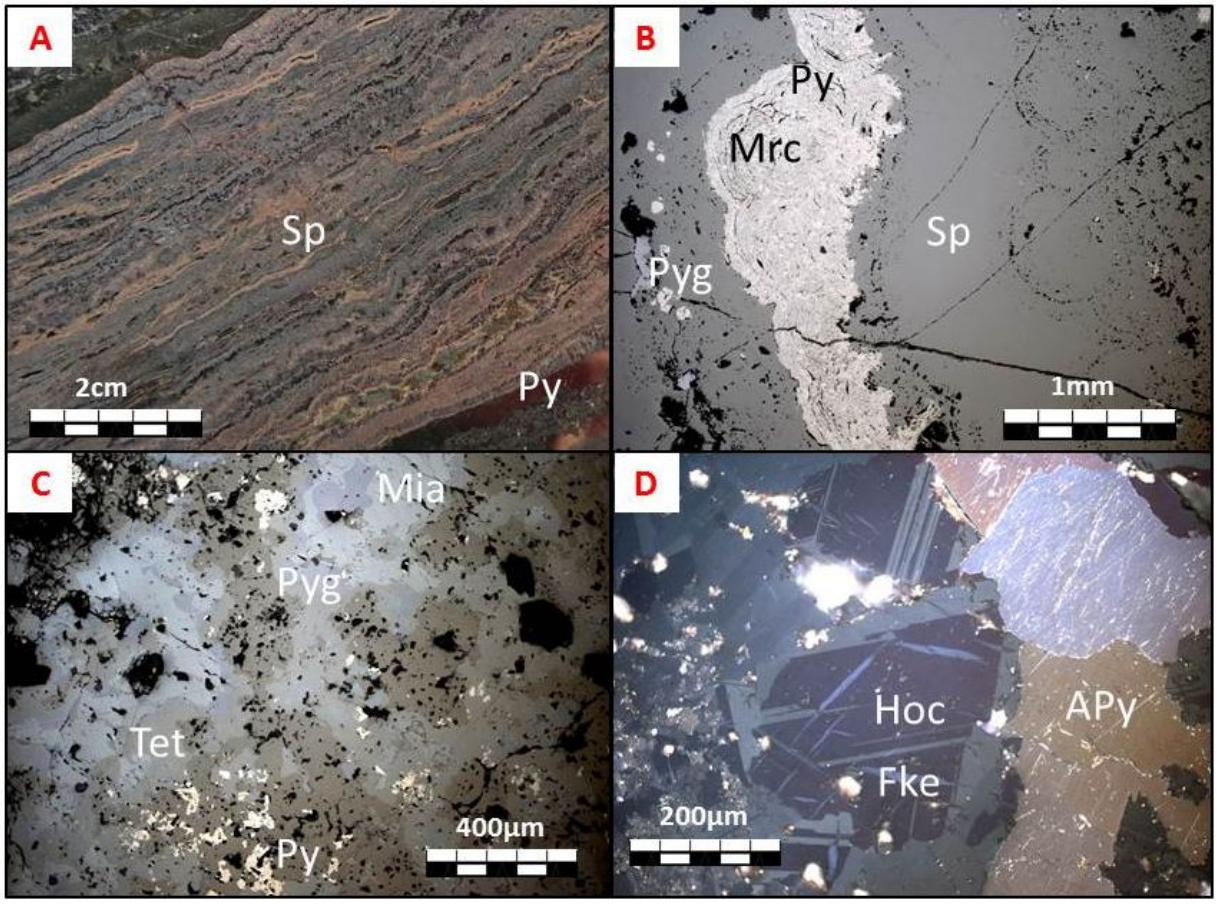

Figure 3. Oploca polymetallic mineralization: A) Dril lcore with banded sphalerite (Sp) and pyrite (Py). B) Reflected plane light photograph of colloform textures of sphalerite (Sp) , pyrargyrite (Pyr), marcasite (Mc). C) Pyrargyrite (Pyg) and miargirite (Mia) crystals surrounded by tetrahedrite (Tet). D) Reflected polarized light photograph of arsenopyrite (APy) associated with hocartite (Hoc) and Ferrokësterite (Fke).

Quartz samples from various occurrences within the Pirquitas mine are mostly recrystallized and a clear classification of primary vs. secondary inclusions is difficult or even impossible due to the high frequency of fluid inclusions in most samples. Furthermore, the Ordovician host rocks contain older metamorphic quartz segregations and veins that are not always easy to distinguish from the Pirquitas veins. To avoid potential ambiguity, our emphasis here is on fluid inclusions hosted in the ore minerals.

Primary and/or pseudosecondary inclusions in sphalerite show variable shapes and mostly occur along growth zones. Secondary inclusions are orientated along healed microfractures. Primary inclusions in hocartite-pirquitasite are clearly defined by regular prismatic or near spherical shapes. They occur isolated or are arranged in fluid inclusion assemblages (FIAs) within individual crystal grains. Pyrargyrite contains primary and secondary inclusions that are clearly distinguishable. The shape of primary inclusions is rectangular prismatic and spherical and they are occur as isolated inclusions or in small FIAs. Secondary inclusions have more irregular or spherical shapes and are arranged along healed microfractures. Cassiterite only rarely hosts fluid inclusions and, when present all inclusions are very small and show rectangular prismatic shape. The L-V ratios of cassiterite-hosted fluid inclusions are considerably lower compared to those hosted in quartz, sphalerite and Ag-sulfosalts (Figure 4 and 5).

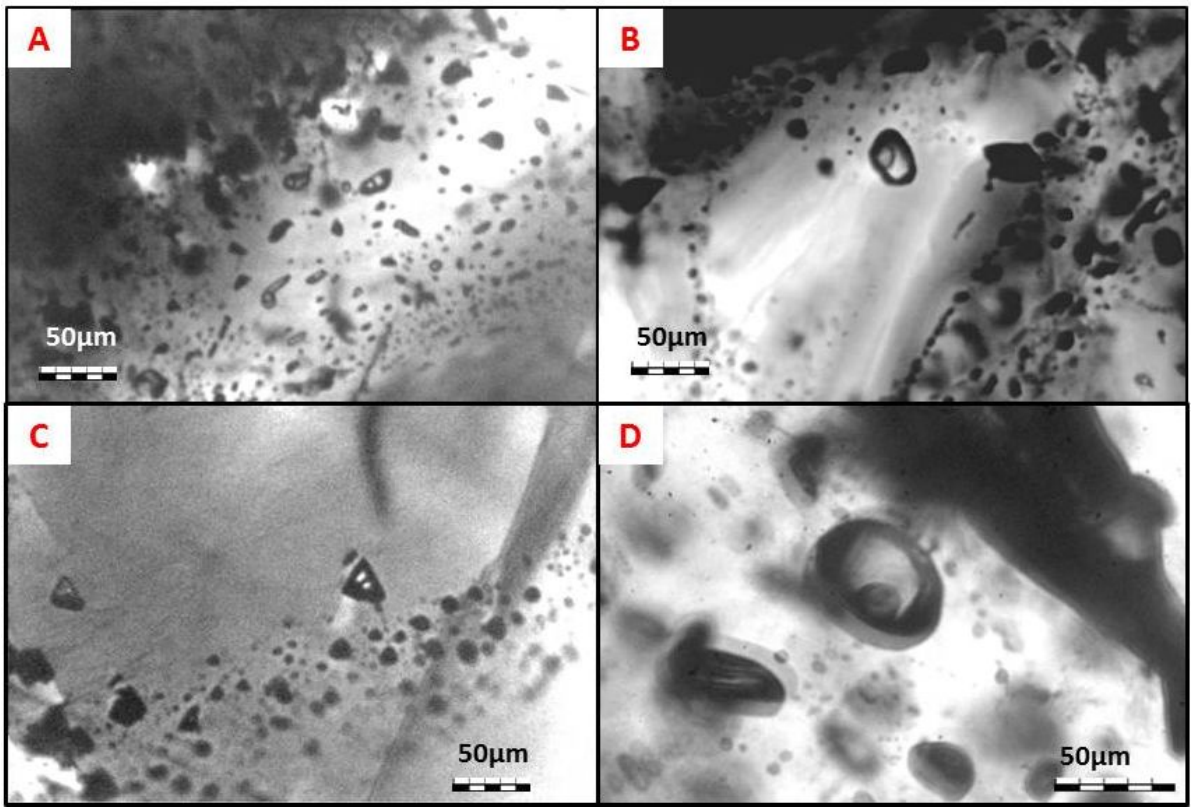

Figure 4. IR photomicrographs of fluid inclusions hosted A), B) and C) hocartite-pirquitasite, D) in Pyrargyite.

2.4.2.Microthermometry

Fluid inclusions hosted in quartz from the ore stages yield salinity between 0 to 9.2 wt. % NaCl equiv. and a broad range of homogenization temperatures in the range between 175° and 300° C.

Fluid inclusions in colloform sphalerite (dark and light), in banded wurzite, hocartite-pirquitasite, and pyrargyrite show variations in salinity and homogenization temperatures from 10.6 to 0.8 wt. % NaCl and 274° to 190° C, respectivly, (Fig. 6). In general, fluid inclusions hosted in hocartite and pyrargyrite yield higher salinity and homogenization temperatures than those in sphalerite.

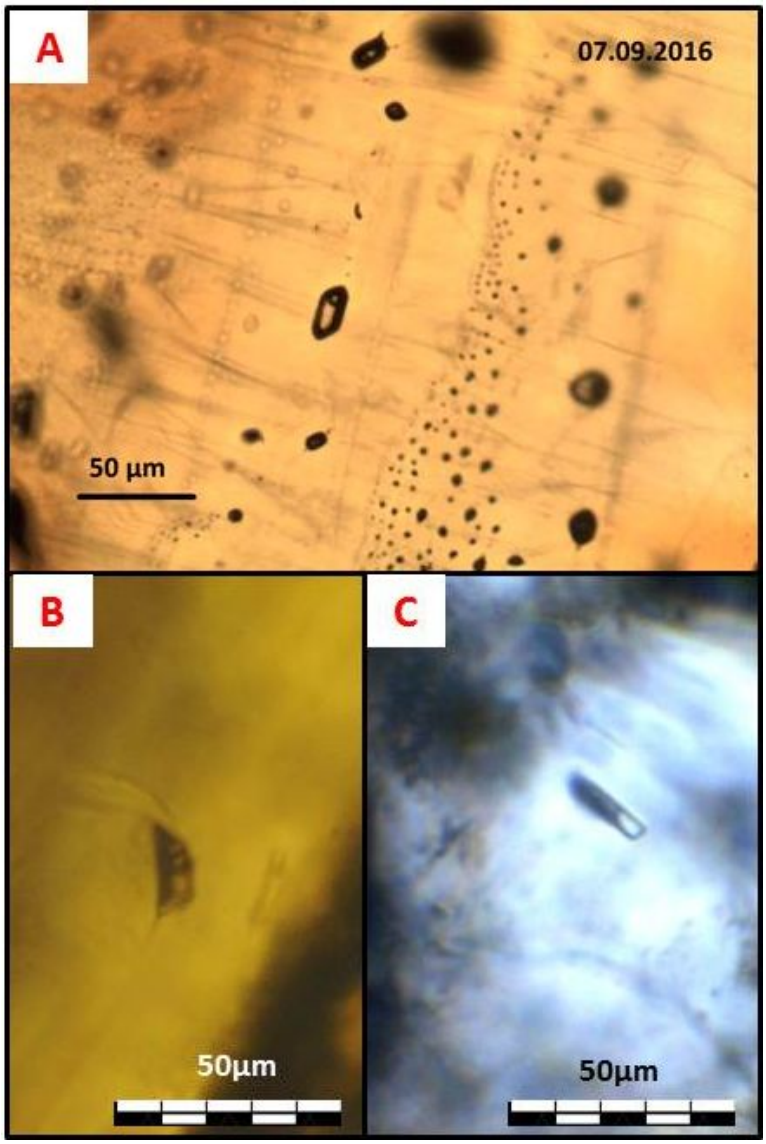

Figure 5. Photomicrographs of fluid inclusions in A) sphalerite, B) and C) cassiterite.

2.5. Discussion

The observed general trend of decreasing salinity and homogenization-temperatures in fluid inclusions hosted in early and late ore minerals from the Oploca vein system (Fig. 6) suggests fluid mixing between a higher temperature and higher salinity fluid with a cooler, low salinity fluid. The origin of the two fluids is still unknown but mixing of a metal-rich (magmatic?) fluid and meteoric water appears likely. The rare and small cassiterite-hosted fluid inclusions showing low L-V ratios can be due to a higher trapping temperature. However, vapor-rich inclusions may also be indicative for boiling of the ore-forming fluid (Bodnar et al., 1985).

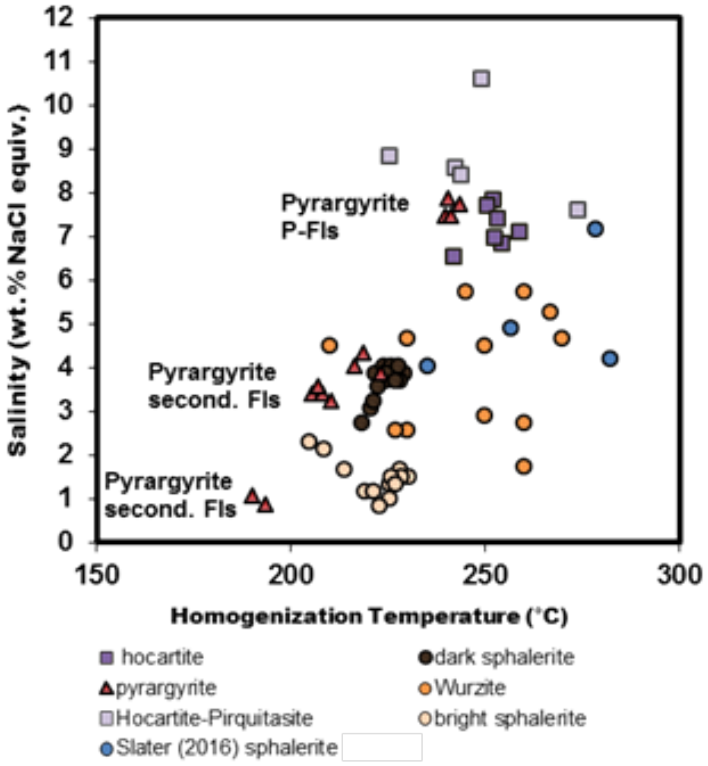

Figure 6.Results of fluid inclusion microthermometry in ore minerals from Oploca and San Miguel vein compared with Slater (2016) data from sphalerite in the Cortaderas breccia zone.

Slater (2016) interpreted fluid inclusion data from the Cortaderas breccia to indicate flashing, where liquid is instantaneously converted to steam, and simple boiling due to rock dilation and depressurization (Brown, 1986). The colloform structure of sphalerite was also attributed to such processes. According Slater (2016), the Ag-Sn sulfosalts formed in the last stage of mineralization when the system was sealed and temperature gradients were higher. However, no clear evidence for boiling was observed in the Oploca samples.

The fluid inclusions results are in agreement with studies of fluids from typical Sn-Ag epithermal deposits in Bolivia. Fluid inclusions in sphalerite from the Potosi district in Bolivia show a range of homogenization temperature and salinity of 174° - 311° C and 6.6 - 9.5 wt. % NaCl equiv.,

respectively. Similarly, the San Rafael deposit near the Argentine border yielded Th between 157° and 317° C and 1.2 - 16 wt% NaCl equiv. (Sugaki & Kitakaze, 1988).

References

Board, W.S., Kennedy, R.B., and Yeomans, T.J. 2011. Technical Report on the Pirquitasmine, Jujuy, Argentina. Silver Standard Ressources Inc. 220 pp.

Bodnar. R.J., Reynolds T.J. and Kuehn, C.A. 1985. Fluid inclusion systematics in epithermal systems. Berger BR, Bethke PM (eds) Geology and geochemistry of epithermal systems. Reviews in Economic Geology 2:73–97

Brown, K.L. (1986). Gold deposition from geothermal discharges in New Zealand. Economic Geology, 81(4):979–983

Gorustovich, S.A., Monaldi, C.R. and Salfity, JA. 2011. Geology and metal ore deposits in Argentine Puna. Cenozoic Geology of the Central Andes of Argentina, SCS Publisher, Salta, Argentina:169-187.

Malvicini, L. 1978. Las vestas de estano y plata de Minas Pirquitas (Pircas) PCIA. de Jujuy, Rebublica Argentina. Revisita de la Asociación Argentina de Mineralogía, Petrología y Sedimentología. 9 (1-2):1-25.

Para. W.H., De Brodtkorb, M., Topa, D., and Sureda, R.J. 1996. Caracterización Mineralógica y Química de Algunas Especies Metalíferas del Yacimiento Pirquitas, Porvinca de Jujuy, República Argentina: Parte 1. XIII Congreso Geológico Argentino y III Congreso de Exploración de Hidrocarburos. 3:141-158.

Para, W.H., Miletich, R., Topa, D., Criddle, A.J., De Brodtkorb, M.K., Amthauer, G., Tippelt, G. 2000. Suredaite, PbSnS3, a new mineral species, from the Pirquitas Ag-Sn deposit, NW-Argentina: Mineralogy and Crystal Structure. American Mineralogist. 85:1066-1075.

Rosas, L.V., Avilia, J.C. 2013. Desarrollo minero de Pirquitas, provincia de Jujuy. Temas de Correlación Geológica III, Serie Correlación Geológica. 29(2):51-62.

Silver Standard [online]:http://www.silverstandard.com/ consulted the 25/02/2017

Slater, E.T. 2016. The Cortaderas zone, Pirquitas Mine, NW Argentina: An exemple of Miocene Epithermal Ag-Zn-Pb-Sn Mineralization in the Andean Tin Belt. M.Sc. thesis, Laurentian University. Sudbury, Ontario :113.

Soler, M.M., Caffe, P.J., Coira, B.L., Onoe, A.T., Mahlburg Kay, S. 2008. Principales aspectos de la geologia, recursos y minado de Mina Pirquitas, Jujuy. In: IIG XVII Congreso Geológico Argentino. Jujuy, Argentina :343-349.

Sugaki, A. Kitakaze, A. 1988. Tin-bearing Minerals from Bolivian Polymetallic Deposits and Their Mineralization Stages. Mining Geology. 38(5):419-435.

3. Formation of epithermal Sn-Ag-(Zn) vein-type mineralization at the Pirquitas deposit, NW Argentina: Fluid inclusion and noble gas isotopic constraints

3.1. Abstract

The Pirquitas Sn-Ag-(Zn) deposit in northwestern Argentina is thought to be an analogue to the Miocene polymetallic epithermal Sn-Ag deposits of the southern Bolivian Tin Belt, but little is known in detail about the origin and evolution of ore-forming fluids at Pirquitas. This paper reports on a microthermometric study of fluid inclusions in quartz, sphalerite, Ag-Sn sulfides, and Ag-rich sulfosalts using transmitted near infrared and visible light, combined with noble gas isotope analyses of fluids released from mineral separates. The study focused on the vein-hosted mineralization, which formed during two major mineralization events, whereby the first event I comprises two stages (I-1 and I-2). All studied minerals exclusively contain aqueous two-phase inclusions, indicating that the ore-forming fluids did not undergo two-phase phase separation (boiling). Salinity of fluid inclusions in I-1 quartz that precipitated along with pyrite and pyrrhotite ranges between 0 and 7.5 wt% NaCl equiv. and homogenization temperatures (Th) are between 233 and 370 °C. Stage I-2 is characterized by abundant Sn-Ag-Pb-Zn-sulfides and a variety of Ag-rich sulfosalts. Fluid inclusions in stage I-2 Ag-Sn sulfides have salinities up to 10.6 wt% NaCl equiv. and Th between 213 and 274 °C. The deposition of stage I-2 ore is likely related to a new pulse of saline magmatic fluids to the hydrothermal system. The mineralization event II deposited the richest Ag ores at Pirquitas. Colloform sphalerite and pyrargyrite deposited during event II contain two-phase aqueous fluid inclusions with homogenization temperatures between 190 and 252 °C and salinities between 0.9 and 4.3 wt% NaCl equiv. Noble gas concentrations and isotopic compositions of ore-hosted fluid inclusions were determined from crushing hand-picked ore minerals from both mineralization events. With one exception, all samples yielded 3He/4He ratios between 1.9 and 4.1 Ra, which is within the range of published data from the volcanic arc and somewhat higher than typical values of meteoric water-derived hot-springs in the region. This demonstrates a significant contribution of magmatic fluids to the Pirquitas mineralization although no intrusive rocks are exposed in the mine region. Taking the noble gas evidence for a

magmatic fluid source, we interpret the trends of decreasing Th and salinity values in fluid inclusions from events I and II to represent waning of the magmatic hydrothermal system and/or increased admixing of meteoric water to the magmatic fluids.

Keywords:

Bolivian tin belt, Pirquitas, Epithermal Ag-Sn deposits; Fluid inclusions, Noble gas

Published as:

Desanois L, Volker L, Niedermann S, Trumbull RB (2019) Formation of epithermal Sn-Ag-(Zn) vein-type mineralization at the Pirquitas deposit, NW Argentina: fluid inclusion and noble gas isotopic constraints. Chem Geol. 508: 78-91

3.2. Introduction

The Pirquitas deposit is an epithermal polymetallic Sn-Ag-(Zn) deposit situated at an elevation of about 4200m on the Puna Plateau in northwestern Argentina near the Bolivian border (Fig. 7). Based on its location and metals association, Malvicini (1978) considered the Pirquitas deposit to be an analogue of the Ag-Sn deposits in the southern part of the Bolivian tin belt (BTB) which is described in detail by e.g. Turneaure (1960), Petersen (1970), Sillitoe (1976), Lehmann and Schneider (1981), Sugaki and Kitakaze (1988), Dill (1998), Mlynarczyk and William-Jones (2005), Wagner et al. (2009), Arce-Burgoa (2009). The origin of the "Bolivian-type" deposits has been related to subvolcanic intrusions of Miocene and Pliocene age (e.g. Grant et al., 1979; Coira et al., 2004). However, in the case of Pirquitas, the age of mineralization is poorly known and there is no evidence of a direct relationship with igneous intrusions. The closest outcropping intrusive body, the Cerro Galán granodiorite (undated), is about 12 km east of the mine. A borehole extending 800m below the mine floor (Soler et al., 2007) failed to intersect intrusive rocks.

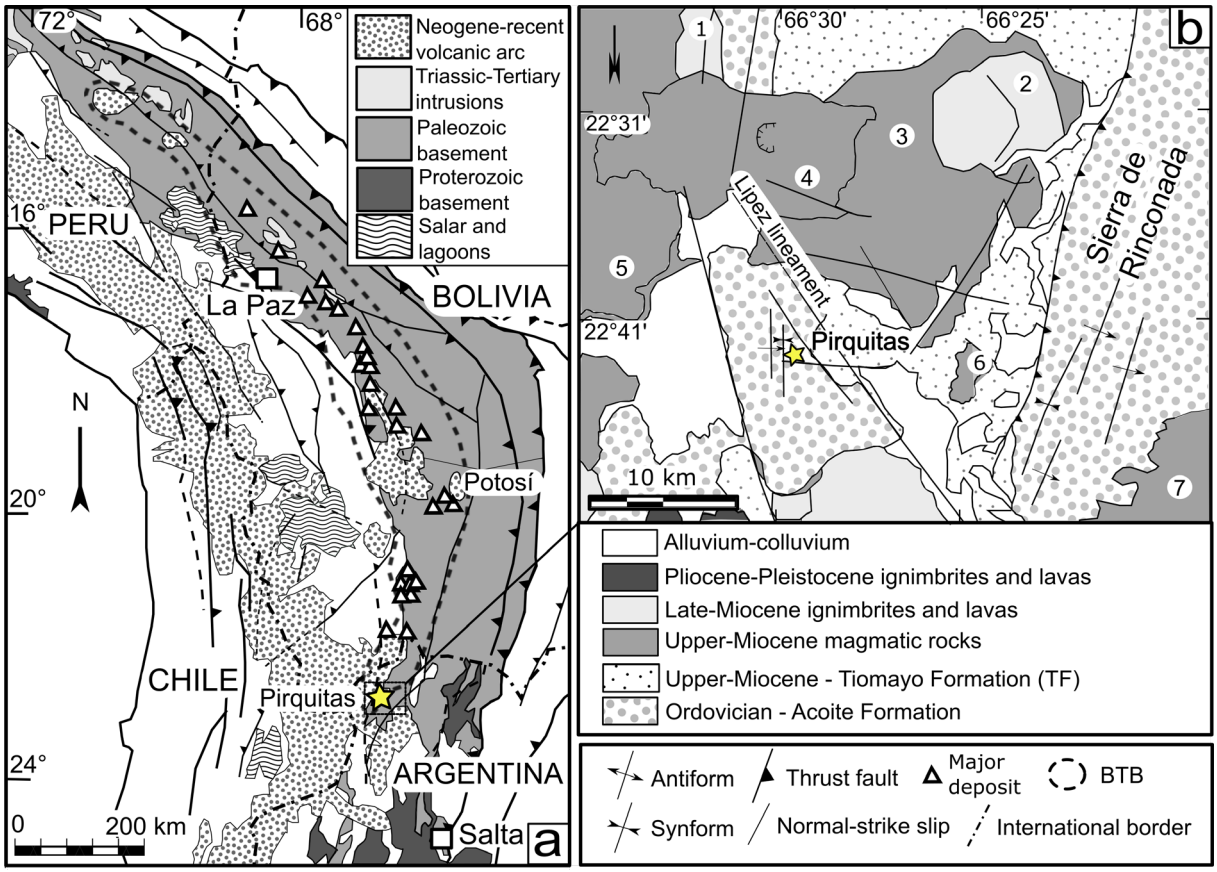

Figure 7.a) Simplified geologic map of the Central Andes showing the location of the Bolivian Tin Belt (BTB) and major polymetallic ore deposits within it, after Jacobshagen et al. (2002), Mlynarczyk and William-Jones (2005), Sugaki and Kitakaze (1988) and Grant et al. (1979). b) Geologic map of the Pirquitas area after Coira et al. (2004) and Soler et al. (2007). 1) Laguinillas ingimbrites 2) Cerro Colorado 3) Granada pyroclastic pumices 4) Cerro Granada 5) Vilama ignimbrites 6) Cerro Galán 7) Coranzuli volcanic complex.

Prospecting for placer gold in the area of Pirquitas led to the discovery of alluvial tin placers which were mined from 1933 until 1949. The source of tin was discovered in the upper valley of the Pircas River and led to small underground mining activities for tin and silver ore. From 1936 until its closure in 2017, the Pirquitas mine became the most important Sn-Ag- (Zn) producer in Argentina (Board, 2011). The deposit was first operated by underground mining and since 2009 by open pit mining. The total silver production was about 295 tons in 2016 (Silver Standard Resources Inc., 2017). The ore mineralization at the Pirquitas deposit occurs in different styles: 1) polymetallic vein-type mineralization which hosts the richest ore grades, 2) Fe-Zn-rich breccia bodies with complex sulfide and sulfosalt associations, and 3) disseminated mineralization in small veinlets and altered host rocks (Ordovician clastic metasediments). The vein-type mineralization is characterized by an abundance of cassiterite and sulfide minerals as well as a large variety of complex Ag, Sn, Sb, As, Fe, Cu, Zn, and Bi sulfosalts (e.g. Malvicini, 1978; Paar et al., 1996), including two for which Pirquitas is the type locality (pirquitasite: Ag2ZnSnS4 and suredaite: PbSnS3: Paar et al., 2000).

The apparent lack of a direct magmatic association and the greater complexity of ore mineralogy at Pirquitas compared with typical Bolivian type deposits (Paar et al., 1996) suggest the need to test the metallogenetic model. This study reports on a microthermometric study of fluid inclusions in quartz and a variety of ore minerals (tin sulfides, sphalerite and Agsulfosalts) from samples of the vein-type

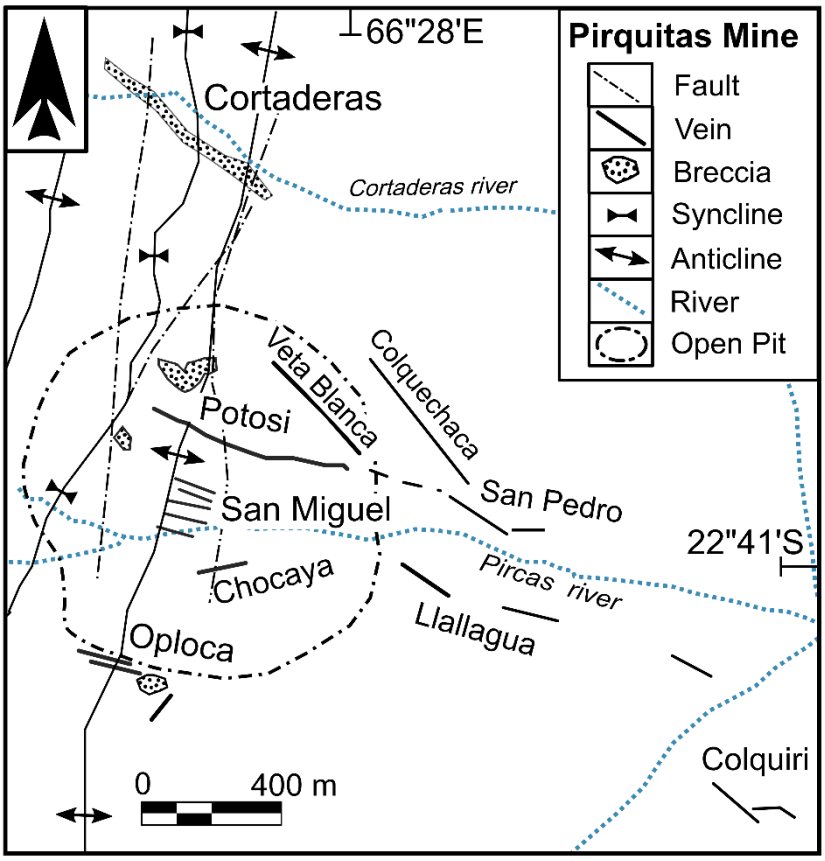

Figure 8. Location map of the Pirquitas mine showing major structures, vein systems and breccia bodies mentioned in the text. Modified after Rosas and Avilia (2013) and Slater (2016).

and breccia ore collected from outcrops in the Pirquitas open pit, former underground galleries and drill cores. The results provide temperature-salinity estimates of the ore-bearing fluids. Furthermore, we conducted noble gas isotope analyses of fluid inclusions hosted in ore minerals (extracted by crushing) in order to decipher the origin of the fluids. This is the first study of fluid inclusions from the vein-type ores in the Pirquitas deposit. We draw comparisons with results of a recent study of fluid inclusions and ore geochemistry in breccia-type ores from the newly-discovered Cortaderas zone (Fig. 8), some 500m north of the Pirquitas open pit (Slater, 2016) and with previous fluid inclusions studies from Ag-Sn-Zn deposits in the southern part of the BTB (e.g. Sugaki et al., 1988).

3.3. Geological setting

3.3.1. Puna plateau

The Pirquitas deposit is located in the northern part of the Puna plateau in the central Andes (Fig. 7). The Puna plateau is dominated by north-northwest trending ranges consisting mainly of folded Ordovician metasediments and metavolcanic units, which are separated by intermountain basins covered by younger sediments and salt flats (Allmendinger et al., 1997; Gorustovich et al., 2011). The geology of the plateau is made up of a strongly deformed metamorphic basement of Neoproterozoic to Cambrian age (Hongn, 1995; Lucassen et al., 2000) overlain by weakly-metamorphosed and folded Ordovician rocks, whose protoliths were shale and sandstone from marine shelf and turbidite facies intercalated with synsedimentary volcanic layers

(Lucassen et al., 2000; Astini, 2003; Coira et al., 2004). The Cenozoic history of the Puna plateau was dominated by compressional deformation and uplift related to the Andean orogeny (Allmendinger et al., 1997; Coutand et al., 2001) and by the widespread magmatic activity of the Andean Central Volcanic Zone. The main volcanic chain of the Andean arc is composed of andesitic-dacitic stratovolcanoes along the western margin of the Puna plateau at the Argentine-Chilean border, but volcanism locally extends far-east of the main arc along a series of NW-SE structural lineaments. The age of magmatism in the northern Puna of relevance to this study ranges mainly from Early Miocene to Pliocene (Caffe et al., 2002). The Mid-Miocene activity (12–16 Ma) in NW Argentina, and particularly in Bolivia, is important because dacitic domes and intrusive stocks of this age show a close association with polymetallic Sn-Ag mineralization similar to Pirquitas (Cunningham et al., 1991; Coira, 1994). Late Miocene to Pliocene volcanism in the Puna was dominated by large-volume felsic ignimbrite eruptions from resurgent calderas of the Altiplano-Puna volcanic complex (de Silva, 1989; Kay et al., 2010). The youngest volcanism in the Puna plateau produced small-volume basaltic to andesitic cones and fissure flows that are associated with extensional or strike-slip faults (Kay et al., 1994; Risse et al., 2013; Maro et al., 2017). The main fault structures in the Puna plateau are Neogene N-S to NNE-SSW striking faults with compressive or transpressive character. Other important structures are regional scale NW-SE striking lineaments, transverse to the strike of the cordillera,

along which Cretaceous, Miocene-Pliocene and Quaternary volcanic centers are aligned. Extensional and transtensional faulting associated with plateau collapse was widespread in the central and southern Puna during the Pliocene, and these faults provided pathways for the emplacement of back-arc mafic lavas (Allmendinger et al., 1989; Marrett et al., 1994). In contrast, no important tectonic activity was registered in the northern part of the Puna since the end of reverse faulting in the late Miocene. Cladouhos et al. (1994) considered the northern Puna as in a near neutral stress state since ca. 9 Ma, but they also report local extensional and strike-slip faulting evidenced by the presence of scarps and faulted colluvium.

3.3.2. Regional geology of the Pirquitas area

The country rocks in the Pirquitas deposit are Ordovician low-grade metasandstones and pelites of the Acoite Formation whose biostratigraphic age falls at the Tremadocian – Floian boundary (ca. 478 Ma; Voldman et al., 2012). These sediments are interpreted to be part of a turbidite system that developed in a back-arc to foreland basin (Voldman et al., 2012). The rocks of the Acoite Formation are folded in the typical deformation style of the Late Ordovician-Lower Devonian Ocloyic Orogeny, with WNW-ESE directed, sub-horizontal compression (Mon and Salfity, 1995; Bahlburg and Hervé, 1997). During the Quechua phase of the Andean orogeny, between 14 and 9 Ma, older normal and strike-slip faults were reactivated as thrust faults (Cladouhos et al., 1994). Some of the reactivated NW-SE fault zones favored magma ascent and hydrothermal fluid migration related to the Miocene volcanic centers (Holdsworth et al., 1997; Riller et al., 2001; Coira et al., 2004; Caffe, 2008). The Acoite Formation is unconformably overlain by the Mid-Miocene Tiomayo Formation, a succession of fluvial lacustrine mudstones, sandstones and conglomerates alternating with ignimbrite deposits which have been dated at 14.9 ± 0.5 Ma in the Pirquitas area (Coira et al., 2004). The structural setting of the Pirquitas deposit (Fig. 7b) is an uplifted block of the Ordovician Acoite Formation. Locally, the mineralization at Pirquitas cuts the base of the Tiomayo Formation and this establishes a maximum age of ca. 15 Ma for the mineralizing event (Slater, 2016). In the region around Pirquitas there are abundant and widespread late Miocene caldera-sourced pyroclastic deposits (1b). The closest of these are dacitic ignimbrites of Cerro Granada of about 9.8–7.8 Ma age (Caffe, 2008) whose eruptive center is about 16 km north of the Pirquitas deposit, ignimbrites of about 8.5 Ma age from Vilama caldera to the west

(Soler et al., 2007), and ignimbrites from the 6.6 Ma Coranzuli complex to the east. The granodiorite of Cerro Galán, some 12 km east of Pirquitas, is assumed to belong to the Coranzuli complex (Caffe, 2008).

3.3.3. Mineralization of the Pirquitas deposit

Essentially two kinds of mineralized structures are distinguished in the Pirquitas deposit: (A) vein systems, locally with peripheral disseminated mineralization; and (B) hydrothermally mineralized breccia bodies. The vein systems of the Pirquitas deposit are named according to their location and orientation (Fig. 8). The Potosí, San Miguel, Chocaya, Oploca, San Pedro, Llallagua, and Colquiri veins are steeplydipping and strike at 105° whereas the Blanca and Colquechaca veins strike near 305°. The veins of the Potosi group have a maximum thickness of 2.5 to 3m whereas the other vein systems have average thicknesses between 0.3 and 0.5 m. disseminated mineralization, with small veinlets and ore minerals dispersed in wall-rocks, occurs around the San Miguel, Veta Blanca and Colquechaca veins (Malvicini, 1978; Paar et al., 1996; Rosas and Avilia, 2013). Fig. 9 shows the Pirquitas open pit with Ordovician strata and exposed galleries in the subvertical San Miguel vein system. Hydrothermal breccia bodies with sulfide and quartz mineralization that were formed concordantly with vein-type mineralization are present in several parts of the Pirquitas area (Fig. 8). The two most important ones are the Potosí breccia in the open pit area, and the Cortaderas breccia located some 500m to the north of the open pit (Slater, 2016). The ore assemblage in breccia bodies comprises pyrite, marcasite, cassiterite, sphalerite, arsenopyrite, galena and various Ag-Sn-As- Sb-Pb-Cu-Bi sulfosalts (Malvicini, 1978; Paar et al., 1996; Slater, 2016), the same as in vein mineralization except that the abundance of galena is higher in the breccia ore. The breccia clasts are dominantly altered metasediments and quartz lenses from the Ordovician country rocks and, locally (Potosí), rare fragments of altered porphyritic dacite of unknown origin, set in a poorly lithified matrix of rock gouge with local sulfide minerals such as banded galena, pyrite, and sphalerite occurring as cements (Slater, 2016).

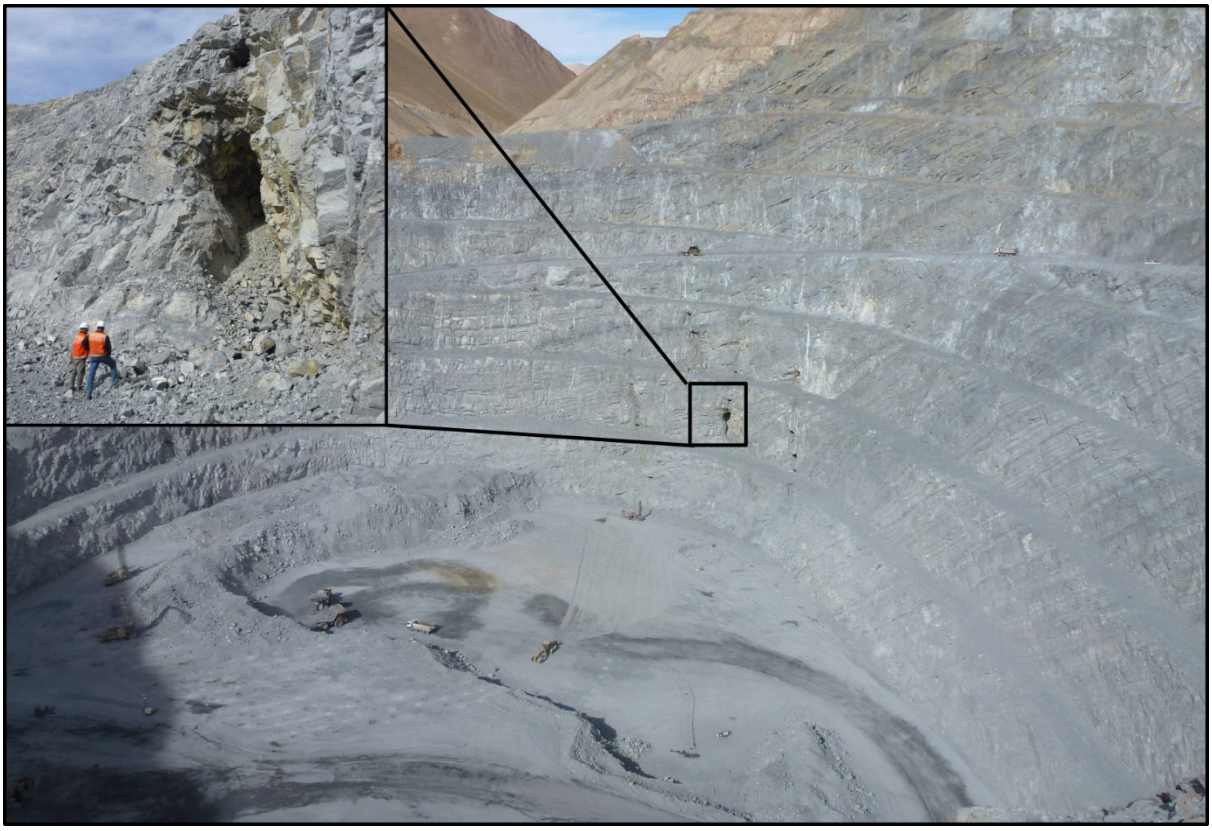

Figure 9. Photograph of the Pirquitas open pit showing folded Ordovician strata and exposed galleries from underground workings of the subvertical San Miguel vein

The focus of this study is on the vein-type mineralization which is the dominant type in the deposit and has been the main source of mined ores. The vein mineralization is multi-stage. Malvicini (1978) identified a pre-ore stage characterized by sericitic wall-rock alteration and two subsequent mineralization events that are here designated I and II, with the first event subdivided into two stages (I-1 and I-2), The mineralization events are illustrated on a paragenetic diagram (Fig. 10), a series of photographs of ore samples (Fig. 11) and a sketch of the vein system evolution (Fig. 12).

During the I-1 stage, fractures and breccia were filled or cemented by quartz, pyrrhotite, pyrite and finally cassiterite. This paragenesis is crosscut by veins of the second stage (I-2) that contain abundant colloform sphalerite, galena, Ag-Sn sulfides, marcasite, Ag-rich tetrahedrite (freibergite), as well as Sb-, Pb- and/or Ag-rich sulfosalts, quartz, kaolinite and alunite. During mineralization event II the earlier assemblages were partly replaced by quartz, cassiterite, chlorite, tin sulfides, abundant Bi-Pb-

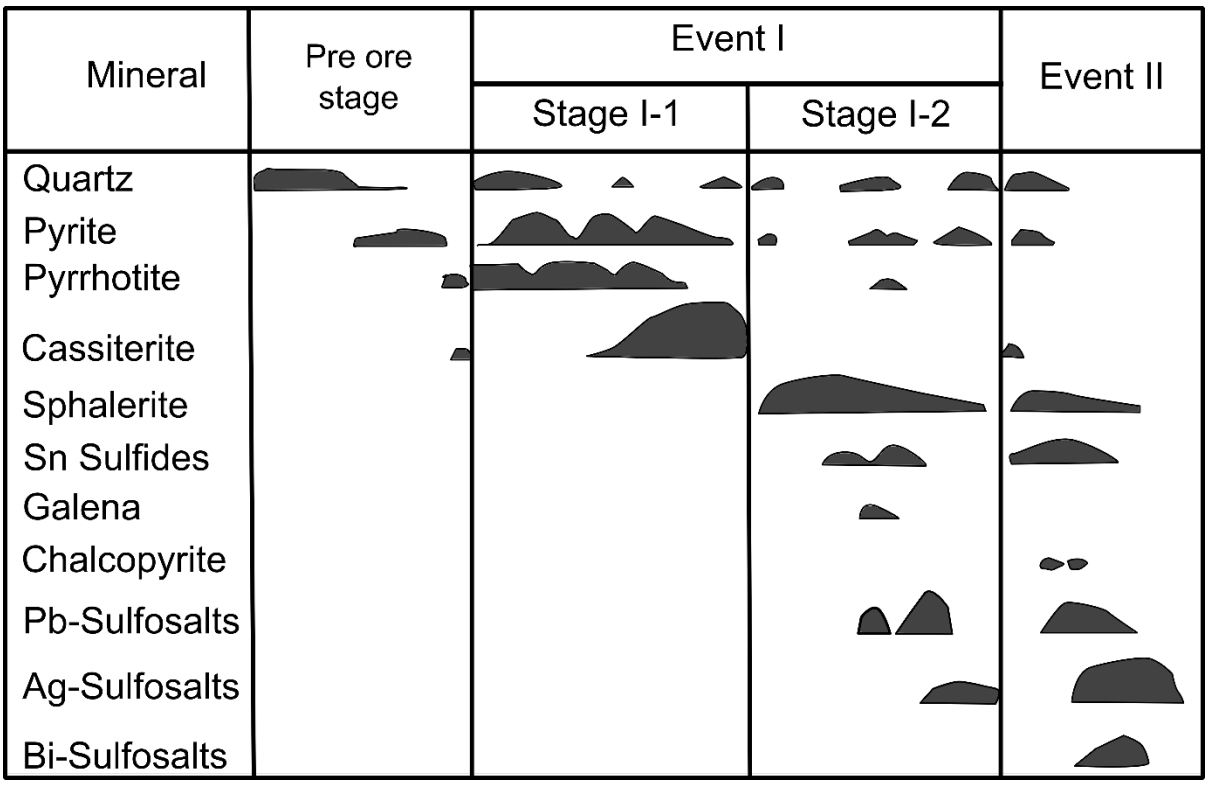

Figure 10. The paragenetic sequence of mineralization at Pirquitas modified from Malvicini (1978).

As-Cu-Sb-Ag sulfosalts, stibnite, alunite, kaolinite and minor barite (Malvicini, 1978). This event produced the high-grade Ag ores, which typically show colloform and/or telescoping textures. The near-surface parts of the mineralized veins and breccias contain quartz and chalcedony and are strongly oxidized, the primary mineralization being replaced by Fe- and Cuoxides, fibrous cassiterite, supergene Ag minerals, native Ag, and a variety of secondary sulfates (Malvicini, 1978).

3.4. Methods

Fluid inclusions in quartz and light-colored sphalerite were measured on doubly-polished mineral plates using a FLUID INC-adapted U.S.G.S. gas-flow heating/freezing system mounted on an Olympus BX50 microscope with a long-distance 40× objective. Fluid inclusions in opaque ore minerals (sphalerite, Ag-rich sulfosalts) were studied using a Linkam FTIR 600 heating-cooling stage coupled to an Olympus BHSM- IR infrared microscope with a 50× IR objective and infrared InGaAs camera that allows observation in the near infrared region in the wavelength range between λ=800 and 1800 nm (Lüders, 2017). The heating-freezing stages were calibrated with Synflinc synthetic inclusions (Sterner and Bodnar, 1984). The precision is±0.1 °C for ice melting temperatures and±1 °C for homogenization temperatures. Salinity in equivalent weight percent

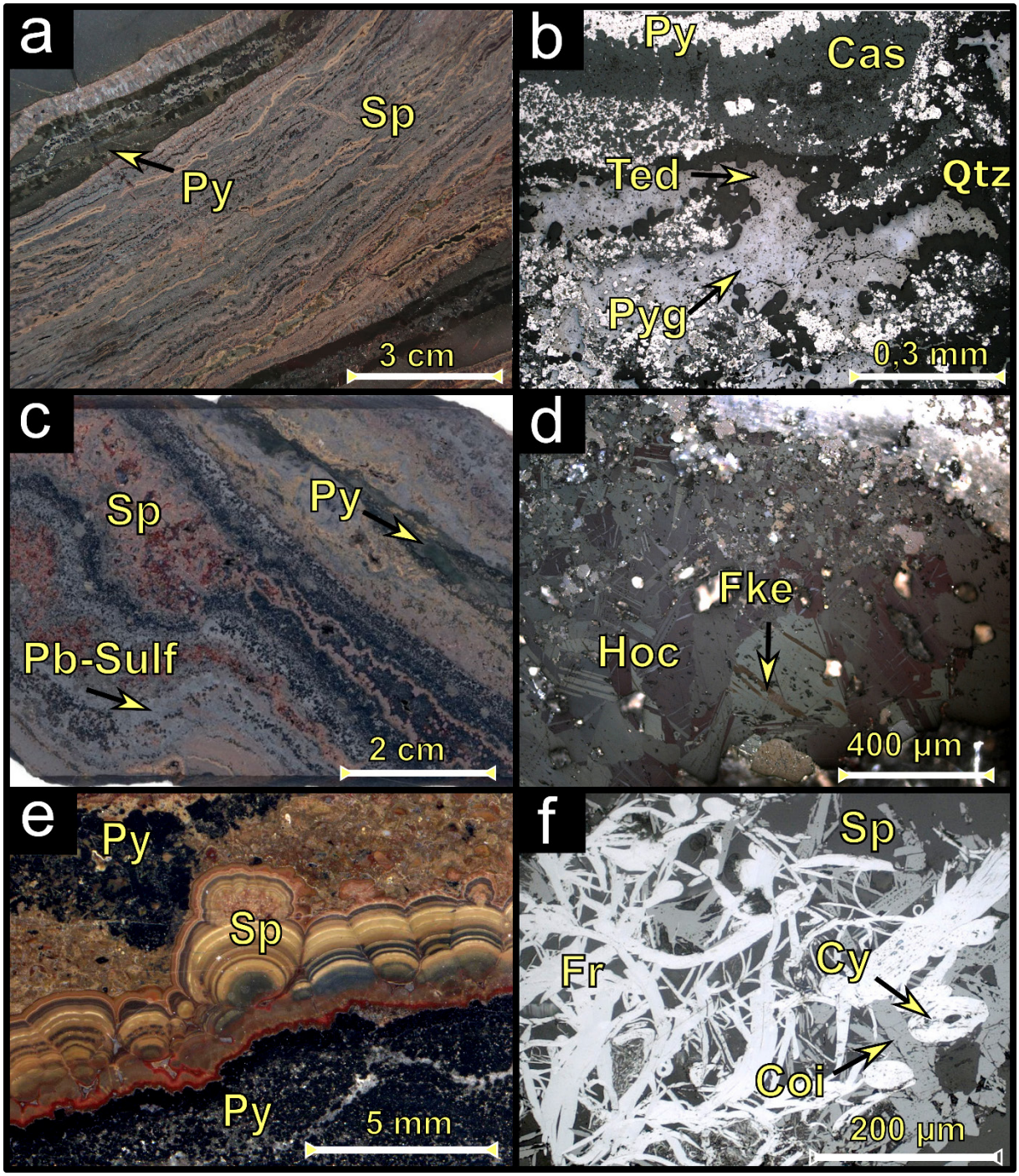

Figure 11.Illustrations of typical features of the mineralization in Pirquitas veins: a, c and e are photographs of polished drill cores, b, d and f are photomicrographs in reflected light. a) stage I-2 pyrite (Py) and banded I-2 sphalerite (Sp); b) stage I-1 pyrite (Py), I-1 cassiterite (Cas), I-1 quartz (Qtz), stage I-2 pyrargyrite (Pyg) and tetrahedrite (Ted); c) stage I-1 pyrite (Py), I-2 sphalerite (Sp) and I-2 Pb-sulfosalts (Pb-Sulf); d) massive stage I-2 hocartite (Hoc) with inclusion of ferrokesterite (Fke); (e) colloform sphalerite II (Sp) replacing earlier pyrite (py), f) intergrowth of Pb-Sn sulfosalts: frankeite (Fr), coiraite (Coi) and cylindrite (Cy) with sphalerite (Sp).

NaCl (wt% NaCl equiv.) was interpreted from low-temperature phase changes using HokieFlincs_H2ONaCl (Steele-MacInnis et al., 2012; Bodnar, 1993). The vapor bubbles of fluid inclusions were tested for probable gas contents using a Jobin-Yvon LabRam confocal laser Raman microspectrometer, equipped with an Olympus optical microscope. All measurements were taken with an MPlan 100×/0.90 objective lens. The excitation radiation used was a 532.6 nm Nd-YAG laser (100

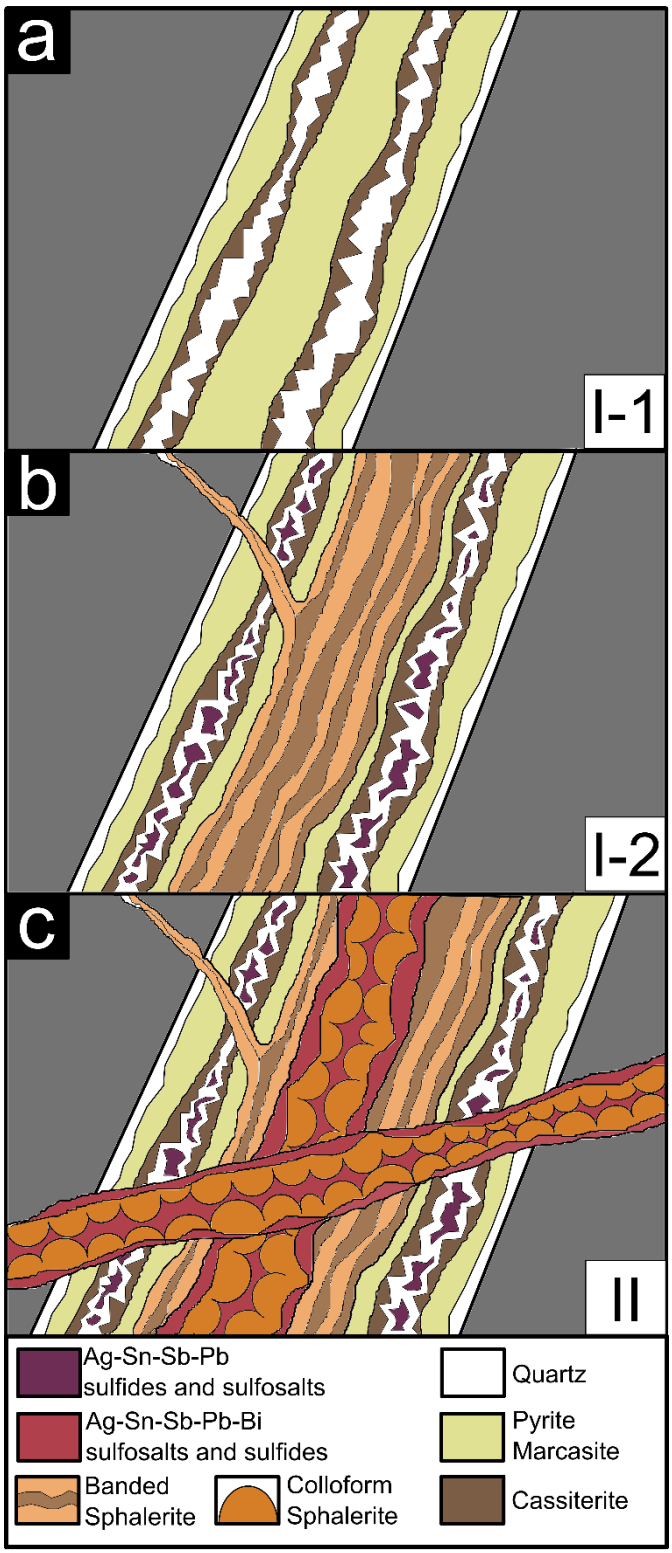

Figure 12. Sketches illustrating the sequence of mineralization in the Pirquitas vein systems. a) stage I-1 with deposition of quartz, pyrite, marcasite (after pyrrhotite) and cassiterite; b) stage I-2 with Ag-Sn-Sb-Pb sulfides and sulfosalts as well as banded sphalerite; c) The second event of mineralization with abundant Ag-Sn-Sb-Pb-Bi sulfides and sulfosalts and colloform sphalerite.

mW). For internal calibration, silicon (520 cm−1) and diamond (1332 cm−1) were used. Raman spectra of aqueous inclusions were collected in the spectral range between 1200 and 3000 cm−1 with a Peltier cooled CCD detector. A 2×45 s acquisition time was used for all checked inclusions.

Noble gas analyses were performed using samples of 0.70 to 0.86 g of hand-picked separates of sphalerite, pyrite, arsenopyrite, galena and Ag-rich sulfosalts (Table 2). The samples were loaded into an ultrahighvacuum spindle crusher, which was pumped at room temperature for 24 h to remove atmospheric gases adsorbed on grain surfaces. For gas extraction the samples were crushed under vacuum, and the gases released were admitted to the preparation line. Water was frozen in a dry ice-cooled trap and other chemically active species were removed in Ti sponge and ZrAl getters. The noble gases were then separated from each other in a cryogenic adsorber, and noble gas concentrations and isotopic compositions were determined in a VG5400 noble gas mass spectrometer according to procedures described by Niedermann et al. (1997). The mineralogy and mineral phase associations were determined by optical microscopy and semi-quantitatively by energy dispersive X-

Ray spectroscopy (EDS) analyses with SEM JEOL JSM-6510 (W filament, 0.5–30 kV acceleration voltage), coupled with an EDS Oxford Instruments INCAx-act. The EDS data compare favorably with electron microprobe analysis reported by Paar et al. (1996).

3.5. Results

3.5.1. Fluid inclusions

The studied sample suite comprises quartz from stage I-1, quartz, Ag-Sn sulfides, sphalerite and pyrargyrite from stage I-2, and quartz, dark and bright sphalerite and pyrargyrite from event II. All minerals without exception contain two-phase aqueous inclusions at room temperature with variable liquid/vapor ratios in the different host minerals. Vapor-rich inclusions and/or boiling assemblages were not observed in any samples although evidence for necking-down of fluid inclusions was found in some samples (especially those from the Potosí breccia), which can mimic vapor-rich primary inclusions. Traces of gases such as CO2 were not observed by clathrate melting nor were they detected by laser-Raman spectroscopy in vapor bubbles of aqueous two phase inclusions. Fluid inclusions were classified as primary, pseudosecondary or secondary using the criteria of Roedder (1984) and Goldstein and Reynolds (1994). All fluid inclusion data are presented in Fig. 13 and ranges of salinity values and homogenization temperatures are summarized in Table 1.

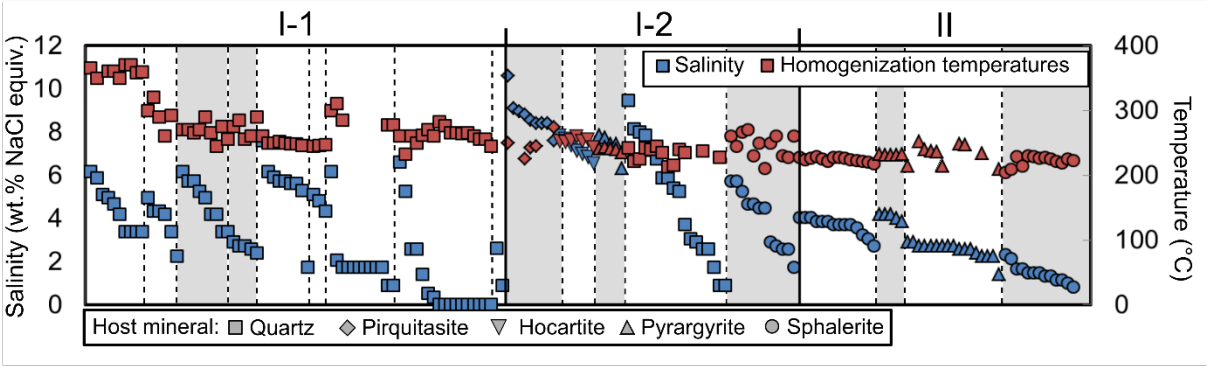

Figure 13. Homogenization temperatures and salinity of fluid inclusions in quartz and ore minerals from mineralization stages I-1, I-2, and event II. The symbol shapes are keyed to mineral phases shown in the legend. The vertical white and gray bands separate samples and the vertical dashed lines separate inclusion assemblages within them. For each assemblage, data are plotted in order of decreasing salinity to the right.

3.5.1.1. Fluid inclusions in quartz

Quartz from various occurrences and mineralization events withinthe Pirquitas mine is commonly recrystallized and a classification of primary vs. secondary inclusions is uncertain or even impossible.

The rare exceptions to this were a few quartz crystals associated with pyrite, cassiterite, sphalerite and/or Ag-Sn sulfides that contain small primary inclusions (not exceeding 5 μm) decorating growth zones; and occasional, isolated, larger fluid inclusions in clear quartz crystals associated with sphalerite. Both of these fluid inclusion assemblages are interpreted as primary. Fluid inclusions in growth zones in quartz from event II are abundant but were too small (1–2 μm) for microthermometric measurements (Fig. 14a). Therefore, only quartz-hosted fluid inclusions from the I-1 and I-2 stages were studied. Fluid inclusions representing stage I-1 show a broad range of homogenization temperatures between 233 and 370 °C and salinities between 0 and 7.6 wt% NaCl equiv. (Fig. 13). In detail, homogenization temperatures above 300 °C were found in fluid inclusions from quartz associated with pyrrhotite (see Fig. 10) whereas the other stage I-1 fluids are mostly in the range of 250 °C–290 °C. Fluid inclusions in stage I-2 quartz show highly variable salinity and homogenization temperatures not exceeding 250 °C (Fig. 13). Fluid inclusions in quartz from the Potosí breccia (event I-2) are rarely large enough for microthermometric measurements. The exceptions are between 30 and 50 μm in diameter and have liquid/vapor ratios between 60/40 and 70/30. Most of the inclusions show features of secondary modifications (necking-down). When heated to temperatures above 290° to 385 °C, fluid inclusions in quartz started leaking so no measurements of homogenization temperature were possible.

3.5.1.2. Inclusions in ore minerals

Fluid inclusions were studied in different ore minerals from vein type mineralization that deposited during the mineralization events I-2 and II. Some As-poor pyrite from the Potosí breccia ore (event I-2) displays good infrared transparency and well expressed zonation (Fig. 14b) but it does not contain measurable fluid inclusions. The pyrite from vein-type mineralization shows no IR transparency which is likely due to the high As content up to 3 wt%. Fluid inclusions in sphalerite from mineralization events I-2 and II range between 10 and 40 μm in size and show variable liquid/vapor ratios of 80/20 to 90/10 (Fig. 14c). Primary fluid inclusions have lenticular, cylindrical and prismatic crystal shapes and mostly occur in growth zones. Secondary inclusions have irregular shapes and are commonly arranged in trails along healed microfractures. Primary fluid inclusions in massive sphalerite from stage I-2 have salinities between 1.7 and 5.7 wt% NaCl equiv. and homogenization temperatures between 210

and 270 °C (Fig. 13). Fluid inclusions in colloform sphalerite from event II show slightly lower salinity of 0.8 to 4.0 wt% NaCl equiv. and homogenization temperatures between 204 and 230 °C

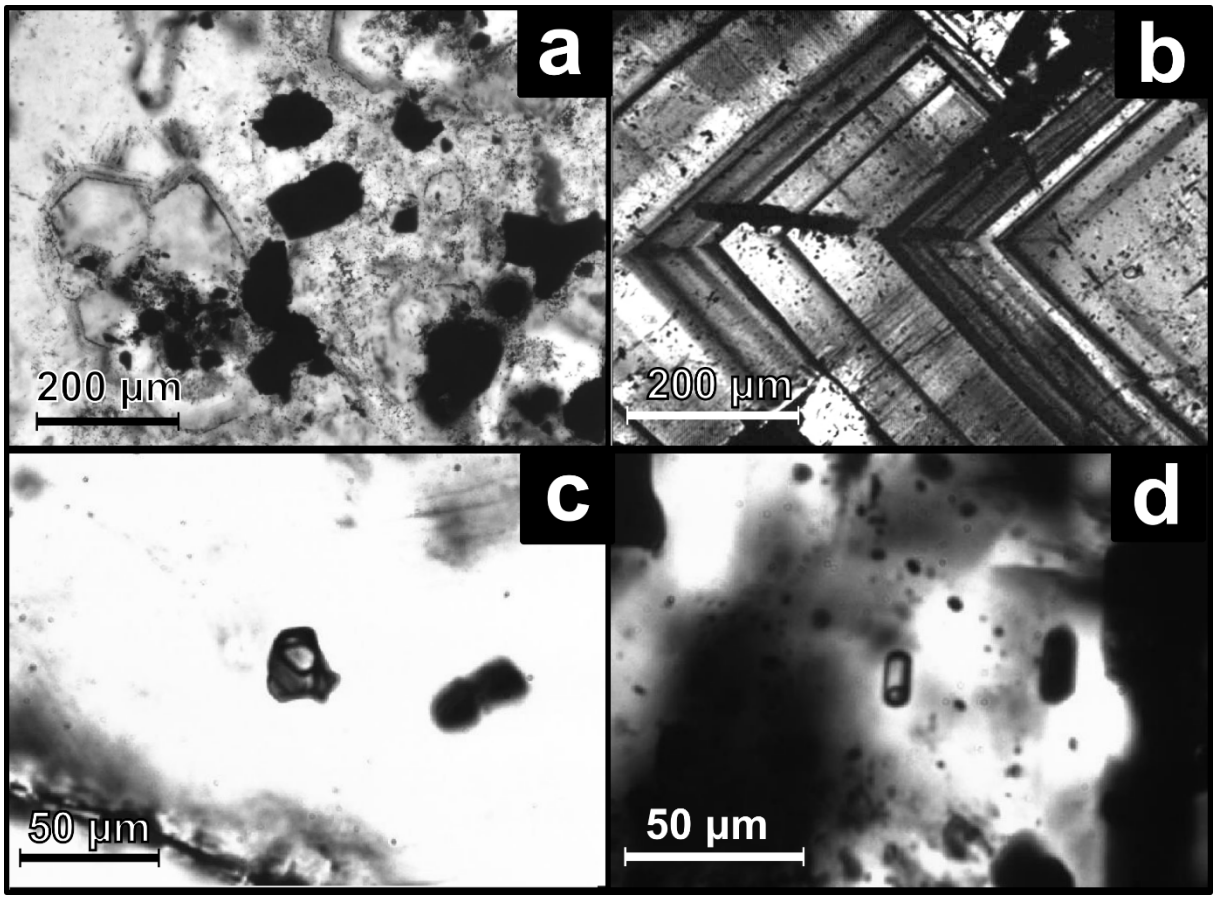

Figure 14. Photomicrographs of fluid inclusion examples under near infra-red and visible transmitted light: a) quartz, and pyrite from event II; note growth zones in quartz, b) zonation in I-1 pyrite, c) primary fluid inclusion in stage I-2 sphalerite, d) primary fluid inclusions in stage I-2 hocartite.

(Fig. 13). Fluid inclusions hosted in Ag-rich ore minerals from stage I-2 show similar homogenization temperatures but slightly higher salinity than fluid inclusions in associated sphalerite (Fig. 13). The highest salinity was found in fluid inclusions hosted by the Ag-Sn sulfides hocartite (Ag2FeSnS4) and pirquitasite (Ag2ZnSnS4). These minerals contain primary two-phase aqueous fluid inclusions with liquid/vapor ratios of about 80/20 or somewhat lower (Fig. 14d).

The inclusions have prismatic, rectangular-prismatic or spherical shapes and sizes between 10 and 40 µm. They generally occur as isolated inclusions or in fluid inclusion assemblages. The ranges of salinity and homogenization temperatures are 6.5 to 10.6 wt% NaCl equiv. and 225 to 274 °C, respectively. Hocartite crystals also host minor secondary fluid inclusions showing higher liquid/vapor ratios of about 95/5 that were not analyzed. Fluid inclusions are abundant in pyrargyrite from both

mineralization events. The inclusions have sizes between<5 μm and 50 μm and liquid/vapor ratios between 80/20 and 90/10. Primary inclusions have rectangular, prismatic or spherical shapes and occur as isolated inclusions or in fluid inclusion assemblages. Secondary inclusions occur in trails along healed microfractures. Primary fluid inclusions hosted in stage I-2 pyrargyrite have salinities of 6.0 to 7.9 wt% NaCl equiv. and homogenization temperatures between 231° and 243 °C, whereas fluid inclusions in pyrargyrite from event II yielded lower salinity (0.9–4.3 wt% NaCl equiv.) and more variable homogenization temperatures between 190 and 252 °C.

Table 1. Ranges of ice melting temperatures, corresponding salinities and homogenization temperatures of fluid inclusions in ore and gangue minerals.

Event	Mineral	Location	Tm ice (°C)	Salinity (wt.% eq. NaCl)	Homogenization Temperature (°C)
I-1	Quartz (Po associated)	San Miguel	(-2.0) - (-3.8)	3.4 - 6.2	350 - 370
	Quartz (Py associated)	San Miguel	(-2.1) - (-3.0)	3.5 - 5.0	260 - 320
	Quartz (post Po-Py)	Oploca	0 - (- 4.8)	0.0 - 7.6	233 - 310
	Quartz (Cas associated)	San Miguel	(-1.4) - (-3.8)	2.4 - 6.2	245 - 290
I-2	Sphalerite	San Miguel	(-1.0) - (-3.5)	1.7 - 5.7	210 - 270
	Pirquitasite	Oploca	(- 4.8) - (-7.1)	7.6 - 10.6	244 - 274
	Hocartite	Oploca	(-4.1) - (-4.9)	6.5 - 7,8	242 - 259
	Pyrargyrite	San Miguel	(-3.9) - (-5.0)	6.3 - 7.9	235 - 243
	Quartz	Oploca	(-0.5) - (6.2)	0.9 - 9.5	213 - 245
II	Sphalerite	Oploca	(-0.4) - (-1.3)	0.8 - 2.3	205 - 228
	Sphalerite	Oploca	(-1.6) - (-2.4)	2.7 - 4.0	218 - 229
	Pyrargyrite	Oploca	(-0.5) - (2.5)	0.9 - 4.2	190 - 252

3.5.2. Noble gas isotopes

Noble gas isotope analyses were performed on fluids released by crushing of hand-picked mineral separates of pyrargyrite, pirquitasite, frankeite, freibergite, sphalerite, pyrite, arsenopyrite and galena from samples that represent mineralization events I and II (Table 2). The majority of analyzed samples come from the vein-type mineralization; only two are from the Potosí breccia (Table 2). Since fluid inclusion petrography in hocartite and sphalerite revealed that primary inclusions are larger and more abundant than secondary inclusions, we consider the results to represent the ore-bearing fluids with

only a minor contribution from secondary fluids. However, the sulfosalts, including pyrargyrite-miargyrite, contain abundant secondary inclusions as well, so the noble gas ratios of these minerals represent a mixture between ore-bearing fluids and secondary fluids. Petrographic examination of fluid inclusions in pyrite and galena was impossible and we have no information on the proportion of primary vs. secondary inclusions in those cases.

The results are plotted in terms of 3He/4He vs. 4He/20Ne ratios in Fig. 15, which distinguishes the relative contributions from mantle, crustal and atmospheric gas sources. All samples, regardless of host mineral and mineralization stage, yielded a range of 3He/4He ratios between 1.9 and 4.1 Ra, with one outlier at 0.5 Ra (where Ra is the atmospheric ratio of 1.39×10−6). The 4He/20Ne ratios are between 2.3 and 600. Considering that the value of this ratio in air is 0.319 (ASW on Fig. 15), we conclude that the atmospheric He contribution is small and in most cases negligible. The other source reservoirs for Pirquitas fluids shown by the mixing curves in Fig. 15 are mantle-derived magmas (3He/4He about 8 Ra) and the continental crust (3He/4He about 0.02 Ra). Also shown are the ranges of 3He/4He compositions reported for hot-springs and volcanic rocks in the central and southern Puna (see discussion). Whereas the He isotope ratios show little influence from the atmospheric, the opposite is true for the heavier noble gases Ne, Ar, Kr and Xe. The values of Ar and of all Ne and Xe isotopic ratios correspond to the atmospheric values within the respective error limits (Table 2). The relative abundances of Ne, Ar and Kr are also very similar to those in air, while Xe tends to be higher by up to a factor of 3 (Table 2, Fig. 16).

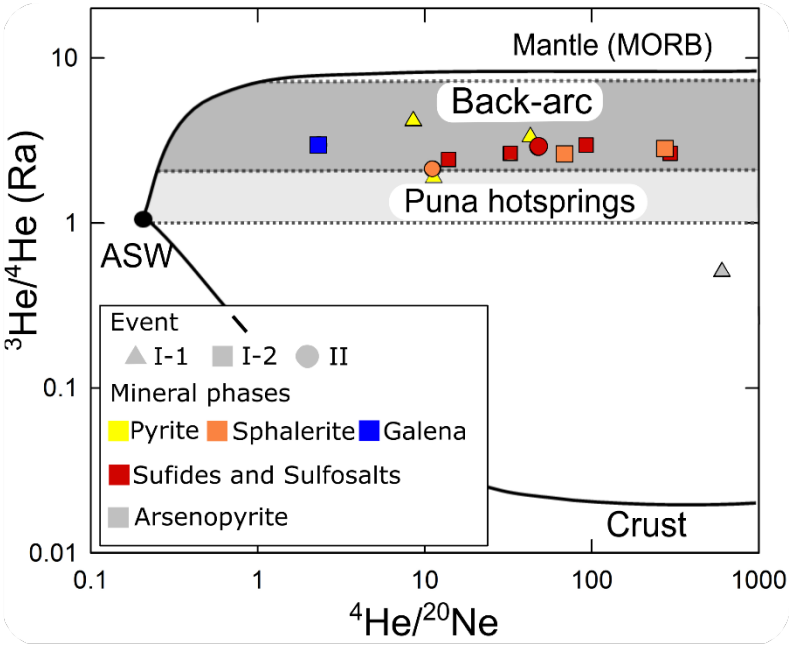

Figure 15. 4He/20Ne vs. 3He/4He diagram (after Sano and Wakita, 1985) for crushreleased fluids from ore minerals in the Pirquitas deposit. ASW (air-saturated water) denotes the atmospheric composition and solid lines labelled MORB and Crust show mixing lines of the atmospheric with mantle and crustal components. The horizontal patterned fields show the 3He/4He range of Puna back-arc lavas and hot-springs for comparison (see text for data sources). No error bars are shown because they are similar to or smaller than the symbol size (see Table 2).

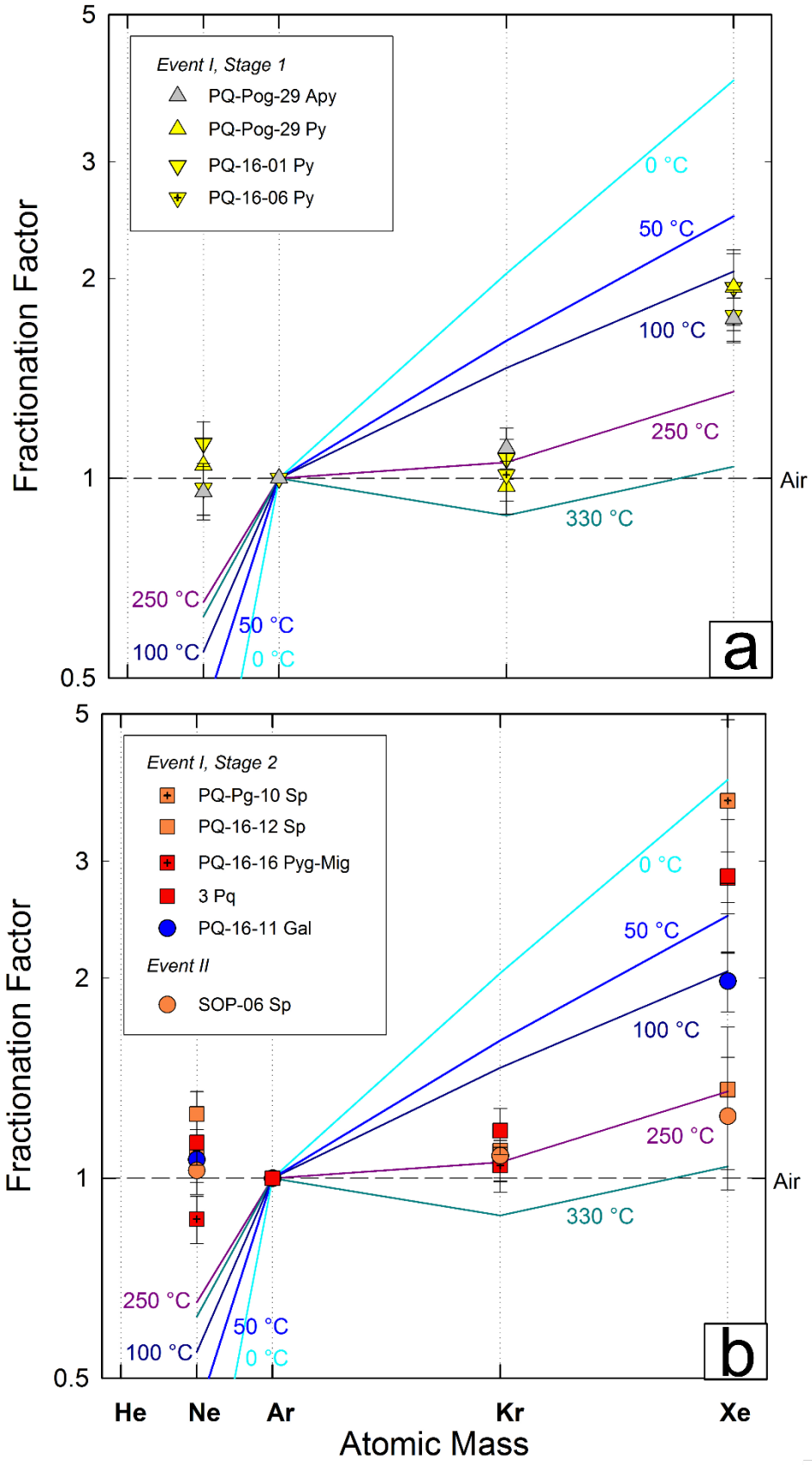

Figure 16 Logarithmic plots of noble gas abundances in Pirquitas ore minerals (a: stage I-1 and b: stage I-2 and event II) expressed as fractionation factors relative to 36Ar and air (iX/36Ar)sample/(iX/36Ar)air, where iX is a noble gas. The labelled curves show dissolution equilibrium of noble gases in water for 0 °C and 50 °C at 5% salinity according to Smith and Kennedy (1983) and for 100 °C, 250 °C and 330 °C at zero salinity according to Crovetto et al. (1982). Helium data are not displayed as they are dominated by non-atmospheric components and would plot well above the shown range. See text for discussion.

Table 2. Results of noble gas analyses of crush-released fluids in ore minerals from vein type mineralizations and *breccia ore. Error limits are 2σ.

Mineral	Sample location	Sample name	Min event	^{4}He	^{20}Ne	^{40}Ar	$^{3}He/^{4}He$	$^{20}Ne/^{22}Ne$	$^{21}Ne/^{22}Ne$	$^{40}Ar/^{36}Ar$	$^{38}Ar/^{36}Ar$	^{84}Kr	^{132}Xe
				10^{-8} cm^3/g	*10^{-12} cm^3/g*	*$10^{-8}cm^3/g$*	*R_a*					*10^{-12} cm^3 STP/g*	*10^{-12} cm^3 STP/g*
As-Pyrite	San Miguel	PQ-Pog-29	I-1	41.1	684	45.7	0.506	9.757	0.02965	333.6	0.1886	30.8	1.794
0.71180 g				±2.5	±52	±2.3	±0.040	±0.049	±0.00058	±1.6	±0.0013	±1.6	±0.098
Pyrite	Oploca	PQ-Pog-29	I-1	12.54	2920	161	3.32	9.766	0.02920	301.1	0.1885	105.2	7.78
0.70816 g				±0.75	±190	±11	±0.13	±0.058	±0.00038	±1.6	±0.0012	±6.6	±0.78
Pyrite	San Miguel	PQ-16-01	I-1	2.35	2070	105.1	1.88	9.744	0.02910	299.9	0.18958	76.0	5.13
0.86034 g				±0.12	±120	±5.3	±0.21	±0.055	±0.00032	±1.2	±0.00092	±3.8	±0.67
Pyrite*	Potosí	PQ-16-06	I-1	0.992	1160	68.7	4.14	9.708	0.02923	298.9	0.1879	47.2	3.04
0.71118 g	breccia			±0.060	±76	±4.1	±0.48	±0.059	±0.00060	±1.5	±0.0011	±2.9	±0.21
Pyrarg.-Miarg.	Oploca	PQ16-16	I-2	11.47	390	26.2	2.64	9.800	0.02930	305.4	0.18777	18.2	1.83
0.70292 g				±0.57	±24	±1.3	±0.15	±0.065	±0.00083	±2.3	±0.00099	±1.3	±0.40
AgSn sulfosalt	Oploca	PQ16-12	I-2	1.624	1167	134	2.42	9.778	0.02933	348.5	-	-	-
0.70084 g				±0.081	±69	±47	±0.20	±0.038	±0.00053	±7.4			
Sphalerite	San Miguel	PQ16-12	I-2	12.60	1790	82.3	2.60	9.824	0.02930	301.5	0.18823	60.1	2.80
0.84846 g				±0.63	±110	±4.1	±0.14	±0.085	±0.00037	±1.3	±0.00098	±4.3	±0.65
Pirquitasite	Oploca	3	I-2	7.68	2350	118.7	2.64	9.791	0.02931	298.3	0.18921	95.0	8.50
0.71036 g				±0.39	±130	±6.0	±0.17	±0.095	±0.00039	±1.2	±0.00097	±5.8	±0.62
Freibergite	San Miguel	NIU-7/30-10-05	I-2	163.5	17660	-	2.961	9.966	0.02936	-	-	-	-
0.70844 g				±8.2	±890		±0.054	±0.060	±0.00032				
Sphalerite	Oploca	PQ-Pg-10	I-2	54.9	1990	105.5	2.741	9.759	0.02914	304.3	0.1887	76.9	9.5
0.70790 g				±2.7	±110	±5.3	±0.074	±0.070	±0.00028	±1.2	±0.0012	±6.8	±3.2
Galena*	Potosí	PQ-16-11	I-2	0.328	1416	75.5	2.97	9.761	0.02917	297.7	0.18909	55.7	3.78
0.80364 g	breccia			±0.016	±82	±3.8	±0.44	±0.048	±0.00035	±1.3	±0.00092	±2.8	±0.34
Frankeite	Oploca	1	II	36.7	7710	-	2.880	9.720	0.02919	332	0.1888	-	-
0.70762 g				±1.8	±440		±0.096	±0.047	±0.00027	±20	±0.0014		
Sphalerite	Oploca	SOP-06	II	1.344	1207	67.3	2.12	9.844	0.02931	299.7	0.18816	49.2	2.08
0.85154 g				±0.067	±75	±3.4	±0.28	±0.036	±0.00040	±1.4	±0.00090	±3.5	±0.46
				Atmosphere			*1*	*9.80*	*0.0290*	*298.56*	0.1885		

3.6. Discussion

3.6.1. Constraints on fluid origin

The He isotope ratios and He/Ne abundance ratios have strong discriminating power for different fluid sources. To put the Pirquitas noble-gas data into perspective, Fig. 15 shows the range of 3He/4He ratios from thermal waters in the region (ca. 1 to 3 Ra) reported by Hilton et al. (1993), Hoke et al. (1994), Pilz (2008) and Newell et al. (2015). Peralta-Arnold et al. (2017) evaluated the fluid chemistry and O isotope composition of northern Puna hotsprings and concluded that they are dominated by meteoric water, with a possible small contribution from a magmatic fluid. The He isotope composition of the local magmatic component is given by 3He/4He ratios from olivine and clinopyroxene phenocrysts from Cenozoic mafic lavas in the arc and back-arc region of the Puna plateau (ca. 3 to 7 Ra) reported by Hilton et al. (1993) and Pilz (2008). The He isotope results from Pirquitas ore minerals demonstrate that the atmospheric He component is minimal (Fig. 15). With one exception the Pirquitas samples yielded 3He/4He ratios between 1.9 and 4.1 Ra, which is consistently higher than the hot-spring meteoric fluids and overlaps with the range of magmatic helium. The exception is an arsenopyrite sample from an open vug that yielded 0.5 Ra (Table 2) and precipitated during event I-1. On this basis, we conclude that helium in Pirquitas ore fluids contains a magmatic component but there are also variable admixtures of helium from crustal fluids, as evidenced most clearly by the vug-hosted arsenopyrite. In contrast to He, the Ne, Ar and Xe isotope ratios of Pirquitas fluids have atmospheric values except for three samples whose 40Ar/36Ar ratios are elevated by up to ~20% relative to air (Table 2). Such 40Ar excesses may originate in both the mantle and the crust, so the heavy noble gas results are not useful to discriminate between mantle and crustal fluid sources. Nevertheless, they are useful to test for isotopic equilibrium at the ca. 200–250 °C mineralization temperature indicated by fluid inclusions. This is shown in Fig. 16, where elemental fractionation factors (Fi=(iX/36Ar)sample/(iX/36Ar)air, where iX=20Ne, 84Kr or 132Xe) are compared with those for air-saturated water calculated for temperatures from 0 to 330 °C (Crovetto et al., 1982; Smith and Kennedy, 1983). For clarity the Pirquitas data are plotted separately for mineralization stages I-1 (Fig. 16a) and for I-2 and II (Fig. 16b). The first point to consider is that there is no significant difference in the noble gas abundances for the different mineralization stages and events. The second point is that

we find agreement with the equilibrium curve for 250 °C in all 10 samples for Kr, whereas the Xe abundances in most samples and the Ne abundances in all of them are too high for equilibrium at the mineralization temperature. Such Xe excesses in hydrothermal fluids have been observed before (e.g. Stuart et al., 1995; Bouabdellah et al., 2015) and may relate to preferential adsorption of Xe on mineral surfaces (Niedermann and Eugster, 1992; Stuart et al., 1995), although the very low Xe concentrations and consequent high analytical uncertainties may also play a role. High Ne abundances relative to dissolution equilibrium at high temperatures are also not uncommon (e.g., Battani et al., 2000; Bouabdellah et al., 2015), but they are more difficult to explain. One factor may be that the ≥100 °C fractionation curves in Fig. 16 apply to freshwater only. Data are not available for saline waters at high temperature but the effect of salinity is to increase the Ne/Ar ratios. Therefore, despite deviations from the expected pattern for some elements the noble gas results are consistent with dissolution of atmospheric gases in a hydrothermal fluid at temperatures near 250 °C.

3.6.2. Evolution of the vein mineralization

Some fluid inclusions hosted in stage I-1 quartz that precipitated along with pyrrhotite and pyrite yielded homogenization temperatures well above 300 °C (Fig. 13), considerably higher than the homogenization temperatures of fluid inclusions in quartz and ore minerals from the subsequent Ag-Sn ore stages. Unfortunately, no pyrite-hosted inclusions from stage I-1 could be analyzed for comparison, but nevertheless, the range of salinities and temperatures in quartz that precipitated episodically during stage I-1 follows a trend of decreasing salinity and a smaller decrease in temperature with time. This is consistent with mixing of magmatic fluids with heated meteoric water, causing a larger impact on salinity than on temperature. Fluid mixing may have caused deposition of the granular cassiterite towards the end of stage I-1 (see Figs. 10, 12) due to the decrease of cassiterite solubility (Heinrich, 1990; Audétat et al., 1998) induced by the drop of salinity (and temperature). The higher salinity of stage I-2 fluids and the greater abundance of ore minerals including Sn and Ag minerals, suggests that after stage I-1 cassiterite formation the fluids became more acidic, probably due to new influx of magmatic fluids, enabling the transport of Sn and other metals along with reduced sulfur species at temperatures below 350 °C (Heinrich and Eadington, 1986; Heinrich, 1990). The neutralization of stage I-2 fluids by wall-rock interaction and cooling may have led to the deposition of

abundant colloform sphalerite, minor galena and the Ag-Sn-Zn (-Pb-As-Sb-Bi-Cu) sulfides and sulfosalts that are characteristic of stage I-2.

The second mineralization event II was responsible for the deposition of most of the economic Ag ore at Pirquitas (Malvicini, 1978). Fibrous, colloform cassiterite in the form of "wood tin" was one of the first ore minerals precipitated at the beginning of the second event. Wood tin commonly precipitates at lower temperature than granular cassiterite (Pan, 1974), but the fluid inclusion temperatures of event II are only slightly lower than those of late stage I-1 and I-2. However, the cassiterite texture is not an exclusive indicator for temperature because colloform cassiterite can form at higher temperatures (300 to 600 °C) in conditions of rapid nucleation from supersaturated solutions (Taylor, 1979; Rye et al., 1990). Fluid inclusions in sphalerite and pyrargyrite from event II generally show lower salinity and lower homogenization temperature compared to minerals from the first event (Fig. 13) and this may reflect continued dilution of magmatic fluids by mixing with meteoric water. However, in this case, the meteoric fluid may have been sulfate-bearing as suggested by the presence of barite towards the end of the mineralization event II in the Chocaya and San Miguel veins (Malvicini, 1978).

3.6.3. Breccia ore mineralization

The presence of various styles of breccia mineralization (e.g. crackle breccia, breccia veins) along some mineralized vein systems (Oploca, Potosí, Cortaderas) suggests episodic fluctuations in pressure during the formation of the Pirquitas ore deposit (Slater, 2016). Mineralization of all breccia ore bodies is similar to vein fillings of the Pirquitas deposit and consists of cassiterite, base and Ag-Sn sulfides as well as a variety of Ag-rich sulfosalts associated with quartz as gangue mineral with kaolinite and other clay minerals. Fluid inclusions in minerals from the Potosí breccia ore body are scarce. Where present (in quartz and sphalerite) they are aqueous two-phase inclusions that show features of secondary modification (necking-down) and began to leak during heating at temperatures above 300 °C prior to reaching homogenization. Thus it is likely that the fluids were trapped under overpressured conditions and had already partially leaked in response to drop of the confining pressure due to the brecciation.

3.6.4. Fluid evolution and the significance of boiling

The ranges of salinity and homogenization temperature from fluid inclusions in ore minerals and quartz show covariations that are consistent with progressive cooling and/or dilution trends caused by fluid mixing. Such trends are commonly observed in distal (i.e., low-sulfidation to intermediate-sulfidation) epithermal systems related to magmatic intrusions (e.g. Hedenquist and Lowenstern, 1994; John, 2001; Lüders et al., 2009). Mixing of magmatic and meteoric fluids is supported by the noble gas results that indicate significant but variable magmatic contributions. In contrast to the fluid inclusion data the noble gas isotopes show no systematic difference between early and late events.

Boiling is an important process in hydrothermal fluid evolution, particularly in epithermal systems like Pirquitas where it is thought to play a key role in the precipitation of precious metals. Thus, Hedenquist et al. (2000) and Moncada et al. (2012) cited examples where Au and Ag grades are concentrated at or above the boiling horizon whereas below it, base metal sulfides such as sphalerite are common and precious metal grades are low or even absent. Evidence for boiling was carefully assessed in this study, but the exclusive presence of aqueous two-phase inclusions in quartz and in all ore minerals examined from the veins and breccia body indicates non-boiling conditions during ore deposition. This has implications for the pressure of mineralization because it means that the ore-forming fluids did not intersect the liquidvapor curve. Taking the fluid in stage I-2 tin sulfides as an example (10 wt% NaCl and temperatures not exceeding 300 °C), this ascending fluid would start boiling at about 325m depth assuming a lithostatic pressure regime (2.4 g/cm3) or at about 900m under hydrostatic pressure conditions (Fig. 17). Above these depths the ore-forming fluid would have undergone phase separation (boiling), which would have led to entrapment of boiling assemblages, yet none were found in this study. Therefore, the depth of mineralization must have been greater than about 350m and consequently, pressure conditions exceeded 150 bars. Given a pressure of about 150 bars, the difference between homogenization and trapping temperature, i.e. the pressure correction, is about 10 °C (Potter, 1977), which is insignificant compared with the observed variations. One may speculate that mineralization took place at depths of about 400–500m but this would not significantly change the minimal pressure correction. It is noted that Slater (2016) did infer boiling of fluids from the Cortaderas breccia body. Sphalerite from Cortaderas breccia contains liquid-rich two-phase fluid

inclusions that yielded homogenization temperatures between 209 and 280 °C and salinities of 0.2 to 7.2 wt% NaCl equiv., in good agreement with our results from vein-hosted sphalerite. However, Slater (2016) also reported coexisting vapor-rich and liquid-rich aqueous inclusions as well as pure vapor-rich inclusions and took these as evidence for boiling and flashing, respectively. We found no such evidence in the veins or the Potosí breccia, but we did observe necking-down in some inclusions of breccia-hosted sphalerite. Judging from the photomicrographs in Slater (2016), we suggest the possibility that necking-down might also have affected the inclusions in Cortaderas breccia and produced the appearance of liquid and vapor-rich fluid inclusion assemblages. If fluid boiling is a necessary condition for Ag deposition as suggested by some studies, one can speculate that the ore-bearing fluids at Pirquitas may have boiled at a deeper level than currently exposed. There is no evidence of this in the inclusions studied here but it cannot be ruled out. Thus, for the same example of 10% saline fluid and a supposed 400 °C temperature to reflect the greater depth, boiling would commence at about 1020m or 3000m depth for lithostatic and hydrostatic conditions, respectively (Fig. 17).

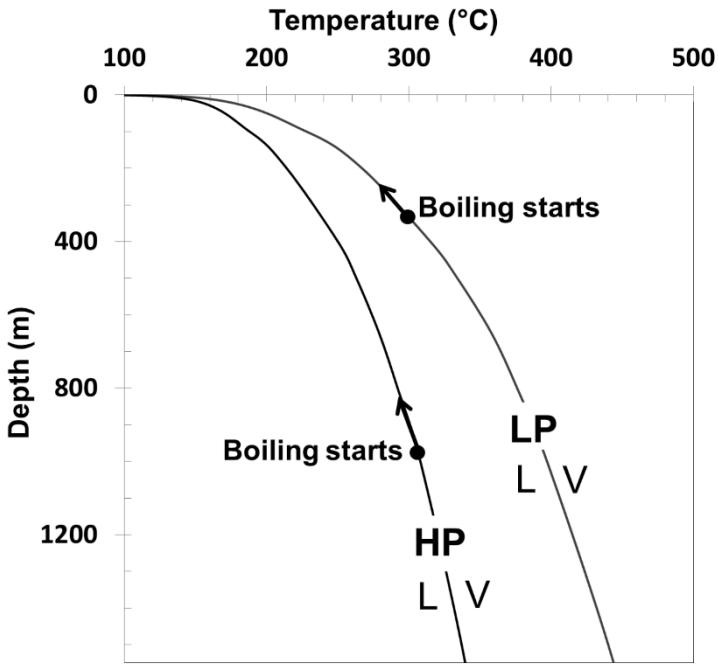

Figure 17. Two-phase (liquid and vapor) curves for a 10 wt% NaCl fluid at hydrostatic pressure (HP) and lithostatic pressure (LP), modified after Cunningham (1978) and Bischoff and Pitzer (1985). Boiling at 300 °C would commence above about 325m for LP and 900m for HP.

If one accepts the possibility of a boiling event at greater depth and the relationship of boiling to Ag deposition, one might predict the existence of a deeper-seated Ag-rich mineralization which could be a source of Ag to the fluids in the Pirquitas vein system. However, it is also possible that the Ag deposited at Pirquitas was directly derived by magmatic fluids and/or leached by alteration of Ordovician shale by heated meteoric water that mixed with magmatic fluids. The noble gas results of fluid inclusions rule out a pure meteoric

fluid origin but give no other constraints on the source of metals. Thus the source(s) for Ag at Pirquitas (as for other Bolivian-type polymetallic Sn-Ag deposits as well) remains unclear.

3.6.5. Mina Pirquitas in the context of the Bolivian Tin Belt

Following the nomenclature for epithermal ore deposits of, e.g., Barton and Skinner (1967), Hedenquist et al. (2000), Sillitoe and Hedenquist (2003), and Einaudi et al. (2003), the polymetallic Sn-Ag ore assemblages in Pirquitas classify it as an intermediate-sulfidation deposit. Many characteristics of the mineral assemblages and ore fluid characteristics of the Pirquitas deposit are similar to those of polymetallic Sn-Ag deposits (e.g. Potosí, Sud Lipez, Quechisia) in the southern part of the BTB (e.g. Turneaure, 1960; Sillitoe, 1976; Malvicini, 1978; Cunningham et al., 1996). Sugaki and Kitakaze (1988) described six stages of mineralization generally found in the BTB deposits: quartz-tourmaline (I), quartz (II), pyrite-quartz (III), sulfide (IV), sulfosalt (V) and sulfate-phosphate (VI). In the Pirquitas deposit, stages (II)–(III)–(IV)–(V)–(VI) are observed but stage (I) is missing. However, stage I fluids are characterized by higher temperatures (260 to 510 °C) and much higher salinities (18.5 to 55.4 wt% NaCl) than found in Pirquitas, which may explain its absence there.

The metallogenetic model for the Bolivian Sn-Ag deposits calls for an important magmatic input, which is consistent with the high temperatures and salinities of stage I fluids just mentioned. Evidence for associated intrusions is clear for several of the Bolivian examples such as Cerro Rico de Potosí (Ludington et al., 1992; Rice et al., 2005) but in the case of Pirquitas, the nearest known intrusion is ca. 12 km distant. Nevertheless, our He isotope results show that Pirquitas fluids must contain a significant magmatic contribution (Fig. 15) which implies an intrusion at greater depth. Our samples were collected between 150m (Oploca) and 300m (San Miguel) below the present surface, and an exploration drill hole to 800m depth below the floor of the open pit did not penetrate magmatic rocks. If an intrusion exists below the deposit as implied by the He-isotope evidence, it must have been deeper than about 1000m at the time of ore deposition and therefore distal with respect to mineralization. A distal magmatic source is consistent with the fact that the Pirquitas deposit is an intermediate-sulfidation system (Turneaure, 1971).

The age of the Pirquitas mineralization is poorly constrained and there is a need for a geochronology study. A maximum age of 15 Ma is indicated by the fact that mineralization affects the Tiomayo Formation of that age (Slater, 2016) and a possible minimum is suggested by the cessation of tectonic activity in the northern Puna block at 9 Ma according to Cladouhos et al. (1994). The range of 15–9 Ma is similar to that of some polymetallic deposits of the southern BTB (Grant et al., 1979) with which Pirquitas may be related. However, we note that magmatic activity in the northern Puna region continued until the early Pliocene (Coira et al., 2004; Caffe, 2008), with several volcanic centers around the Pirquitas deposit being younger than 9 Ma including the Coranzuli complex (6.6 Ma) with which the Cerro Galán intrusion nearest Pirquitas has been correlated (Caffe, 2008).

3.7. Conclusions

The mineral assemblages at the epithermal Pirquitas Ag-Sn-(Zn) deposits classify it as intermediate to low-sulfidation type. The mineralization resembles that found in the polymetallic vein deposits in the southern part of the Bolivian Tin Belt, suggesting a similar origin as a distal magmatic-hydrothermal system. The vein mineralization at the Pirquitas deposit is hosted in Ordovician metasediments and igneous intrusions are not exposed. However, noble gas ratios in ore-hosted fluid inclusions provide direct evidence of a magmatic contribution to the Pirquitas ore fluids.

Vein quartz and ore minerals precipitated from low to moderately saline fluids at temperatures below 400 °C. The highest homogenization temperatures were found in aqueous two-phase fluid inclusions in quartz that precipitated during the first mineralization event. Ore deposition during subsequent stages occurred at lower temperatures (< 300 °C) probably due to cooling of magmatic fluids by mixing with meteoric water. Variations of fluid inclusion homogenization temperatures and salinity during the different stages of mineralization suggest that the supply of magmatic fluids occurred in pulses, causing deposition of different ore associations. Fluid inclusion evidence for boiling was not observed in any samples. Since boiling is widely recognized as a likely mechanism for the deposition of precious metals in epithermal deposits, the contemporaneous deposition of Ag-rich ores and base metal sulfides at Pirquitas is hard to explain. One possible scenario is that boiling occurred at a deeper

level and caused a pre-enrichment in silver which was remobilized by the Pirquitas mineralizing fluids.

References

Allmendinger, R.W., Strecker, M., Eremchuk, J.E., Francis, P., 1989. Neotectonic deformation of the southern Puna Plateau, northwestern Argentina. J. S. Am. Earth Sci. 2, 111–130.

Allmendinger, R.W., Jordan, T.E., Kay, S.M., Isacks, B.L., 1997. The evolution of the Altiplano-Puna Plateau of the Central Andes. Annu. Rev. Earth Planet. Sci. 25, 139–174.

Arce-Burgoa, O., 2009. Metalliferous Ore Deposits of Bolivia, 2nd edition. SPC Impresores S.A, La Paz, Bolivia, pp. 233.

Astini, R.A., 2003. The Ordovician proto-Andean basins. In: Benedetto, J.L. (Ed.), Ordovician fossils of Argentina. Secretaría de Ciencia y Tecnología Universidad Nacional, Cordoba, pp. 1–74.

Audétat, A., Günther, D., Heinrich, C.A., 1998. Formation of a magmatic-hydrothermal ore deposit: insights with LA-ICP-MS analysis of fluid inclusions. Science 279, 2091–2094.

Bahlburg, H., Hervé, F., 1997. Geodynamic evolution and tectonostratigraphic terranes of northwestern Argentina and northern Chile. Geol. Soc. Am. Bull. 109, 869–884.

Barton Jr., P.B., Skinner, B.J., 1967. Sulfide mineral stabilities. In: Barnes, H.L. (Ed.), Geochemistry of Hydrothermal Ore Deposits. Holt, Rinehart and Winston, New York, pp. 236–333.

Battani, A., Sarda, P., Prinzhofer, A., 2000. Basin scale natural gas source, migration and trapping traced by noble gases and major elements: the Pakistan Indus basin. Earth Planet. Sci. Lett. 181, 229–249.

Bischoff, J.L., Pitzer, K.S., 1985. Phase relations and adiabats in boiling seafloor geothermal systems. Earth Planet. Sci. Lett. 75, 327–338.

Board, W.S., 2011. Technical Report on the Pirquitas Mine, Jujuy, Argentina. pp. 52–78.

Bodnar, R.J., 1993. Revised equation and table for determining the freezing point depression of H2O-NaCl solutions. Geochim. Cosmochim. Acta 57, 683–684.

Bouabdellah, M., Niedermann, S., Velasco, F., 2015. The Touissit-Bou Beker Mississippi Valley-type district of northeastern Morocco: relationships to the Messinian Salinity Crisis, late Neogene-Quaternary alkaline magmatism, and buoyancy-driven fluid convection. Econ. Geol. 110, 1455–1484.

Caffe, P.J., 2008. The Granada ignimbrite: a compound pyroclastic unit and its relationship with Upper Miocene caldera volcanism in the northern Puna. J. S. Am. Earth Sci. 25, 464–484.

Caffe, P.J., Trumbull, R.B., Coira, B.L., Romer, R.L., 2002. Petrogenesis of Early Neogene magmatism in the northern Puna; implications for magma genesis and crustal processes in the Central Andean Plateau. J. Petrol. 43, 907–942.

Cladouhos, T.T., Allmendinger, R.W., Coira, B., Farrar, E., 1994. Late Cenozoic deformation in the Central Andes: fault kinematics from the northern Puna, northwestern Argentina and southwestern Bolivia. J. S. Am. Earth Sci. 7, 209–228.

Coira, B., 1994. Metallogenetic events in the framework of magmatic-tectonic evolution of the Northern Puna of Argentina during the late Cenozoic. Communicacion 45, 67–76.

Coira, B., Caffe, P.J., Ramirez, A., Chayle, W., Diaz, A., Rosas, S., 2004. Hoja Geológica 2366-I/2166-III Mina Pirquitas. Provincia de Jujuy. In: Programa Nacional de Cartas Geológicas de la República Argentina. Vol. 1 (250 000(269)).

Coutand, I., Cobbold, P.R., de Urreiztieta, M., Gautier, P., Chauvin, A., Gapais, D., Rosello, E.A., López-Gamundi, O., 2001. Style and history of Andean deformation, Puna plateau, northwestern Argentina. Tectonics 20, 210–234.

Crovetto, R., Fernández-Prini, R., Japas, M.L., 1982. Solubilities of inert gases and methane in H2O and D2O in the temperature range of 300 to 600 K. J. Chem. Phys. 76, 1077–1086.

Cunningham, C.G., 1978. Pressure gradients and boiling as mechanism for localizing ore in porphyry systems. US Geol. Surv. J. Res. 6 (6), 745–775.

Cunningham, C.G., McNamee, J., Vásquez Pinto, J., Ericksen, E., 1991. A model of volcanic dome-hosted precious metal deposits in Bolivia. Econ. Geol. 86, 415–421.

Cunningham, C.G., Zartman, R.E., McKee, E.H., Rye, R.O., Naeser, C.W., Sanjinés, O.V., Ericksen, G.E., Tavera, F.V., 1996. The age and thermal history of Cerro Rico de Potosi, Bolivia. Mineral Deposits 31, 374–385.

De Silva, S.L., 1989. Altiplano-Puna volcanic complex of the Central Andes. Geology 17, 1102–1106.

Dill, H.G., 1998. Evolution of Sb mineralization in modern fold belts: a comparison of the Sb mineralisation in the Central Andes (Bolivia) and the Western Carpathians (Slovakia). Mineral Deposits 33, 359–378.

Einaudi, M.T., Hedenquist, J.W., Inan, E.E., 2003. Sulfidation state of fluids in active and extinct hydrothermal systems: transitions from porphyry to epithermal environments. Soc. Econ. Geol. Spec. Publ. 10, 285–312.

Goldstein, R.H., Reynolds, T.J., 1994. Systematics of fluid inclusions in diagenetic minerals. In: SEPM Short Course. Vol. 31. pp. 1–199.

Gorustovich, S.A., Monaldi, C.R., Salfity, J.A., 2011. Geology and metal ore deposits in Argentine Puna. In: Cenozoic Geology of the Central Andes of Argentina. SCS Publisher, pp. 169–187.

Grant, J.N., Halls, C., Salinas, W.A., Snelling, N.J., 1979. K-Ar ages of igneous rocks and mineralization in part of the Bolivian Tin Belt. Econ. Geol. 74, 838–851.

Hedenquist, J.F., Lowenstern, J.B., 1994. The role of magmas in the formation of hydrothermal ore deposits. Nature 370, 519–527.

Hedenquist, J.F., Arribas, R.A., Gonzales-Urien, E., 2000. Exploration for epithermal gold deposits. In: SEG Reviews. 13. pp. 245–277.

Heinrich, C.A., 1990. The chemistry of hydrothermal tin (–tungsten) ore deposition. Econ. Geol. 85, 457–481.

Heinrich, C.A., Eadington, P.J., 1986. Thermodynamic predictions of the hydrothermal chemistry of arsenic, and their significance for the paragenetic sequence of some cassiterite arsenopyrite-base metal sulfide deposits. Econ. Geol. 81, 511–529.

Hilton, D.R., Hammerschmidt, K., Teufel, S., Friedrichsen, H., 1993. Helium isotope characteristics of Andean geothermal fluids and lavas. Earth Planet. Sci. Lett. 120, 265–282.

Hoke, L., Hilton, D.R., Lamb, S.H., Hammerschmidt, K., Friedrichsen, H., 1994. ^{3}He evidence for a wide zone of active mantle melting beneath the Central Andes. Earth Planet. Sci. Lett. 128, 341–355.

Holdsworth, R.E., Butler, C.A., Roberts, A.M., 1997. The recognition of reactivation during continental deformation. J. Geol. Soc. 154, 73–78.

Hongn, F.D., 1995. Estructuras precámbricas y paleozoicas del basamento de la Puna oriental, su aplicación para el análisis regional de la faja eruptiva. Rev. Asoc. Geol. Argent. 49 (3–4), 256–268.

Jacobshagen, V., Müller, J.P., Wemmer, K., Manoutsoglou, E., 2002. Hercynian deformation and metamorphism in the Cordillera Oriental of Southern Bolivia, Central Andes. Tectonophysics 345 (1–4), 119–130.

John, D.A., 2001. Miocene and Early Pliocene epithermal gold-silver deposits in the northern Great Basin, Western United States: characteristics, distribution, and relationship to magmatism. Econ. Geol. 96, 1827–1853.

Kay, S.M., Coira, B., Viramonte, J., 1994. Young mafic back arc volcanic rocks as indicators of continental lithospheric delamination beneath the Argentine Puna plateau, Central Andes. J. Geophys. Res. 99, 24,323–24,339.

Kay, S.M., Coira, B.L., Caffe, P.J., Chen, C.-H., 2010. Regional chemical diversity, crustal and mantle sources and evolution of central Andean Puna plateau ignimbrites. J. Volcanol. Geotherm. Res. 198, 81–111.

Lehmann, B., Schneider, H.J., 1981. Stratabound tin deposits. In: Wolf, K.H. (Ed.), Handbook of Stratabound and Stratiform Ore Deposits. 9. Elsevier, Amsterdam, pp. 743–771.

Lucassen, F., Becchio, R., Wilke, H.G., Thirlwall, M.F., Viramonte, J., 2000. Proterozoic–Paleozoic development of the basement of the Central Andes (18°S–26°S) – a mobile belt of the South American craton. J. S. Am. Earth Sci. 13, 697–715.

Lüders, V., 2017. Contribution of infrared microscopy to studies of fluid inclusions hosted in some opaque ore minerals: possibilities, limitations, and perspectives. Mineral. Deposita 52, 663–673.

Lüders, V., Romer, R.L., Gilg, A., Bodnar, R.J., Pettke, T., Misantoni, D., 2009. A geochemical study of the Sweet Home Mine, Colorado Mineral Belt, USA: hydrothermal fluid evolution above a hypothesized granite cupola. Mineral. Deposita 44, 415–434.

Ludington, S., Orris, G.J., Cox, D.P., Long, K.R., Asher-Bolinder, S., 1992. Mineral deposit models: geology and mineral resources of the Altiplano and Cordillera Occidental, Bolivia. U.S. Geol. Surv. Bull. 1975, 63–90.

Malvicini, L., 1978. Las vestas de estano y plata de Minas Pirquitas (Pircas) PCIA. De Jujuy, Rebublica Argentina. Rev. Asoc. Argent. Mineral. Petrol. Sedimentol. 9 (1–2), 1–25.

Maro, G., Caffe, P.J., Trumbull, R.B., Romer, R.L., 2017. Neogene mafic magmatism in the Northern Puna plateau, Argentina: generation and evolution of a back-arc volcanic suite. J. Petrol. 58, 1591–1618.

Marrett, R.A., Allmendinger, R.W., Alonso, R.N., Drake, R.E., 1994. Late Cenozoic tectonic evolution of the Puna Plateau and adjacent foreland, northwestern Argentine Andes. J. S. Am. Earth Sci. 7, 179–208.

Mlynarczyk, M.S., William-Jones, A.E., 2005. The role of collisional tectonics in the metallogeny of the Central Andean Tin Belt. Earth Planet. Sci. Lett. 240, 656–667.

Mon, R., Salfity, J.A., 1995. Tectonic evolution of the Andes of northern Argentina. In: Tankard, A.J., Suarez, R., Welsink, H.J. (Eds.), Petroleum Basins of South America. Am. Assoc. Petr. Geol. Mem. 62. pp. 269–283.

Moncada, D., Mutchler, S., Nieto, A., Reynolds, T.J., Rimstidt, J.D., Bodnar, R.J., 2012. Mineral textures and fluid inclusion petrography of the epithermal Ag–Au deposits at Guanajuato, Mexico: application to exploration. J. Geochem. Explor. 114, 20–35.

Newell, D.L., Jessup, M.J., Hilton, D.R., Shaw, C., Hughes, C., 2015. Mantle-derived helium in hot springs of the cordillera Blanca, Peru: implications for mantle-to-crust fluid transfer in a flat-slab subduction setting. Chem. Geol. 417, 200–209.

Niedermann, S., Eugster, O., 1992. Noble gases in lunar anorthositic rocks 60018 and 65315: acquisition of terrestrial krypton and xenon indicating an irreversible adsorption process. Geochim. Cosmochim. Acta 56, 493–509.

Niedermann, S., Bach, W., Erzinger, J., 1997. Noble gas evidence for a lower mantle component in MORBs from the southern East Pacific rise: decoupling of helium and neon isotope systematics. Geochim. Cosmochim. Acta 61, 2697–2715.

Paar, W.H., Brodtkorb, M.K., Topa, D., Sureda, R.J., 1996. Caracterización mineralógica y química de algunas especies metalíferas del Yacimiento Pirquitas, Provinca de Jujuy, República Argentina: Parte 1. In: XIII Congr. Geol. Argent y III Congreso de Exploración de Hidrocarburos (III), pp. 141–158.

Paar, W.H., Melitich, R., Topa, D., Criddle, A.J., Brodtkorb, M.K., Amthauer, G., Tippelt, G., 2000. Suredaite, PbSnS3, a new mineral species from the Pirquitas Ag-Sn depotis, NW-Argentina: mineralogy and crystal structure. Am. Mineral. 85, 1066–1075.

Pan, Y.S., 1974. The Genesis of the Mexican-Type Tin Deposits in Acidic Volcanics (Ph.D. thesis). Columbia Univ. (286 p).

Peralta-Arnold, Y., Cabassi, J., Tassi, F., Caffe, P.J., Vaselli, O., 2017. Fluid geochemistry of a deep-seated geothermal resource in the Puna plateau (Jujuy Province, Argentina). J. Volcanol. Geotherm. Res. 338, 121–134.

Petersen, U., 1970. Metallogenic provinces in South America. Geol. Rundschau B. 1, 174–183.

Pilz, P., 2008. Ein neues magmatisch-tektonisches Modell zur Asthenosphärendynamik im Bereich der zentralandinen Subduktionszone Südamerikas (Ph.D. thesis). Institut für Geowissenschaften, Mathematisch-Naturwissenschaftliche Fakultät der Universität Potsdam.

Potter, R.W., 1977. Pressure corrections for fluid inclusion homogenization temperatures based on the volumetric properties of the system NaCl-H2O. US Geol. Surv. J. Res. 5, 603–607.

Rice, C.M., Steele, G.B., Barfod, D.N., Boyce, A.J., Pringle, M.S., 2005. Duration of magmatic, hydrothermal, and supergene activity at Cerro Rico de Potosi, Bolivia. Econ. Geol. 100, 1647–1656.

Riller, U., Petrinovic, I., Ramelow, J., Strecker, M., Oncken, O., 2001. Late Cenozoic tectonism, collapse caldera and plateau formation in the Central Andes. Earth Planet. Sci. Lett. 188, 299–311.

Risse, A., Trumbull, R.B., Kay, S.M., Coira, B., Romer, R.L., 2013. Petrology of late Neogene mafic volcanism in the southern Puna Plateau, Argentina: insights on the source, generation and evolution of mantle melts in a back-arc setting. J. Petrol. 54, 1963–1995.

Roedder, E., 1984. Fluid inclusions. Mineral. Soc. Am. Rev. Mineral. 12, 149–180.

Rosas, L.V., Avilia, J.C., 2013. Desarrollo minero de Pirquitas, provincia de Jujuy. In: Temas de Correlación Geológica III, Serie Correlación Geológica. 29(2). pp. 51–62.

Rye, R.O., Lufkin, J.L., Wasserman, M.D., 1990. Genesis of the rhyolite-hosted tin occurrences in the Black Range, New Mexico, as indicated by stable isotope studies. In:

Stein, H.J., Hannah, J.L. (Eds.), Ore-bearing Granite Systems: Petrogenesis and Mineralizing Processes. Geol. Soc. Am. Spec. Paper Vol. 246. pp. 233–250.

Sano, Y., Wakita, H., 1985. Geographical distribution of 3He/4He ratios in Japan: implications for arc tectonics and incipient magmatism. J. Geophys. Res. 90, 8729–8741.

Sillitoe, R.H., 1976. Andean mineralization: a model for the metallogeny of convergent plate margins. Geol. Assoc. Can. Spec. Pap. 14, 59–100.

Sillitoe, R.H., Hedenquist, J.W., 2003. Linkages between volcanotectonic settings, ore fluid compositions, and epithermal precious-metal deposits. Soc. Econ. Geol. Spec. Publ. 10, 315–343.

Silver Standard Resources Inc., 2017. Puna operation; Brownfields Development for Mine Life Extension. http://www.ssrmining.com/operations/production/puna/, Accessed date: 13 November 2017.

Slater, E.T., 2016. The Cortaderas Zone, Pirquitas Mine, NW Argentina: An Example of Miocene Epithermal Ag-Zn-Pb-Sn Mineralization in the Andean Tin Belt (MSc thesis). Laurentian University Sudbury, Ontario, Canada (113 p).

Smith, S.P., Kennedy, B.M., 1983. The solubility of noble gases in water and NaCl brine. Geochim. Cosmochim. Acta 47, 503–515.

Soler, M.M., Caffe, P.J., Coira, B.L., Onoe, A.T., Kay, S.M., 2007. Geology of the Vilama caldera: a new interpretation of a large-scale explosive event in the Central Andean plateau during the Upper Miocene. J. Volcanol. Geotherm. Res. 164, 27–53.

Steele-MacInnis, M., Lecumberri-Sanchez, P., Bodnar, R.J., 2012. HokieFlincs_H2O-NaCl: a Microsoft Excel spreadsheet for interpreting microthermometric data from fluid inclusions based on the PVTX properties of H2O-NaCl. Comput. Geosci. 49, 334–337.

Sterner, S.M., Bodnar, R.J., 1984. Synthetic fluid inclusions in quartz I. Compositional type synthesized and application to experimental geochemistry. Geochim. Cosmochim. Acta 48, 59–68.

Stuart, F.M., Burnard, P.G., Taylor, R.P., Turner, G., 1995. Resolving mantle and crustal contributions to ancient hydrothermal fluids: He-Ar isotopes in fluid inclusions from Dae Hwa W-Mo mineralisation, South Korea. Geochim. Cosmochim. Acta 59, 4663–4673.

Sugaki, A., Kitakaze, A., 1988. Tin-bearing minerals from Bolivian polymetallic deposits and their mineralization stages. Min. Geol. 38, 419–435.

Sugaki, A., Kojima, S., Shimada, N., 1988. Fluid inclusion studies of the polymetallic hydrothermal ore deposits in Bolivia. Miner. Depos. 23, 9–15.

Taylor, R.G., 1979. Geology of tin deposits. Dev. Econ. Geol. 11, 543.

Turneaure, F.S., 1960. A comparative study of major ore deposits of Central Bolivia. Part I. Econ. Geol. 55, 217–254.

Turneaure, F.S., 1971. The Bolivian tin-silver province. Econ. Geol. 66, 215–225.

Voldman, G.G., Albanesi, G.L., Ortega, G., Monaldi, C.R., Zeballo, F.J., Giuliano, M.E., 2012. Biostratigraphy of the Santa Rosita Formation (Furongian-Tremadocian) in its type area, Eastern Cordillera, NW Argentina. Geophys. Res. Abstr. 14.

Wagner, T., Mlynarczyk, M.S., William-Jones, A.E., Boyce, A.J., 2009. Stable isotope constraints on ore formation at the San Rafael tin-copper deposit, Southeast Peru. Econ. Geol. 104, 223–248.

4. Lead and sulfur isotopic composition of ore minerals from the polymetallic Pirquitas Ag-Sn-(Zn) deposit, Jujuy, Argentina.

4.1. Abstract

The Pirquitas Sn-Ag-(Zn) deposit is situated in the Northern Puna Plateau in NW Argentina, near the Bolivian border. It has been exploited since the early 1930's and was one of the most important Sn-Ag producing mine of the country. During a long time, little is known in detail about the origin and evolution of ore-forming process at Pirquitas. This paper reports an isotopic study of sulfur, lead and uranium in sulfates and sulfosalt ore crystals with U-Pb dating on wolframite from the late mineralization event II. The Pb isotopic ratios of sulfides and sulfosalt minerals are similar, with no spatial patterns standing out ($^{206}Pb/^{204}Pb$: 18.77 – 18.82; $^{207}Pb/^{204}Pb$: 15.67 – 15.73; $^{208}Pb/^{204}Pb$: 38.89 – 39.07). This is in agreements with data from pluton related polymetallic deposits in the Bolivian Tin Belt (BTB) and area close to Pirquitas. Fragments of wolframite shows variable lead isotopes ratios ($^{206}Pb/^{204}Pb$: 18.82 - 19.05; $^{207}Pb/^{204}Pb$ 15.64 - 15.74; $^{208}Pb/^{204}Pb$ 38.81 - 39.01) as well as Pb and U contents ranging from 2 to 11 ppm and from 13 to 63 ppm respectively. The relatively U-rich wolframite reflects more oxidizing conditions during the wolframite deposition. The $\delta^{34}S$ values of sulfide and sulfosalt minerals mostly plot in the range for sulfur derived from igneous rocks (-1 to +1.7‰ with rare exception in pyrite and marcasite between -6.3‰ and +2.5‰). Those values are similar to most of the $\delta^{34}S$ values measured in sulfides from pluton related polymetallic Sn-Ag deposits in the southern part of the BTB. They suggest that the main contribution of sulfur to the hydrothermal system at Pirquitas is likely to be magma-derived. The U-Pb calculated regression line corresponds to a theoretical "age" of 2.9 ± 9.1 Ma. Pirquitas mineralization are partly hosted by rocks of the Tiomayo Formation dated from 12 to 16 Ma and suggests that the late mineralization event is younger than 12 Ma.

Keywords:

Bolivian tin belt, Pirquitas, Sulfur isotopes, lead isotopes, Sn-Ag deposit, U/Pb dating.

Published as:

Desanois L, Lüders V, Romer RL, Trumbull RB, Caffe PJ (in preparation) Lead and sulfur isotopic composition of ore minerals from the polymetallic Pirquitas Ag-Sn-(Zn) deposit, Jujuy, Argentina.

4.2. Introduction

The Pirquitas Sn-Ag-(Zn) deposit is situated in the Northern Puna Plateau in NW Argentina, close to the Bolivian border (. 1). Underground mining for silver and tin at Pirquitas commenced in 1936 and continued until 1990 and restart with open pit mining in 2009 (Board 2011). From 2011 until its temporary closure in 2017, the deposit was operated by open pit mining and became the largest silver and tin producer in Argentina. Pirquitas shares many features with the well-known Sn-Ag deposits in the Bolivian Tin Belt (BTB) to the north, but there are also important differences. Many of the polymetallic Sn-Ag deposits in the BTB are directly related to magmatic-hydrothermal systems established during the Late Oligocene through Mid Miocene (e.g. Turneaure 1960; Sugaki and Kitakaze 1988; Dill 1998; Lehmann et al. 2000). Common features of the BTB deposits are widespread tourmalinization and/or the presence of salt-rich, high-temperature fluid inclusions in early stage mineralization (Sugaki et al. 1988; Lehmann et al. 2000). Both of those features are lacking at Pirquitas, and there is no geologic evidence of magmatism coeval with the mineralization at Pirquitas although a magmatic source of fluids was inferred from noble-gas isotope ratios of fluid inclusions trapped in ore minerals (Desanois et al., 2018). To better constrain the role of magmas in the hydrothermal mineralization at Pirquitas and to allow more detailed comparisons with the Sn-Ag deposits in the neighboring BTB, we determined the Pb and S isotopic composition of a suite of ore minerals from Pirquitas vein and breccia-hosted ores. We also report results of testing U-Pb isotope dating on wolframite from the deposit.

4.3. Mineralization at the Pirquitas deposit

The Pirquitas deposit is hosted by Ordovician metasediments (Santa Victoria Group; Turner, 1960) and comprises three ore types, namely: (1) polymetallic veins, (2) disseminated mineralization and (3) hydrothermal breccia ore bodies (Malvicini 1978; Paar et al. 1996; Slater 2016). Two main

mineralization events were distinguished by Malvicini (1978). The first event includes two stages (I-1 and I-2), the first of which is characterized by pyrrhotite partly replaced by pyrite, and accessory cassiterite and arsenopyrite. In stage I-2, colloform sphalerite precipitated with stannite and other Sn-sulfides, minor galena and various Sn-Ag sulfosalts which locally replace pyrrhotite, cassiterite, sphalerite and galena. The second mineralization event was responsible for the richest silver mineralization, with deposition of Pb-Sb-Ag-Bi-Cu-As sulfosalts which defines the end of hydrothermal activity in the Pirquitas deposit. Desanois et al. (2018) concluded from a fluid inclusion study that ore formation at Pirquitas involved at least 3 pulses of hydrothermal fluids giving the Event I-1, I-2, and II. Temperatures and salinity values from inclusions representing all pulses range from 190 to 370°C and 0 to 10.6 wt% NaCl, respectively. The highest Homogenization temperatures were measured in aqueous two-phase inclusions hosted in stage I-1 quartz. The temperature and fluid salinity decreased from early to late mineralization events, which was attributed to waning of the magmatic-hydrothermal system and/or increased admixing of meteoric water to the magmatic fluids.

The age of mineralization at Pirquitas is unknown but a maximum age of 12 to 16 Ma is inferred by the fact that mineralization is partly hosted by rocks of the Tiomayo Formation of that age (Slater, 2016; Caffe and Coira, 2002). Other polymetallic ore deposits in the northern Puna and the southern BTB, with which Pirquitas may be related, yielded ages between 13 and 16 Ma (e.g., Chinchillas, 13 ± 1 Ma, Pan de Azúcar 12 ± 2 Ma, Potosí 13.8 ± 0.2 Ma, Chocaya 13.8 ± 0.2 Ma, Tatasi 15.6 ± 0.3 Ma) (Grant et al. 1979; Linares and Gonzalez 1990; Cunningham et al. 1991; Coira 1994; Zartman and Cunningham 1995). There is extensive mid- to late Miocene magmatic activity in the region around Pirquitas, but no igneous rocks occur at the mine site, nor did drilling to 800 m depth intersect an intrusion (Soler et al. 2008). The closest outcrops of igneous rocks are dacitic ignimbrites of Cerro Granada, and the granodiorite of Cerro Galán. The first one is dated between 9.8 and 7.8 Ma (Caffe, 2008) and its eruptive center is located 16 km north of the deposit. The granodiorite of Cerro Galán is located some 12 km east of Pirquitas but is undated. It is assumed to belong to the 6.6 Ma Coranzuli caldera complex (Caffe, 2008).

The polymetallic Sn-Ag-(Zn) mineralization at Pirquitas is considered to be of the low to intermediate sulfidation type (Slater 2016; Desanois et al. 2018), and comparable to those in the southern part of the

BTB (e.g. Potosí, Sud Lipez, Quechisia) the world-class polymetallic Sn-Ag deposit Cerro Rico de Potosí, the Sud Lipez deposits, and the Quechisia deposit (Sugaki et al. 1983; Zartman et al. 1995; Cunningham et al. 1996).

4.4. Lead and sulfur isotope ratios in the Bolivian Tin Belt

Before presenting the results of this study it is useful to summarize existing information on Pb-S isotopic composition of ores in the BTB, which provide an important context for the Pirquitas results. Two distinct types of metal deposits occur in this belt. The first is mostly located in the northern part of the BTB and is defined by deep-seated hydrothermal (mesothermal-hypothermal) vein-type tin–tungsten mineralization related to different periods of granitic intrusions (Late Paleozoic, late Triassic, early and middle Tertiary) (Turneaure 1971). The second type is typical for the southern part of the BTB and it involves polymetallic epithermal deposits with Sn, Ag, Pb, W, Zn, Sb, and Bi mineralization related to subvolcanic intrusions and dome complexes of Miocene to Pliocene age (Turneaure 1971; Sugaki et al. 1988; Coira et al. 2004). Generally, the age and style of polymetallic deposits in the southern part of the BTB changes from north to south. Late Oligocene-Early Miocene high-sulfidation ore deposits in the north are separated from younger (Middle Miocene to early Pliocene), intermediate to low-sulfidation ore associations in the south (Sillitoe et al. 1975; Grant et al. 1979; Sugaki and Katakaze 1988; Sugaki et al. 1990). Tilton (1981) and later workers (Macfarlane et al. 1990; Petersen 1993; Aitcheson et al., 1995; Kamenov et al. 2002; Mamani et al. 2008) have defined a regional provinciality of lead isotope ratios, using data from ore deposits including the BTB, as well as from the Central Andes magmatic arcs and basement rocks. Three lead isotope provinces were so first defined (Macfarlane et al. 1990) and a fourth one was defined later by Kamenov et al. (2002) (Fig. 18), with province I in the coastal magmatic arc of Chile and southern Peru, province II in the Mesozoic sedimentary belt in the western Cordillera in Peru and northern Chile, province III located in the eastern Cordillera of SE Peru, central Bolivia and the northern Puna from NW Argentina; and province IV crosscutting the latter two.

Province III hosts the ore deposits in the BTB and the Pirquitas deposit as well. This lead-isotope province is distinguished from the others by higher values of $^{208}Pb/^{204}Pb$ and $^{207}Pb/^{204}Pb$ relative to $^{206}Pb/^{204}Pb$, and also by a wider range in Pb-isotope ratios overall compared to other provinces. Within this range, Macfarlane et al. (1990) recognized a division located near the Bolivia-Peru border, which they related to the local basement (see Fig. 18). Ores in the southern part of the province (IIIa), which includes Pirquitas and most of the BTB, has less-radiogenic Pb than those from northern province, (IIIb). Macfarlane et al. (1990) explained this difference by a change in the regional geology, with Precambrian basement in the northern province and Paleozoic sedimentary strata in the southern. The distinctive Pb-isotope composition of the San Cristobal Ag-Zn deposit, which lies in domain IIIa, led Kamenov et al. (2002) to define a fourth province (IV). This last one extend from the coastal area of southern Peru and western Bolivia to the San Cristobal mining district (Fig. 18 with the major part of ore lead originating from the local metamorphic basement).

Sugaki et al. (1990a) determined the sulfur isotopic composition of galena, sphalerite, pyrite and other sulfides and sulfosalts from several deposits in the BTB. Ore deposits in the northern Oruro-Potosí district, in the central to northern BTB, have negative $\delta^{34}S$ values down to -8.6‰ (cf. Morcocala, Fig. 21). Sulfide $\delta^{34}S$ values from the southern part of the district show a minimum of -2.0‰ (e.g., Porco, Fig. 21). Deposits in the north of the district are hosted by Silurian sedimentary formation (quartzite, sandstones, and slate). In comparison, southern deposits are hosted by Ordovician metasediments (sandstone and slate) and have less negative $\delta^{34}S$.

It shows a bimodal distribution of $\delta^{34}S$ between the north and the south of the Oruro-Potosi district, with wider $\delta^{34}S$ ranges in the north from -8.6 to 15.6‰ (cf. Morococala and Viloco). The authors explained the regional variations by different sources for sulfur, which they related to the contrasting geologic settings of deposits in the northern and southern parts of the BTB. For the north, Sugaki et al. (1990a) proposed that sulfur is mainly derived from magmatic sources but with some mixing with sulfur leached from sedimentary units of the country rocks. The sulfide minerals from polymetallic vein-type Sn-Ag deposits in the southernmost part of the BTB, the closest geographically from Pirquitas, mostly have $\delta^{34}S$ values between -2.5 and 3.5‰ (Fig. 21).

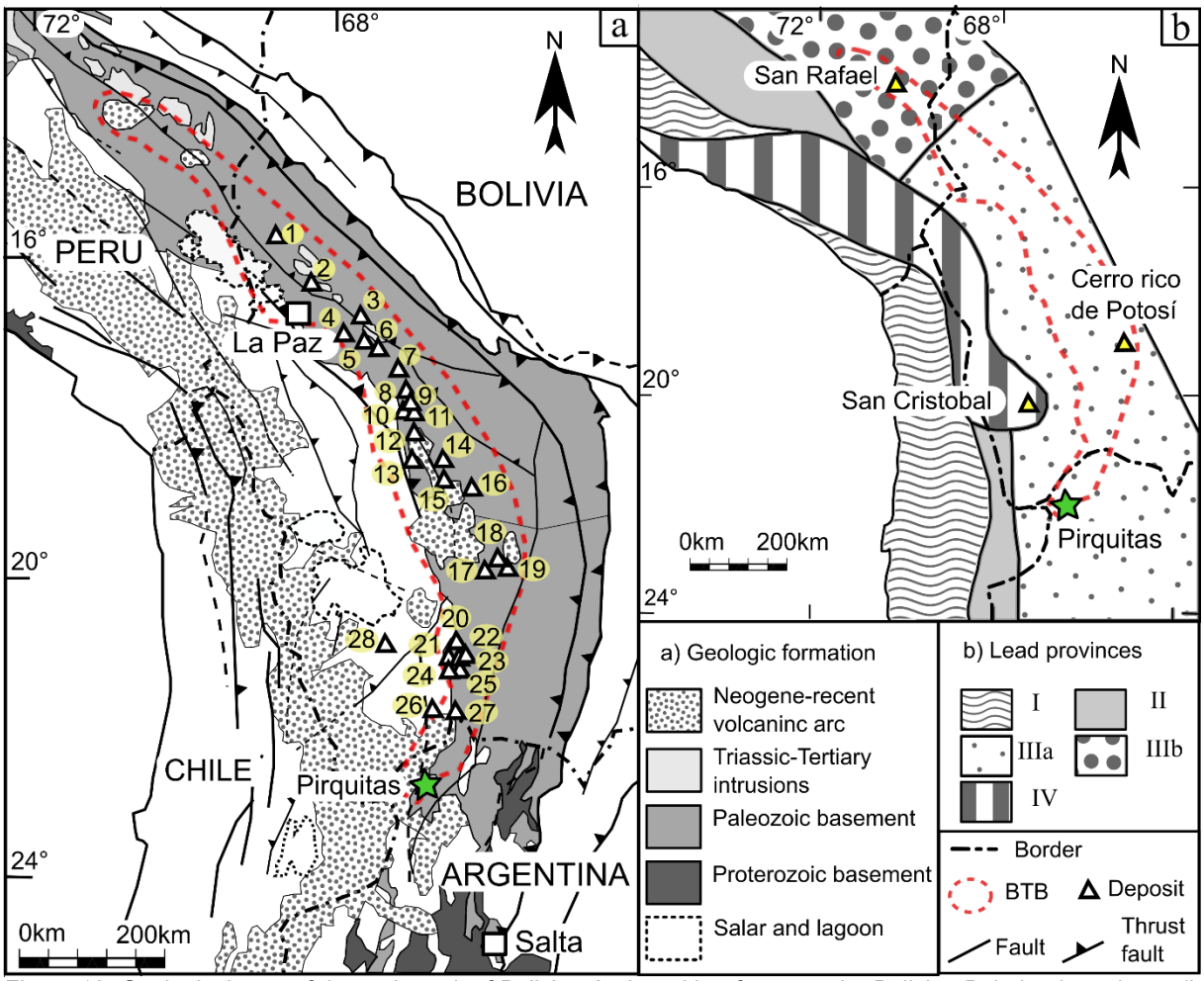

Figure 18. Geological map of the major unit of Bolivian Andes with a focus on the Bolivian Belt, lead provinces (I, II, III; IV) and major deposits: Matilde (1), Kellhuani (2), Chojilla (3), Milluni (4), Caracoles (5), Colquiri (6), Colquiri (7), San Jose (8), Japo (9), Huanuni (10), Bolivar (11), Oruro (12), Avicaya (13), Morococala (14), Llallagua (15), Colquechaca (16), Kumurana (17), Cerro Rico de Potosí (18), Illimani (19), Tasna (20), Animas (21), Sieste Suyos (22), Chorolque (23), Chocaya (24), Tatasi (25), San Antonio de Lipez (26), Santa Rosa (27) San Cristobal (28).

4.5. Sampling and methods

Fifteen samples were selected for S-isotopic analyses to represent the different mineralization stages and localities in the Pirquitas mine area, from the Oploca and San Miguel veins to the Potosí breccia described in Desanois et al. (2018). The hand-picked minerals include pyrite, marcasite, and arsenopyrite from mineralization stage I-1; pyrargyrite, pirquitasite and sphalerite from stage I-2; and cylindrite, frankeite, suredaite and galena from mineralization stage II. The sulfur isotope measurements on these minerals were performed at the Geologisch-Paläontologisches Institut, Westfälische Wilhelms-Universität Münster, Germany. Pure mineral separates (visual inspection) were thoroughly mixed with V_2O_5 and measured directly online for their sulfur isotopic composition using an Elemental Analyzer connected to a Thermo Finnigan Delta V Plus mass spectrometer. Reproducibility was better than 0.2‰ and reported in the standard delta notation against the Vienna-Canyon Diablo troilite standard (VCDT).

A subset of 6 sulfide and sulfosalt minerals were also analyzed for Pb isotopic compositions at GFZ German Research Centre for Geosciences (Potsdam), following the analytical procedure described by Romer et al. (2005). The samples originate from the Potosí breccia and veins at Oploca and San Miguel. They comprise both mineralization events I and II. Hand-picked, visibly pure separates of andorite, cylindrite, galena, pyrite, and sphalerite were dissolved in 7N HNO_3 overnight on a hot plate at 180°C. In addition, a wolframite sample from the Oploca veins and associated to event II mineralization was analyzed. Wolframite is intensely intergrown with quartz and sulfide minerals. The sulfide minerals were selectively dissolved using 1N HNO_3. A mixed ^{205}Pb–^{235}U tracer was added to the wolframite samples prior to dissolving in 40% HF overnight in closed screw-top Teflon vials on a 160°C hot plate. Lead and U were separated in ion exchange columns. Lead and U were loaded with silica-gel and H_3PO_4 on separate Re single-filament. Their isotopic composition was measured at 1200 – 1260 °C and at 1300-1380°C, respectively, using a Thermo-Fisher Scientific TRITON TIMS mass spectrometer operated in static or dynamic multi-collection using Faraday collectors. Instrumental fractionation was corrected with 0.1%/a.m.u. Precision of Pb measurements were better than 0.1% at the 2-sigma level. For the Pb-rich sulfide minerals, no age correction was calculated.

4.6. Results

4.6.1. Pb and U isotopes

The Pb isotopic ratios of sulfides and sulfosalt minerals are listed in Table 3 and plotted in Figure 19. Wolframites Pb and U/Pb ratios are listed in Table 4. The six sulfide and sulfosalt samples show similar lead isotope ratios ($^{206}Pb/^{204}Pb$: 18.77 – 18.82; $^{207}Pb/^{204}Pb$: 15.67 – 15.73; $^{208}Pb/^{204}Pb$: 38.89 – 39.07). No spatial patterns stand out, nor is there a difference according to the mineralization event. The most radiogenic and the least radiogenic Pb-isotope ratios in the sulfide and sulfosalts were measured respectively in galena and in cylindrite, both from the event II of mineralization. All Pb-isotope ratios plot near the border between lead compositions of Province II and IIIa (Fig. 19). Millimeter size fragments of a wolframite crystal were hand-picked for dating (Fig. 20) yielded variable lead isotope ratios ($^{206}Pb/^{204}Pb$: 18.82 - 19.05; $^{207}Pb/^{204}Pb$ 15.64 - 15.74; $^{208}Pb/^{204}Pb$ 38.81 - 39.01).

Table 3.Lead isotope composition of sulfide minerals from Mina Pirquitas, Argentina.

Samples [a]	Event	^{206}Pb [b] / ^{204}Pb	^{207}Pb [b] / ^{204}Pb	^{208}Pb [b] / ^{204}Pb
Pyrite Pq-16-07	I-1	18.808	15.713	39.028
Pyrite Pq-Pag-24	I-1	18.801	15.715	39.032
Galena PQ-16-11	I-2	18.819	15.725	39.070
Sphalerite Pq-16-11	I-2	18.807	15.710	39.021
Cylindrite 4	II	18.767	15.671	38.890
Andorite 3112	II	18.799	15.717	39.034

[a] For details on samples dissolution and separation of Pb see Romer et al. (2005) and Romer and Hahne (2010).

[b] Lead isotope analyses were performed at Deutsches GeoForschungsZentrum (GFZ), Potsdam, Germany, using a TRITON multi-collector mass-spectrometer. The lead isotopic composition is corrected for mass discrimination with 0.1%/a.m.u., as estimated from the repeated measurement of Pb reference material NBS981. Overall 2□ uncertainties, including measurement error and uncertainties for corrections of mass discrimination, are less than 0.1%.

Wolframite is an extremely rare mineral at Pirquitas. It formed at the beginning second mineralization event (Paar pers. comm.), but it has special importance because of the potential for U-Pb dating (Romer and Lüders 2006). The U and Pb contents and Pb-isotope ratios of Pirquitas wolframite are listed in Table 4. The four wolframite fragments yielded more radiogenic Pb-isotope ratios compared

to those of sulfides and sulfosalts. Wolframite is also characterized by variable Pb and U content ranging from 2 to 11 ppm and from 13 to 63 ppm, respectively. The original crystal shows no particular zonation. By comparison, wolframite worldwide typically has uranium concentrations that are less than 5 ppm (e.g. Swart and Moore 1982; Tindle and Webb 1989; Ferenc and Uher 2007; Goldmann et al. 2013).

The U and Pb isotope ratios of wolframite are plotted on an isochron diagram in Figure 20. Linear regression of all four points failed to define an isochron, but the slope of the line on Figure 20 corresponds to an age of 2.9 Ma, which is relatively consistent with geologic constraints showing that the mineralization is younger than 16 Ma, but provides no further constraints on the age.

Table 4. Results of uranium and lead isotope dating of wolframite from the Pirquitas deposit

Sample [c]	Pb [a] [ppm]	U [a] [ppm]	^{206}Pb [b] / ^{204}Pb	^{207}Pb [b] / ^{204}Pb	^{208}Pb [b] / ^{204}Pb	^{238}U [b] / ^{204}Pb
1	11.01	63.14	18.931	15.654	38.809	369
2	2.524	28.77	19.052	15.642	38.747	734
3	4.16	13.67	18.942	15.741	39.009	212
4	3.98	14.65	18.817	15.645	38.745	236

[a] Concentrations determined by isotope dilution using a mixed ^{205}Pb-^{235}U tracer.

[b] Lead isotope analyses were performed at GeoForschungsZentrum Potsdam, Germany, using a Thermo-Fisher Triton multicollector mass spectrometer. The lead isotopic composition is corrected for mass discrimination with 0.1%/a.m.u. and Pb contributions from blank and tracer. 2□uncertainties are less than 0.1%.

[c] Samples 1 to 4 are fragments from the same crystal.

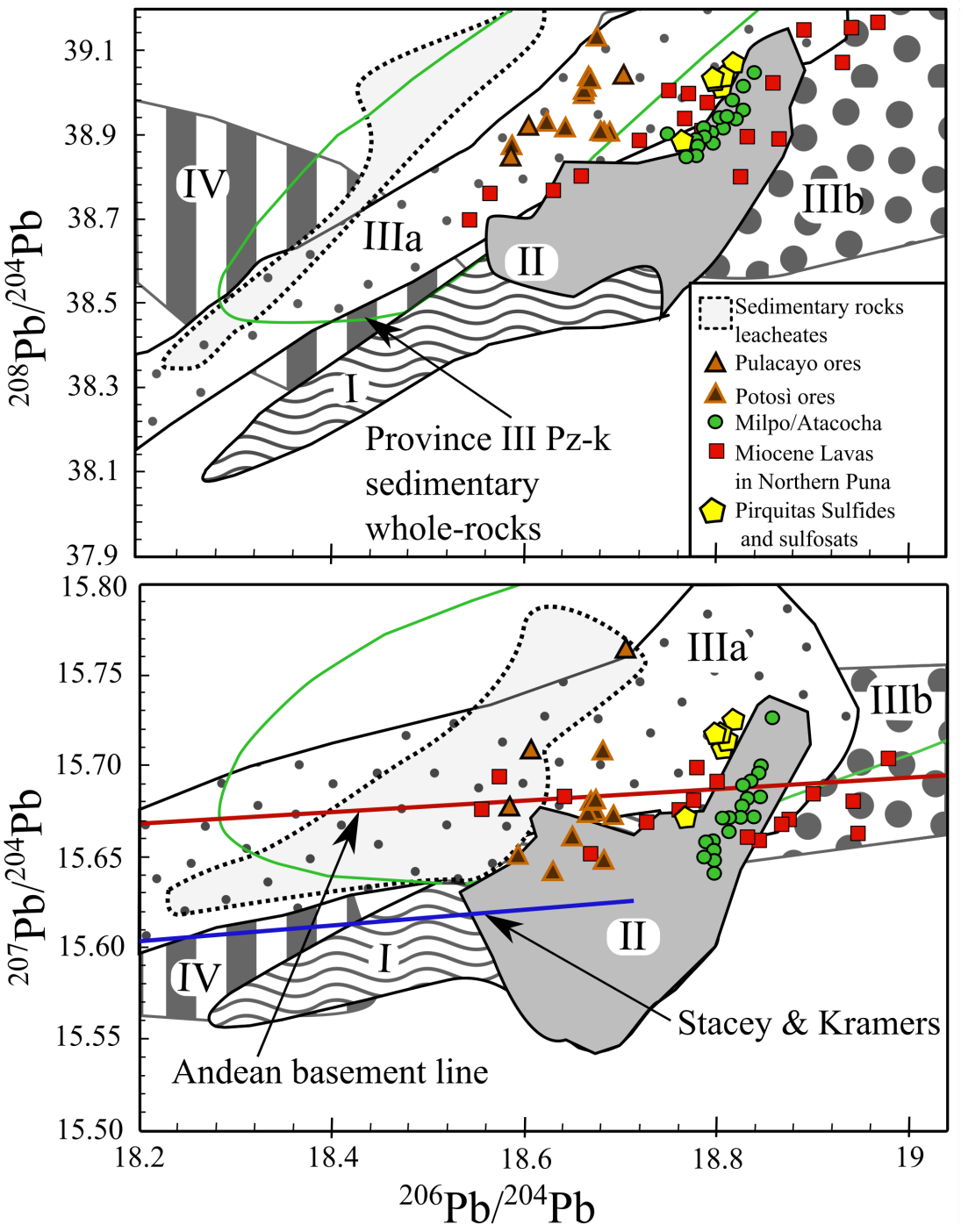

Figure 19. Pb isotope ratios of Pirquitas plot in 207Pb/204Pb vs 206Pb/204Pb and 208Pb/204Pb vs 206Pb/204Pb diagrams with BTB deposits and lead provinces defined by (Macfarlane et al. 1990), Petersen et al. (1993), and Kamenov et al. (2002). Data fields of Pulacayo, Potosì and Milipo/Atachocah where build with data from Macfarlane et al. (1990) and Kamenov et al. (2002); the Miocene Lavas in Northern Puna data field was build with data from Ort et al. (1996) Zentilli et al. (1988), Matteini et al. (2002), Caffe et al. (2002) and unpublished data. Stacey & Kramers line is corresponding to the Crustal lead development line (S and K) from Stacey and Kramers (1975) and the Andean basement line is described by a Post-Archean 238U/204Pb ratio (A-ratio) of 10 and fits many of the whole rock lead data from the Central Andes in Lucassen et al. (2002).

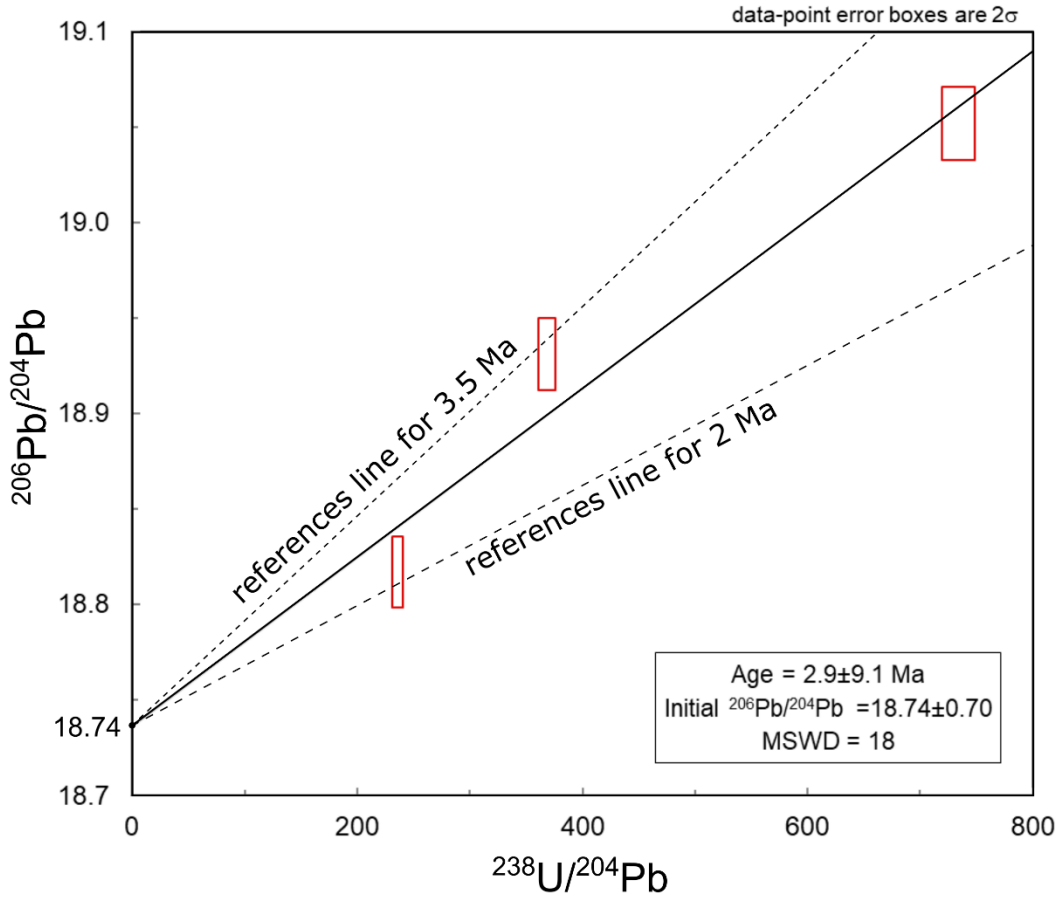

Figure 20. Pb isochron diagram of the fragments from a single wolframite crystal from Pirquitas mineralizations. With only three point it is difficult to build a clear reference line. The calculated age for the wolframite fragments is 2.9±9.1 Ma.

4.6.2. Sulfur isotopes

The sulfur isotope ratios of sulfide and sulfosalt minerals from Pirquitas are shown in Table 5. The widest range of $\delta^{34}S$ values was obtained from stage I-1 pyrite and marcasite from the San Miguel vein system, which vary between -6.3‰ and +2.5‰. All samples from later mineralization stages yielded a much narrower range of $\delta^{34}S$ between -1 and +1.7‰, suggesting a homogeneous sulfur source. Sulfur isotope thermometry could not be applied because mineral pairs have form contemporaneously in equilibrium but many of the selected samples did not occurred during the same mineralization event. That leaves us only the galena-sphalerite pair from the Potosí breccia, which is too weak to constrain an isotopic temperature. Furthermore, Sugaki et al. (1990) found S-isotope disequilibrium pairs in ore minerals in the BTB and then restricted use of the thermometer.

Table 5. Sulfur Isotope composition of ore minerals from the Pirquitas deposit.

Sample [a]	Event	Location	Mineral	$\delta^{34}S$ [b] (‰)
PQ-POG-24	I-1	Oploca	Pyrite	1.5
PQ-POG-29	I-1	Oploca	Arsenopyrite	0.9
PQ-POG-29	I-1	Oploca	Pyrite	2.4
PQ-16-07	I-1	San Miguel	Pyrite	2.5
PQ-16-12A	I-1	San Miguel	Marcasite	-3.7
PQ-16-03	I-1	San Miguel	Pyrite-Marcasite	-6.3
PQ-16-01	I-2	San Miguel	Pyrargyrite	-0.9
PQ-16-12A	I-2	San Miguel	Sphalerite	1.7
3	I-2	Oploca	Pirquitasite	1.1
PQ-16-09	I-2	Potosi	Galena	-1
PQ-16-11	I-2	Potosi	Sphalerite	1.5
1	II	Oploca	Frankeite	0.2
4	II	Oploca	Cylindrite	0.6
PQ-POG-29	II	Oploca	Sphalerite	1
N7-SN4-G4	II	Oploca	Suredaite	0.5

[a] For details on samples dissolution and separation of S see Lin et al. (2017).

[b] The sulfur isotope measurements were performed at the Westfälische Wilhelms-Universität Münster, Germany usning a Elemental Analyzer connected to a Thermo Finnigan Delta V Plus mass spectrometer. The suflur isotopic composition was estimate with a reproducibility better than 0.2‰ and reported in the standard delta notation against the Vienna-Canyon Diablo troilite standard (VCDT).

4.7. Discussion

Sulfur isotope constraints on the sulfur source

Sulfur isotope composition of sulfide minerals can be a strong tool for tracing interactions of magmas with their country rocks. It is possible if the S isotopic composition of the magma is clearly different from that of the country rock (Seal 2006). The majority of $\delta^{34}S$ values of sulfides and sulfosalts from Pirquitas plot in the range for sulfur derived from igneous rocks (e.g. MORB; $\delta^{34}S = -0.3 \pm 2.3$‰; andesites: $\delta^{34}S = 2.6 \pm 2.3$‰) (Rye et al. 1984; Luhr and Logan 2002; Seal 2006). The same holds true for most of the $\delta^{34}S$ values measured in sulfides from polymetallic Sn-Ag deposits in the southern part of the BTB that show direct relationship with subvolcanic intrusions. A north-south variation in S-isotopic ratios in the BTB was noted above and shows in the Figure 21, which was attributed to a regional difference in the country rocks (Sugaki et al., 1990). However, the majority of BTB $\delta^{34}S$ values cluster between -5 and 5‰ and are consistent with a magmatic origin of the sulfur with minor

but significant influence of the country rocks (Ohmoto and Goldhaber 1997; Seal 2006). Thus, we suggest that the main contribution of sulfur to the hydrothermal system at Pirquitas is likely to be magma-derived. This supports the evidence for magmatic fluids given by He-isotope ratios in Pirquitas ore minerals (Desanois et al., 2018).

However, the sulfur isotope ratios of Pirquitas pyrite and marcasite from the San Miguel vein system are lower than the rest (-6.3 to -3.9‰) and extend outside the "magmatic" range. These minerals

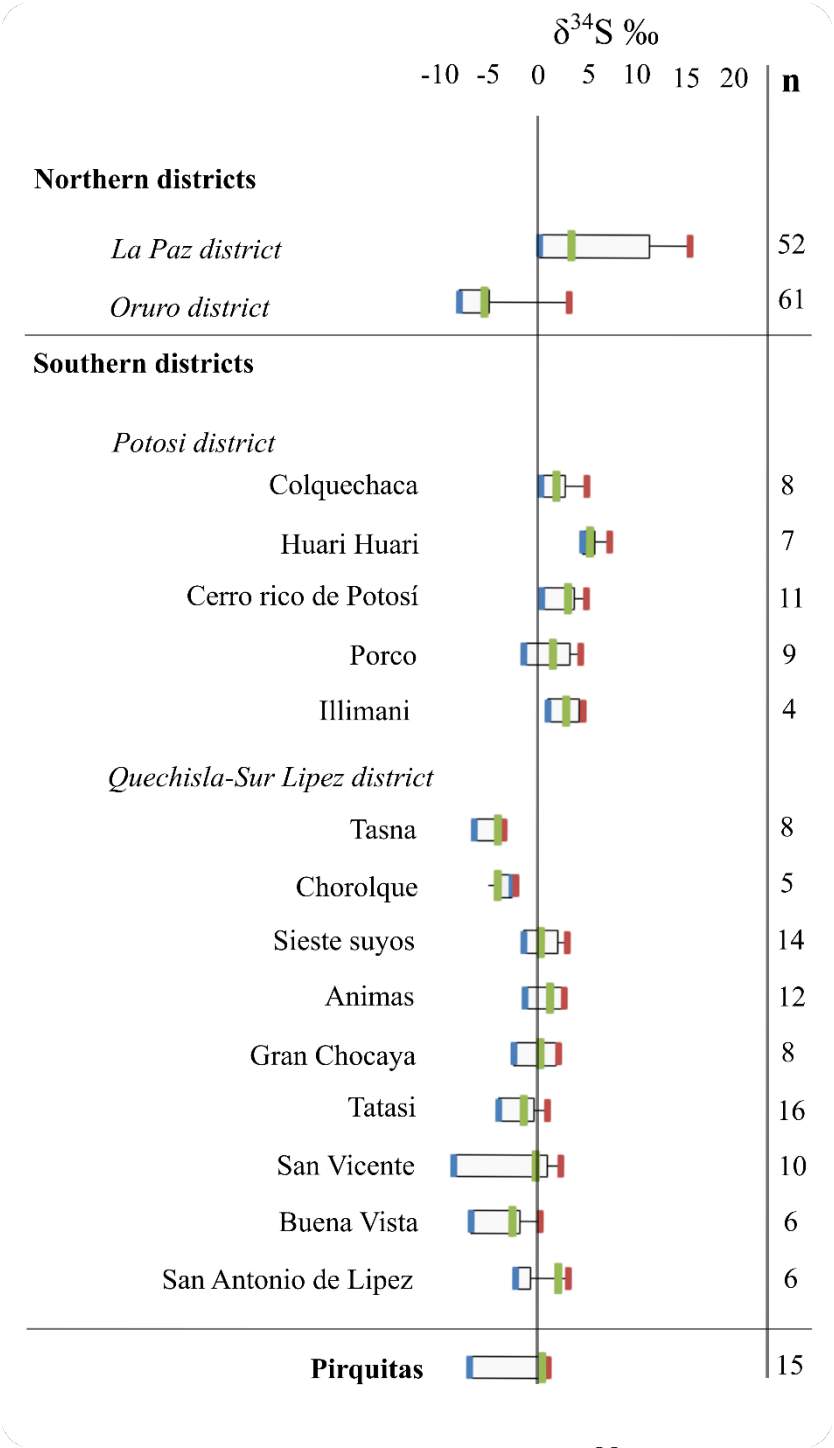

Figure 21. Sulfur isotope ratios in Pirquitas compared with data from southern BTB deposits reported by Sugaki et al. (1990). Deposits are listed from top to bottom on the vertical axis according to latitude. Blue, red, and green lines represent the minimum, maximum and median values for each deposit, respectively; n gives the number of analyses from each deposit.

correspond to the earliest mineralization stage I-1, which is not rich in tin or silver. Negative $\delta^{34}S$ values are not common in the Sn-Ag deposits of the BTB but they do occur, notably at Buena Vista, Tasna, and Chorolque (Fig. 21). Sugaki et al. (1990a) suggested that these low values reflect the influence of sulfur derived from the sedimentary country rocks, and given that Pirquitas is hosted by similar, early Paleozoic (meta)sedimentary rocks. This explanation seems reasonable for Pirquitas as well and is supported by the isotopic data of sulfides (AsPy, Py, and Galena) in the Paleozoic basement, whose δ34S range between -9.5 and -13.7‰ (Rodriguez 2004).

It is significant that negative $\delta^{34}S$ values in our study were found only in samples representing the first event of mineralization, which also yielded the widest range of values (-6.3 to 2.4‰). An explanation for this can be that the hydrothermal system initially involved more assimilation of sulfur from the country rocks but, as the mineralization intensified, the hydrothermal fluid was more homogeneous and carried mostly magmatic-derived sulfur. Interestingly, the first mineralization stage was also distinctive in terms of He-isotope data reported by Desanois et al. (2018). Stage I-1 minerals yielded the largest range of $^{3}He/^{4}He$ ratios (0.5 to 4.1 Ra), which was explained by mixing of magmatic and meteoric-derived helium. The lowest value, 0.5 Ra, corresponds to negligible magmatic input. Similar to the S-isotope results, the He-data from later mineralization stages are more homogeneous and suggest a significant magmatic input.

Lead isotopes and metal sources

The lead isotope ratios of ore minerals from the Pirquitas deposit are plotted in Figure 19 with data from other ore deposits in the BTB and the Central Andes lead provinces from Macfarlane et al. (1990) and Kamenov et al. (2002). On the Pb-Pb isotope plots, the Pirquitas samples show relatively high $^{206}Pb/^{204}Pb$ ratios compared with ratios from the sulfide minerals of Cerro Rico de Potosí in the province IIIa. In fact, the Pb isotope range of the Pirquitas ores is very similar to that of the Milpo-Atachocha deposit from lead province II in the western cordillera of southern Peru (Kamenov et al., 2002). Similar signature were found in the region nearby Pirquitas (Sangster, 2002). These data suggest that most Pb bearing ores in the area are identical to Cerro Rico de Potosi, and then typically from province IIIa. Macfarlane et al. (1990) argued from Pb and Sr isotope evidence that deposits in

the southern part of province II have a stronger crustal signature and thus more radiogenic Pb than those farther norths. Such signature is possibly related to the greater crustal thickness in the Altiplano region in the south. Deposits of the southern province II shows Pb ratios close to Pirquitas ratios. It is reasonable that a stronger assimilation of crustal Pb can explain the difference between Potosí and Pirquitas Pb isotope compositions despite their similar mineralogy and S-isotopic compositions. However, other deposits in the northern Puna as Minas Viejas, Concordia, Salle, Armonia, and La Esperanza are all similar to Pirquitas, and oppositely to what Macfarlane speculate, these are closely related to sedimentary Cretaceous rocks, either regionally or directly emplaced on a Cretaceous basement.

An important feature of the Pb isotope composition of ores plotted on Fig. 19 are the parallel linear trends defined by Potosí, Pulacayo and Milpo/Atacocha ores, Interestingly, Pirquitas shows the same trend. It can be noticed that the Pirquitas trend is essentially made up of a cluster of 5 points and an outlier corresponding to cylindrite of event II (Table 3). As pointed out earlier by Kamenov et al. (2002), these trends are not parallel with Pb-evolution lines (cf. Stacey-Kramer and Andean evolution lines, Fig. 19b), and therefore represent mixing between two or more Pb sources. Macfarlane et al. (1990) and Kamenov et al. (2002) proposed two fundamental sources: (1) the magma source region, which includes the mantle wedge and the lower crust (the MASH zone of Hildreth and Moorbath 1988), and (2) lead source(s) in the upper crust. The latter can be Paleozoic or Mesozoic sedimentary rocks or Precambrian basement depending on location. For Pirquitas, the upper crustal source would be the Ordovician sedimentary units of the Acoite formation.

Kamenov et al. (2002) determined the whole-rock isotopic composition of Pb in early Paleozoic sediments from the southern BTB, and they also analyzed the Pb-isotope ratios of experimental leachates designed to mimic hydrothermal alteration of these units at 200°C by acidic and saline fluids. The results (Fig. 19) showed a wide range of Pb-isotope ratios for the whole-rock data that covers all Pb compositions from BTB ores, but the composition of leachates was more restricted, much less radiogenic, and thus no longer fitting the ore-lead compositions. The authors concluded that Pb mobilized from upper-crustal sediments by hot fluids is not able to explain the radiogenic ores

compositions, but that assimilation of radiogenic Pb from the country rocks must take place via partial melting and incorporation into the magmas.

Studies of the isotopic composition and petrogenesis of Cenozoic arc and back-arc magmas in the northern Puna are consistent with the scenario proposed by Kamenov et al. (2002) (Tilton and Clark, 1981; Aitcheson et al., 1995; Caffe et al., 2002). For example, Caffe et al. (2002) concluded that trace-element and isotopic composition of mid-Miocene magmas in northern Argentina require assimilation of upper crustal partial melts by mafic arc magmas. We consider it is significant that the Pb isotope data from the magmatic rocks also defines a linear trend on Fig. 19 and is parallel to that of the ore lead. In other words, the Cenozoic magmas also contain a mixed Pb-isotope signature that seems to have been inherited in the BTB ore deposits and in Pirquitas ores. The source of the radiogenic Pb component in this mixing scenario is in the Ordovician sedimentary sequence.

Wolframite composition and attempted U-Pb dating

As mentioned above, the U and Pb contents of wolframite from Pirquitas are giving variable U/Pb ratios between 212 and 734 (Fig 20). Given that the redox state and the capacity to form ligand complexes are major factors controlling the mobility of U in aqueous solution (Langmuir 1976). The high U contents in wolframite may have implications for the fluids that formed it. Uranium is mobile in the hexavalent form, typically complexed with O as (UO_2^{2+}), while it is poorly soluble in its reduced, tetravalent form (U^{4+}). Therefore, redox conditions may influence the U content in wolframite crystals in addition to the U availability in the hydrothermal system (Harlaux et al., 2018). U-rich wolframite of Pirquitas may thus reflect oxidizing conditions at the time of deposition. Wolframite in Pirquitas is a rare mineral and it forms during event II, corresponding to last pulse of acidic magmatic fluid (Desanois et al. 2018) that allowed the transport of metals such as Sn, Sb, Zn, Pb and W, beside reduced sulfur. Cassiterite and other Sn sulfosalt from the event I seems to not have been dissolved. It indicate that tin in minerals of the Event 2 was exsolved from a magmatic fluid or remobilized from the wall rock by hydrothermal leaching, as well as U and W. Then the dilution with meteoric fluids allowed the deposition of those metals in sulfides and sulfosalts associated to tin oxide (wood tin cassiterite) and wolframite reflecting more oxidizing condition. The tin hydrothermal

transportation in such oxidizing conditions is possible as Sn(IV) chloride complexes as suggested by Schmidt (2018).

The U-Pb isotopic composition of wolframite fragments failed to define an isochron (Fig. 19b) and the calculated regression line corresponds to a theoretical "age" of 2.9 ± 9.1 Ma, to which no geological significance can be attached. To date, only a few dating attempts on wolframite have been published (Frei et al. 1998; Romer and Lüders 2006; Pfaff et al. 2009; Lecumberri-Sanchez et al. 2014; Harlaux et al., 2018). Also, while the Pirquitas wolframite has relatively high U contents compared to most wolframite found worldwide, it still has much lowers U contents than wolframites usually used in studies cited above for U-Pb dating. Lower U concentration can be a source of complication in dating because the amount of radiogenic Pb will be low and the influence of common Pb variations, due to Pb-bearing phases (e.g. sulfides) in micro-cracks, grain boundaries or inclusions, will be correspondingly strong. The most important identified factor that influences the measurement in our case was the presence of lead sulfide and sulfate inclusions in the wolframite crystal.

The previous age estimation of Pirquitas made by structural observation gives an upper limit of the mineralization age under 15Ma. Despite the unprecise measurement of the U-Pb, the new estimation definitely gives an age younger than 15Ma for the mineralization. Even if no mineralization related to volcanism was clearly observed, it is possible that the Pirquitas mineralization were influenced by the magmatic activity during the late Quechua phase (9 to 6 Ma) as suggest the age of volcanic centers in the Pirquitas district area. The possibility that Sn stays in the magma and redistribution occurs by later fluids has been considered. In such condition, the fluids may have leached the magmatic rocks distinctly after emplacement of these rocks and mobilized W, U, and Sn.

4.8. Conclusions

Sulfur isotope compositions of Pirquitas ores show $\delta^{34}S$ typical for magmatic sources. $\delta^{34}S$ is similar to most of the BTB polymetallic deposits, which unlike Pirquitas, are in direct relationship with subvolcanic intrusions. The hydrothermal system at Pirquitas most probably evolved from an initial, larger assimilation of sulfur from the country rocks at the onset of mineralization, indicated by lowest $\delta^{34}S$ values measured in stage I-1 pyrite. However, in subsequent mineralization stages when

deposition of the majority of silver and tin occurred, the hydrothermal fluid was isotopically more homogeneous and carried mostly magmatic-derived sulfur. Regarding overall lead isotopes studies in the Central Andes and the strong magmatic sulfur isotopic component with trace of sediment assimilation in Pirquitas, we suggest that magmatic assimilation of lead was more important than hydrothermal leaching causing a reduction of the impact on radiogenic lead remobilization by leaching.

The lead isotope compositions measured in Pirquitas ores fall in the range of values measured in ore minerals from the southern BTB. There is a significant difference in the Pb isotope composition of Pirquitas and the well-studied Ag-Sn deposit of Potosí in the central BTB. Although the mineralization style and S-isotope ratios of both deposits are similar, ore lead from Pirquitas is significantly more radiogenic, which can be explained by a stronger crustal input in the southern BTB. The radiogenic lead signature of Pirquitas is interpreted to result from assimilation of Paleozoic (or compositionally equivalent) metasediments in the inferred magmatic source (not outcropping). This is consistent with the Pb-isotope variations in nearby Miocene volcanic and subvolcanic rocks. In the case of Pirquitas and other southern BTB deposits, magmatic Pb assimilation was probably more important than hydrothermal leaching at the site of ore deposition.

The presence of wolframite with relatively high U-contents in association with late ores as wood tin cassiterite of event II suggest relatively oxidizing conditions at the time of deposition.

The U-Pb dating of wolframite did not yield a valid isochron age, which is mostly due to the presence of lead from sulfide inclusions in the wolframite. Nevertheless, the reference lines calculated shows that the late event II of mineralization could occurred between 3 and 6 Ma which is consistent with geological constraints of < 15 Ma. Furthermore, the event II seems too much younger than the maximum age inferred from the age of the host rocks that less suppose, at least for the final event, a younger episode of mineralization.

References

Allègre, C.J. Luck, J.M. 1980. Osmium isotopes as petrogenetic and geological tracers. Earth Planet Sci Let 48:148–154

Allmendinger, R.W., Jordan, T.E., Kay, S.M., Isacks, B.L. 1997. The evolution of the Altiplano-Puna Plateau of the Central Andes. Annu Rev Earth Planet Sci. 25:139–174

Allmendinger, R.W., Strecker, M., Eremchuk, J.E., Francis, P. 1989. Neotectonic deformation of the southern Puna Plateau, northwestern Argentina. J S Am. Earth. Sci. 2:111–130.

Alonso, R., Gutiérrez, R., Viramonte, J. 1984. Puna Austral—Bases para el subprovincialismo geológico de la Puna austral. IX Congr Geol Argent Actas I. pp 43–63

Astini, R.A. 2003. The Ordovician proto-Andean basins. Benedetto, J.L., ed., Ordovician fossils of Argentina. Cordoba: Secretaría de Ciencia y Tecnología Universidad Nacional. pp. 1-74

Aitcheson, S.J., Harmon, R.S., Moorbath, S., Scneider, A., Soler, P., Soria-Escalante, E., Steele, G., Swainbank, I., Wörner, G. 1995. Pb isotopes define basement domains of the Altiplano, central Andes: Geology. 23:555–558

Bahlburg, H., Hervé, F. 1997. Geodynamic evolution and tectonostratigraphic terranes of northwestern Argentina and northern Chile. Geol Soc Am Bull. 109:869–884

Barreiro, B.A. 1984. Lead isotopes and Andean magmagenesis, in Harmon, R. S., and Barreiro, B. A., eds., Andean magmatism chemical and isotopic constraints. Cheshire, U, K, Shiva. pp 21-30.

Board, W.S. 2011. Technical Report on the Pirquitas mine, Jujuy, Argentina. Silver Standard Resources Inc. pp. 52-78.

Caffe, P.J. 2008. The Granada ignimbrite: A compound pyroclastic unit and its relationship with Upper Miocene caldera volcanism in the northern Puna. J South Am Earth Sci. 25:464-484

Caffe, P.J., Trumbull, R.B., Coira, B.L., Romer, R.L. 2002. Petrogenesis of Early Neogene magmatism in the northern Puna; implications for magma genesis and crustal processes in the Central Andean Plateau. J. Petrol. 43:907–942

Cardon, O. 2007. Datation Re-Os sur pyrite et traçage des sources des métaux dans des gisements de type porphyre et épithermal neutre: Exemple des gisements de Bolcana, Troita et Magura, Monts Apuseni, Roumanie. G2R. Université Henri Poincaré. Nancy. France.

Cladouhos, T.T. Allmendinger, R.W., Coira, B., Farrar, E. 1994. Late Cenozoic deformation in the Central Andes: fault kinematics from the northern Puna, northwestern Argentina and southwestern Bolivia. J South Am Earth Sci. 7:209–228

Coira, B. 1994. Metallogenetic events in the framework of magmatic-tectonic evolution of the Northern Puna of Argentina during the late Cenozoic. Communicaciones. 45:67–76

Coira, B., Caffe, P.J., Ramirez, A., Chayle, W., Diaz, A., Rosas, S. 2004. Hoja Geológica 2366-I/ 2166-III Mina Pirquitas. Provincia de Jujuy. Programa Nacional de Cartas Geológicas de la República Argentina 1:250 000(269)

Coutand, I., Cobbold, P.R., de Urreiztieta, M., Gautier, P., Chauvin, D., Gapais, A., Rossello, E.A., López-Gamundí, O. 2001. Style and history of Andean deformation, Puna plateau, northwestern Argentina. Tectonics. 20: 210–234

Cunningham, C.G., McNamee, J., Pinto Vásquez, J., Ericksen, G.E. 1991 A model of volcanic dome-hosted precious metal deposits in Bolivia. Econ Geol. 86: 415–421

Cunningham, C.G., Zartman, R.E., McKee, E.H., Rye, R.O., Naeser, C.W., Sanjinés, V.O., Eriksen, G.E., Tavera, V.F. 1996. The age and thermal history of Cerro Rico de Potosí, Bolivia. Miner Depos. 31: 374 – 385

Davidson, J.P., Mcmillan, N., Moorbath, S., Wörner, G., Harmon, R.S., Lopez-escobar, L. 1990. The Nevados de Payachata volcanic region (18°S/69°W, N. Chile) II. Evidence for widespread crustal involvement in Andean magmatism. Contributions to Mineralogy and Petrology. 105(4):412-432

Desanois, L., Volker, L., Niedermann, S., Trumbull, R.B. 2018. Formation of epithermal Sn-Ag-(Zn) vein-type mineralization at the Pirquitas deposit, NW Argentina: fluid inclusion and noble gas isotopic constraints. Chem Geol. https://doi.org/10.1016/j.chemgeo.2018.04.024

Dill, H.G. 1998. Evolution of Sb mineralization in modern fold belts: a comparison of the Sb mineralisation in the Central Andes (Bolivia) and the Western Carpathians (Slovakia). Miner Depos. 33:359–378

Ferenc, S., Uher, P. 2007. Magnesian wolframite from hydrothermal quartz veins in the Rochovce granite exocontact, Ochtiná, Western Carpathians, Slovakia. N Jb Miner Abh. 183:165–172

Frei, R., Nägler, T.F., Schönberg, R., Kramers, J.D. 1998. Re-Os, Sm-Nd, UPb, and stepwise lead leaching isotope systematics in shear-zone hosted gold mineralization: genetic tracing and age constraints of crustal hydrothermal activity. Geochim Cosmochim Acta. 62:1925–1936

Grant, J.N., Halls, C., Salinas, W.A., Snelling, N.J. 1979. K-Ar ages of igneous rocks and mineralization in part of the Bolivian Tin Belt. Econ Geol. 74:83 –851

Goldmann, S., Melcher, F., Gäbler, H.E., Dewaele, S., De Clercq, F., Muchez, P. 2013. Mineralogy and trace element chemistry of ferberite/reinite from tungsten deposits in Central Rwanda. Miner. 3, 121–144.

Gorustovich, S.A., Monaldi, C.R., Salfity, J.A., 2011. Geology and metal ore deposits in Argentine Puna. Cenozoic Geology of the Central Andes of Argentina, pp. 169-187.

Gubbels, T., Isacks, B., Farrar, E., 1993. High-level surfaces, plateau uplift, and foreland development, Bolivian Central Andes. Geology. 21, 695-698.

Grant, J.N., Halls, C., Salinas, W.A., Snelling, N.J., 1979. K-Ar ages of igneous rocks and mineralization in part of the Bolivian Tin Belt. Econ. Geol. 74, 838-851.

Harlaux, M., Romer, R.L., Mercadier, J., Morlot, C., Marignac, C., Cuney, M., 2018. 40 Ma of hydrothermal W mineralization during the Variscan orogenic evolution of the French Massif Central revealed by U-Pb dating of wolframite. Miner. Depos. 53. 21-51.

Hildreth, S and Moorbath, S. Crustal contributions to arc magmatism in the Andes of central Chile. Contributions to Mineralogy and Petrology. 139:206-226.

Holdsworth, R.E., Butler, C.A., Roberts, A.M., 1997. The recognition of reactivation during continental deformation. Journal of the Geological Society 154, 73–78.

Hongn, F.D., 1995. Estructuras precámbricas y paleozoicas del basamento de la Puna oriental, su aplicación para el análisis regional de la faja eruptiva. Rev. Asoc. Geol. Argent. 49 (3-4), 256-268.

John, F. A., Hofstra, A. H., Fleck, R. F, Brummer, J. E., Saderholm, E.C., 2003. Geologic setting and genesis of the Mule Camyon low-sulfidation epithermal gold silver deposit, North-Central Nevada. Econ. Geol. 98, 425-463

Kamenov, G., Macfarlane, A.W., Riciputi, L. 2002. Sources of lead in the San Cristobal, Pulacayo, and Potosí Mining Districts, Bolivia, and a reevaluation of regional ore lead isotope provinces. Econ Geol. 97:573–592

Kay, S.M., Coira, B., Viramonte, J. 1994. Young mafic back arc volcanic rocks as indicators of continental lithospheric delamination beneath the Argentine Puna plateau, central Andes. J Geophys Res. 99:24,323–24,339.

Kay, S.M., Mpodozis, C., Coira, B. 1999. Neogene magmatism, tectonism and mineral deposits of the Central Andes (22° to 33° latitude): Soc Econ Geol. Special Publication 7:27–59.

Langmuir, D. 1976. Uranium solution-mineral equilibria at low temperatures with applications to sedimentary ore deposits. Geochim Cosmochim Acta. 42:547–569.

Lecumberri-Sanchez, P., Romer, R.L., Lüders, V., Bodnar, R.J. 2014. Genetic relationship between silver-lead-zinc mineralization in the Wutong deposit, Guangxi Province and Mesozoic granitic magmatism in the Nanling belt, southeast China. Miner Depos. 49:353–369.

Lehmann, B., Dietrich, A., Heinhorst, J., Metrich, N., Mosbah, M., Palacios, C., Schneider, H.J., Wallianos, A., Webster, J., Winkelmann, L. 2000. Boron in the Bolivian tin belt. Mineralium Deposita 35: 223-232

Levresse, G., Cheilletz, A., Gasquet, D., Reisberg, L., Deloule, E., Marty, B., Kyser, K. 2004. Osmium, sulphur, and helium isotopic results from the giant Neoproterozoic epithermal Imiter silver deposit, Morocco: evidence for a mantle source. Chem Geol. 207:59–79.

Li, W.C., Yu, H.J., Yin, G.H., Cao, X.M., Huang, F.Z., Dong, T. 2012 Re-Os dating of molybdenite from Tongchanggou Mo-polymetallic deposit in northwest Yunnan and its metallogenic environment. Geological Survey Bureau.

Linares, E., González, R.R. 1990. Catálogo de edades radimétricas de la República Argentina 1957–1987. Asoc Geol Argent. Publicaciones Especiales. 19:628

Lin, Z., Sun, X., Strauss, H., Lu, Y., Gong, J., Xu, L., Lu, H., Teichert, B.M.A, Peckmann, J. 2017. Multiple sulfur isotope constraints on sulfate-driven anaerobic oxidation of methane: Evidence from authigenic pyrite in seepage areas of the South China Sea. Geochimica et Cosmochimica Acta. 211:153-173.

Lucassen, F., Becchio, R., Wilke, H.G., Thirlwall, M.F., Viramonte, J. 2000. Proterozoic–Paleozoic development of the basement of the central Andes (18°S–26°S) – a mobile belt of the South American craton. J S Am Earth Sci. 13:697–715

Luhr, J.F., Logan, A.V. 2002. Sulfur isotope systematics of the 1982 El Chichón trachyandesite: an ion microprobe study. Geochim Cosmochim Acta. 66:3303-3316

Maksaev, V., Munizaga, F., McWilliams, M., Fanning, M., Mathur, R., Ruitz, J., Zentilli, M. 2004. New Chronology for El Teniente, Chilean Andes, from U-Pb, $^{40}Ar/^{39}Ar$, Re-Os, and Fission-Track Dating: Implications for the Evolution of a Supergiant Porphyry Cu-Mo Deposit. In Sillitoe RH, Perelló J, and Vidal CE (eds). New Discoveries, Concepts, and Updates. Soc Econ Geol. Special publication. 11:15-54.

Macfarlane, A.W., Marcet, P., Lehuray, A.P., Petersen, U. 1990. Lead isotope provinces of the Central Andes inferred from ores and crustal rocks. Econ Geol. 85:1857–1880

Malvicini, L. 1978. Las vestas de estano y plata de Minas Pirquitas (Pircas) PCIA. de Jujuy, Rebublica Argentina. Revista de la Asociación Argentina de Mineralogía, Petrología y Sedimentología. 9:1–25

Mamani, M., Tassara, A., Woerner, G., 2008. Composition and structural control of crustal domains in the central Andes. Geochem Geophys Geosys. 9: Q03006, doi:10.1029/2007GC001925. 9:

Marrett, R.A., Allmendinger, R.W., Alonso, R.N., Drake, R.E. 1994. Late Cenozoic tectonic evolution of the Puna Plateau and adjacent foreland, northwestern Argentine Andes. J South Am Earth Sci. 7:179–208

Mathur, R., Ruiz, J.R., Munizaga, F.M. 2001. Insights into Andean metallogenesis from the perspective of Re-Os analyses of sulfides. South American symposium on isotope geology. Extended abstracts.

Matteini, M., Mazzuoli, R., Omarini, R.. 1999. Geochemical, petrographic and isotopic characterisation of Tultul, Del Medio and Pocitos volcanoes, Central Andes. XIV Congreso ArgentinoSalta Acta II. 228-231.

Mon, R., Salfity, J.A. 1995. Tectonic evolution of the Andes of northern Argentina. In: Tankard AJ, Suarez R, Welsink HJ (Eds.), Petroleum basins of South America. Am Assoc Petr Geol Mem. 62:269–283.

Myers, J.D., Marsh, B.D. 1987. Aleutian lead isotopic data: Additional evidence for the evolution of lithospheric plumbing systems: Geochim et Cosmochim Acta. 51:1833–1842

Ohmoto, H., Goldhaber, M.B. 1997. Sulfur and carbon isotopes. In: Barnes, H.L. (Ed.), Geochemistry of Hydrothermal Ore Deposits, 3rd ed. Wiley, New York. 517–611.

O'Neil, J.R., Silberman, M.L., Fabbi, B.P., Chesterman, C.W. 1973. Stable isotope and chemical relations during mineralization in the Bodie Mining District , Mono County, California. Econ Geol. 68:765–784

Ort, M., Coira, B. & Mazzoni, M. Contrib Mineral Petrol. 1996. Generation of a crust-mantle magma mixture: magma sources and contamination at Cerro Panizos, central Andes. Contributions to Mineralogy and Petrology. 123(3): 308-322.

Paar, W.H., Brodtkorb, M.K., Topa, D., Sureda, R.J. 1996. Caracterización mineralógica y química de algunas especies metalíferas del Yacimiento Pirquitas, Provinca de Jujuy, República Argentina: Parte 1. XIII Congr. Geol. Argent y III Congreso de Exploración de Hidrocarburos(III), pp. 141–158

Petersen, U., Macfarlane, A.W., Danielsen, A. 1993. Lead isotopic provinces in Perú, Bolivia and northern Chile: 2nd International Symposium on Andean Geodynamics, Oxford University, England, ORSTOM. 477–480

Pfaff, K., Romer, R.L., Markl, G. 2009. U-Pb ages of ferberite, chalcedony, agate, 'U-mica' and pitchblende: constraints on the mineralization history of the Schwarzwald ore district. Eur J Mineral. 21:817–836

Richards, J.P., 2009. Post-subduction porphyry Cu-Au and epithermal Au deposits: products of remelting of subduction-modified lithosphere. Geology. 37:247–250

Richards, J.P. 2011. Magmatic to hydrothermal metal fluxes in convergent and collided margins. Ore Geol Reviews. 40:1–26

Riller, U., Petrinovic, I., Ramelow, J., Strecker, M., Oncken, O. 2001. Late Cenozoic tectonism, collapse caldera and plateau formation in the central Andes. Earth Planet Sci Lett. 188:299–311

Rodriguez, G.A. 2004. Naturaleza y condiciones de emplazamiento de la mineralización aurífera en Minas Azules, sierra de Rinconada, Jujuy, Argentina. PhD Thesis (unpublished), Universidad Nacional de Cordoba, 347 pp.

Romer, R.L., Heinrich, W., Schröder-Smeibidl, B., Meixner, A., Fischer, C.O., Schulz, C. 2005. Elemental dispersion and stable isotope fractionation during reactive fluidflow and fluid immiscibility in the Bufa del Diente aureole, NE-Mexico: evidence from radiographies and Li, B, Sr, Nd, and Pb isotope systematics. Contributions to Mineralogy and Petrology. 149:400–429

Romer, R.L., Lüders, V. 2006. Direct dating of hydrothermal W mineralization: U–Pb age for hübnerite ($MnWO_4$), Sweet Home Mine, Colorado. Geochim et Cosmochim Acta. 70:4725–4733

Rosas, L.V., Avilia, J.C. 2013. Desarrollo minero de Pirquitas, provincia de Jujuy. Temas de Correlación Geológica III, Serie Correlación Geológica. 29:51–62

Rye, R.O., Luhr, J.F., Wasserman, M.D. 1984. Sulfur and oxygen isotope systematics of the 1982 eruptions of El Chichón volcano, Chiapas, Mexico. J Volcanol Geotherm Res. 23:109-123

Salfity, J.A., Gorustovich, S.A., Moya, M.C., Amengual, R. 1984. Marco tectónico de la sedimentación y efusividad Cenozoicas en la Puna Argentina Actas. Asoc. Geol. Argent., S.C. de Bariloche, Argentina. Congr Geol Argentino IX :539–554.

Saunders, J.A., Unger, D.L., Kamenov, G.D., Frayek, M., Hames, W.E., Utterback, W.C. 2008. Genesis of Middle Miocene Yellowstone-hotspot-related bonanza epithermal Au-Ag deposits, Northern Great Basin region, USA. Mine. Deposita. 43:715–734

Seal, R.R. 2006. Sulfur isotope geochemistry of sulfide minerals. Rev. Mineral. Geochem. 61:633–667

Schmidt, C. 2018. Formation of hydrothermal tin deposits: Raman spectroscopic evidence fo an important role of aqueous Sn(IV) species. Geochim Cosmochim Acta. 220:199–211 .

Sillitoe, R.H., Halls, C., Grant, J.N. 1975. Porphyry tin deposits in Bolivia. Econ Geol. 70:913–927

Simmons, S.F., White, N.C., John, D.A. 2005. Geological characteristic of epitheröal precious and base metal deposits. 100th Anniv Vol Econ Geol. 63:210–223

Slater, E.T. 2016. The Cortaderas zone, Pirquitas Mine, NW Argentina: An example of Miocene epithermal Ag-Zn-Pb-Sn mineralization in the Andean Tin Belt. MSc thesis Laurentian University Sudbury, Ontario, Canada. 113 p.

Stacey, J.S. Kramers, J.D. 1975. Approximation of terrestrial lead isotope evolution by a two-stage model. Earth and Planetary Science Letters. 26(2):207–221.

Sugaki, A., Ueno, H., Shimada, N., Kusachi, I., Kitakaze, A., Kojima, S., Sanjines, V.O. 1983. Geological study on the polymetallic ore deposits in the Potosí district, Bolivia. Sci Rept Tohoku Univ Ser. III:327–352

Sugaki, A., Kitakaze, A. 1988. Tin-bearing minerals from Bolivian polymetallic deposits and their mineralization stages. Min. Geol. 38:419–435

Sugaki, A., Ueno, H., Hayashi, K. 1990. Sulfur Isotope Reconnaissance of Bolivian Hydrothermal Deposits. Mine Geol. 40:219–312

Swart, P.K., Moore, F. 1982. The occurrence of uraniumin association with cassiterite, wolframite, and sulphide mineralization in south-West England. Mineral Mag. 46:211–215

Tilton, G.R., Pollak, R.J., Clark, A., Robertson, R.C. 1981. Isotopic composition of Pb in central Andean ore deposits: Geol Soc Am Mem. 154:791–816

Tindle, A.G., Webb, P.C. 1989. Niobian wolframite from Glen Gairn in the eastern highlands of Scotland: a microprobe investigation. Geochim Cosmochim Acta. 53:921–1935

Thorn, P.G. 1988. Fluid Inclusion and Stable Isotope Studies at the Chicote Tungsten Deposit, Bolivia. Econ geol. 83:62–68

Tosdal, R.M., Gibson, P.C., Wallace, A.R., Hardyman, R.F., Koeppen, R.P., Vilca, N.C., Quispesivana, Q.L., Tejada, G.R., Jimenez, C.N., Lizeca, B.J.L., Murillo, S.F., Moscoso, D.R., Cuitino, G.L., Maksaev, J.V., and Diaz, F.F. 1993. Summary of Pb isotopic compositions in epithermal preciousmetal deposits, Orcopampa area of southern Peru, Berenguela area of western

Bolivia, and Maricunga Belt in north-central Chile: in Investigacion de metales preciosos en los Andes Centrales, Proyecto BID/TC-88-02- 32-5, Banco Interamericano de Desarrollo, Washington, DC, United States (USA) pub Chap. 3:47–55.

Taylor, S.R., McLennan, S.M. 1985. The continental crust: its composition and evolution. Blackwell, Oxford. 312.

Titley, S.R. 1987. The crustal heritage of silver and gold ratios in Arizona ores. Geol Soc Am Bull. 99:814–826

Titley, S.R. 2001. Crustal Affinities of Metallogenesis in the American Southwest. Econ Geol. 96:1323–1342

Turneaure, F.S. 1960. A comparative study of major ore deposits of central Bolivia. Part I Econ Geol. 55:217–254

Turneaure, F.S. 1971. The Bolivian Tin-Silver Province. Econ Geol. 66:215–225

Turner, J.C.M. 1960. Estratigrafía de la Sierra de Santa Victoria y adyacencias, Provincias de Saltay Jujuy. Boletín de la Academia Nacional de Ciencias de Córdoba. 41(2): 163-196

Voldman, G.G., Albanesi, G.L., Ortega, G., Monaldi, C.R., Zeballo, F.J., Giuliano, M.E. 2012. Biostratigraphy of the Santa Rosita Formation (Furongian-Tremadocian) in its type area, Eastern Cordillera, NW Argentina. Geophysical Research Abstracts p 14.

Wörner, G., Moorbath, S., Harmon, R.S. 1992. Andean Cenozoic volcanic centers reflect basement isotopic domains. Geology. 20:1103–1106

Yao, J.M., Hua, R.M., Qu, W.J., Qi, H.W., Lin, J.F., Du, A.D. 2007. Re-Os isotope dating of molybdenites in the Huangshaping Pb-Zn-W-Mo polymetallic deposit, Hunan Province, South China and its geological significance. Sci China Ser D. 50:519–526

Zartman, R. Cunningham, C. 1995. U-Th-Pb zircon dating of the 13.8 Ma dacite volcanic dome at Cerro Rico de Potosí, Bolivia. Earth Planet Sci Lett. 133:227–237

Zentilli M, Doe B, Hedge CE, Alvarez O, Tidy E, Daroca JA. 1988. Isotopos de plomo en yacimientos de tipo porfido cu-prifero comparados con otros depositos metalíferos en los Andes del norte de Chile y Argentina. In: Actas 5th Congr Geol Chileno, pp B331–369

5. General conclusions

Two major events of mineralization in the Pirquitas vein system were identified. The first one can be divided into two stages: (1) I-1 mainly characterized by the deposition of pyrite, arsenopyrite, quartz and cassiterite, and (2) I-2 corresponds to the deposition of Ag-Sn-Sb-Pb-Zn sulfides and sulfosalts. These stages are followed by event II with the deposition of colloform sphalerite and a large variety of complex Ag-Sn-Sb-Pb-Bi sulfides and sulfosalts.

Vein-type mineralization precipitated from moderately saline fluids at temperature below 400°C during the two major events. These events are characterized by at least three pulses of mineralizing fluids, Salinity and homogenization temperature variations suggest different pulses of ore mineralizing fluids. The highest homogenization temperatures were measured in aqueous two-phase fluid inclusions hosted in quartz from the first mineralization event. Ores precipitated at lower temperatures during subsequent stages, which indicates a possible mixing of magmatic fluids with cooler meteoric water. Wolframite with high U-contents in association with late ores, like wood tin cassiterite from event II, reveals relatively oxidizing conditions during this late episode of mineralization. No boiling evidence in any samples was observed. This makes the contemporaneous deposition of Ag-rich ores and base metal sulfides at Pirquitas difficult to explain as boiling is a major phenomenon responsible of precious and base metal deposition.

It was the first time that noble-gases ratios were measured in ore-hosted fluid inclusion from BTB deposits. With one exception, the Pirquitas samples yielded $^{3}He/^{4}He$ ratios between 1.9 and 4.1 Ra, which is consistently higher than the bear-by hot-spring meteoric fluids and overlaps with the range of magmatic helium. Those ratios provide direct evidence of a magmatic contribution to the Pirquitas ore fluids.

The lowest $\delta^{34}S$ measured in pyrite from the event I-1 (-6.3‰) indicating that the hydrothermal system contained an initially higher assimilation of sulfur from the country rocks, whereas during the tin and silver deposition stages in event I-2 and II, the hydrothermal fluid was isotopically more homogeneous and carried mostly magmatic-derived sulfur (-1 to +1.7‰). The Ag-Sn-(Zn) mineralization of Pirquitas is similar to that described in other pluton-related epithermal polymetallic deposits in the

southern BTB. It is classify as an intermediate to low-sulfidation deposit type. Sulfur and lead isotope compositions of Pirquitas resemble those measured in ore minerals from other polymetallic deposits of the southern BTB. This suggests a similar origin as a distal magmatic-hydrothermal system, even if no direct relationship with a subvolcanic body has been discovered by mining or exploration drilling.

As well as the noble-gases isotopes in the fluid, the sulfur isotopes in sulfides and sulfosalts show a clear magmatic input in the mineralizing system. Although the mineralization style and S-isotope ratios of both Pirquitas and the well-studied Ag-Sn deposit of Potosí in the central BTB are similar, lead from Pirquitas is significantly more radiogenic. This significant difference in the Pb isotope composition can also be interpreted as the result of assimilation of Paleozoic (or compositionally equivalent) metasediments in the inferred magmatic source in the southern BTB. This hypothesis is supported by Pb-isotope variations observed in nearby Miocene volcanic and subvolcanic rocks. It is suspected that magmatic Pb assimilation was probably more important than hydrothermal leaching at the site of ore deposition. Indeed, Pirquitas mineralization can be explained by the same metallogenetic model as the others polymetallic epithermal deposits of the BTB. Then, following this model, our results strongly suggest that a buried felsic intrusion exists beneath the deposit.

The attempt of U-Pb dating did not succeed in determining a valid isochron age. This difficulty can be attributed mostly to the presence of lead from sulfide inclusions in the wolframite. Notwithstanding, with the calculated reference line, it is still possible to constrain the late event II to an age of 3 to 9 Ma, which is consistent with ages of volcanic centers in the close area and geological constraints that defined the deposit younger than 15 Ma.